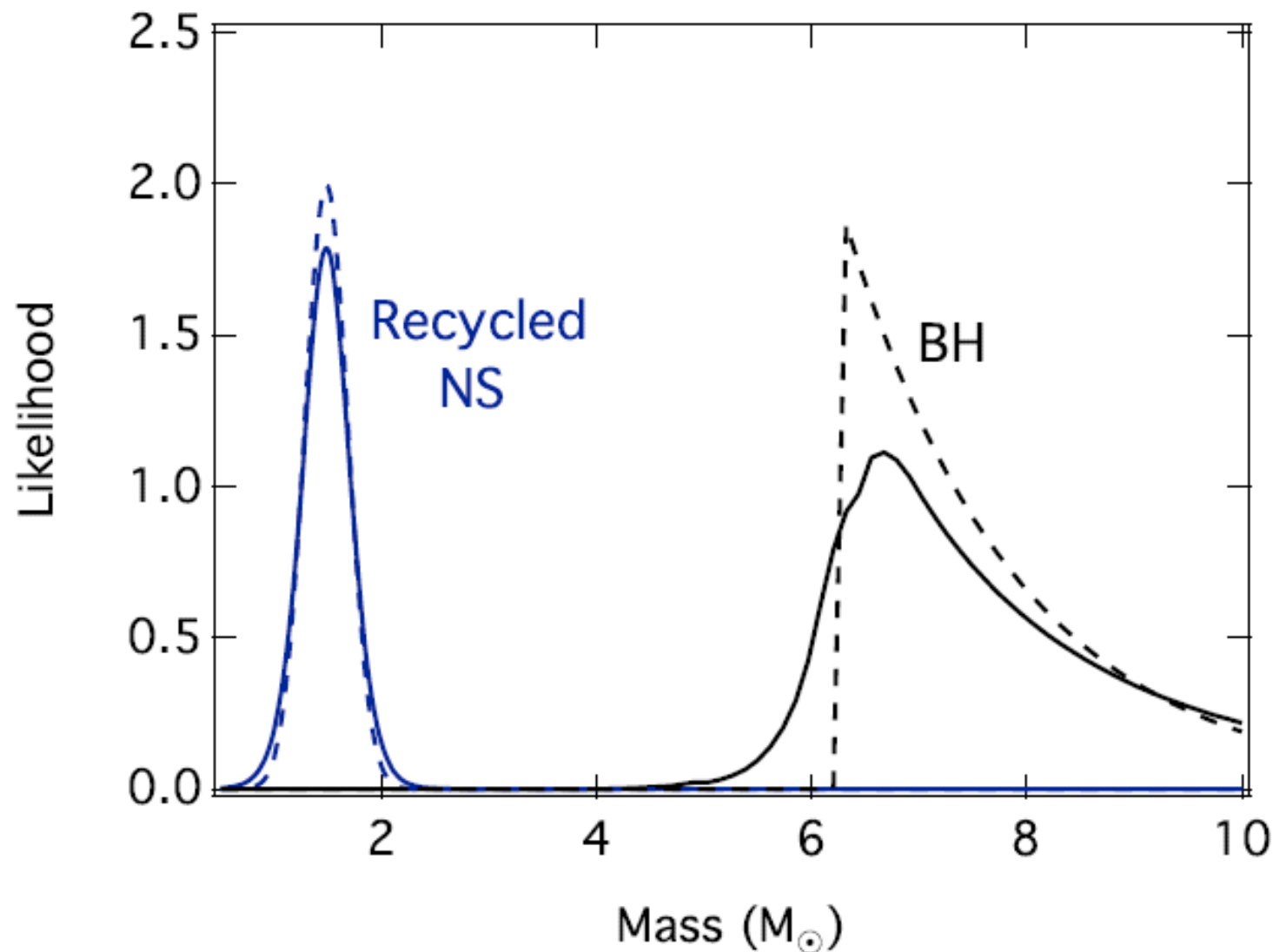


«Возможность отождествления какого-либо компактного объекта с ЧД зависит, в частности, от того, позволяют ли имеющиеся данные категорически утверждать, что масса наблюдаемого объекта больше **максимально допустимой массы нейтронной звезды** (или **белого карлика**).»

(Шапиро и Тьюкольски, том.2, гл.9)



А какая максимальная масса НЗ допустима?



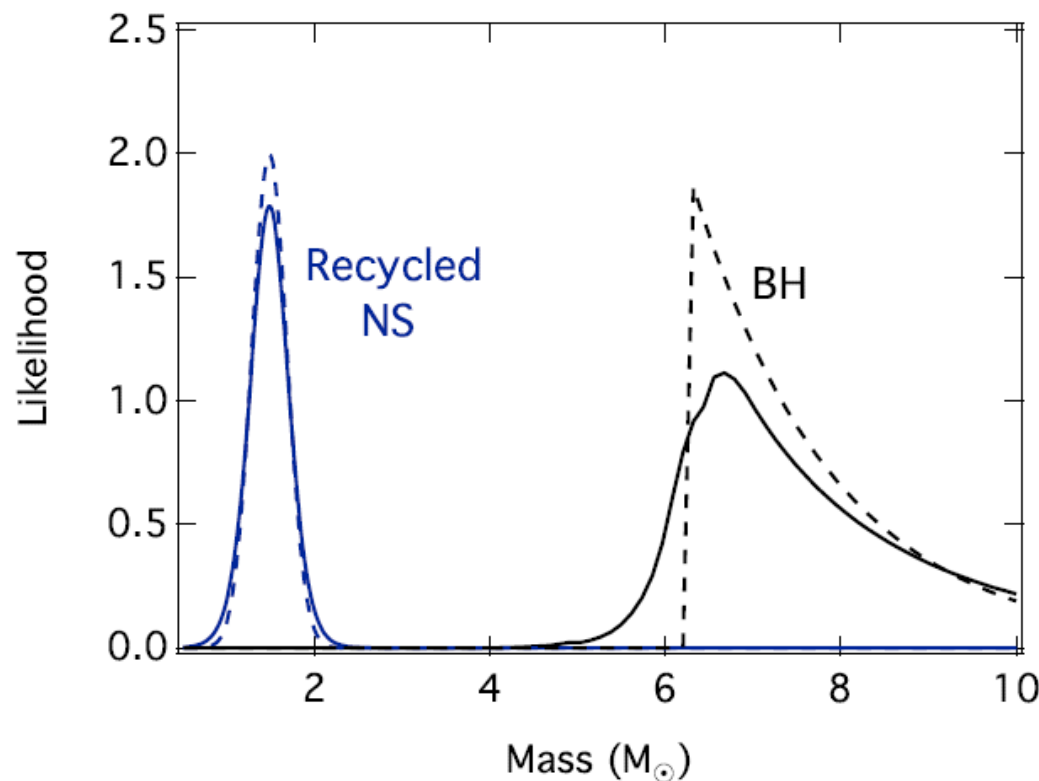
Гравидинамика (скалярно-тензорная гравитация) и дискретный спектр масс звездных компактных объектов.

- (1) Наблюдаемый спектр масс нейтронных звезд и кандидатов в черные дыры показывает явное отсутствие компактных объектов с массами в **интервале 2-6 солнечных**, а в тесных двойных звездных системах с маломассивными оптическими компаньонами самое вероятное (**пик в распределении** массы кандидатов в черные дыры) значение близко к **7 массам Солнца**.
- (2) В полностью неметрической, полевой/скалярно-тензорной модели гравитационного взаимодействия релятивистский компактный объект с предельно сильным гравитационным полем (аналог черных дыр в ОТО) имеет полную массу ≈ 6.7 **солнечных** масс с радиусом области, занятой веществом (кварк-глюонной плазмой), ≈ 10 км.
- (3) Поляризованное излучение гамма-всплесков, чернотельную компоненту в их спектре и другие наблюдательные свойства можно объяснить прямым проявлением **поверхности** у таких коллапсаров.



1.

On the mass gap + a strong peak around 7 Θ



«Само существование черных дыр не очевидно для многих ученых. Это, быть может, самый драматичный спор в науке, который даст ключ к ОТО. Сам Эйнштейн не верил в черные дыры, которые только и могут спасти его теорию. И сегодня **половина** физиков не верит в черные дыры, утверждая, что из реальною вещества такие объекты построить нельзя. Уже открыто 300 черных дыр, но споры продолжаются.

Потому что остается вероятность того, что *будут открыты объекты такой же массы, как черные дыры, но с границей поверхности и магнитным полем.* »



Ну спасибо и на том!



Из доклада А.М.Черепашку (Москва, ИКИ РАН, декабрь 2005 г.)

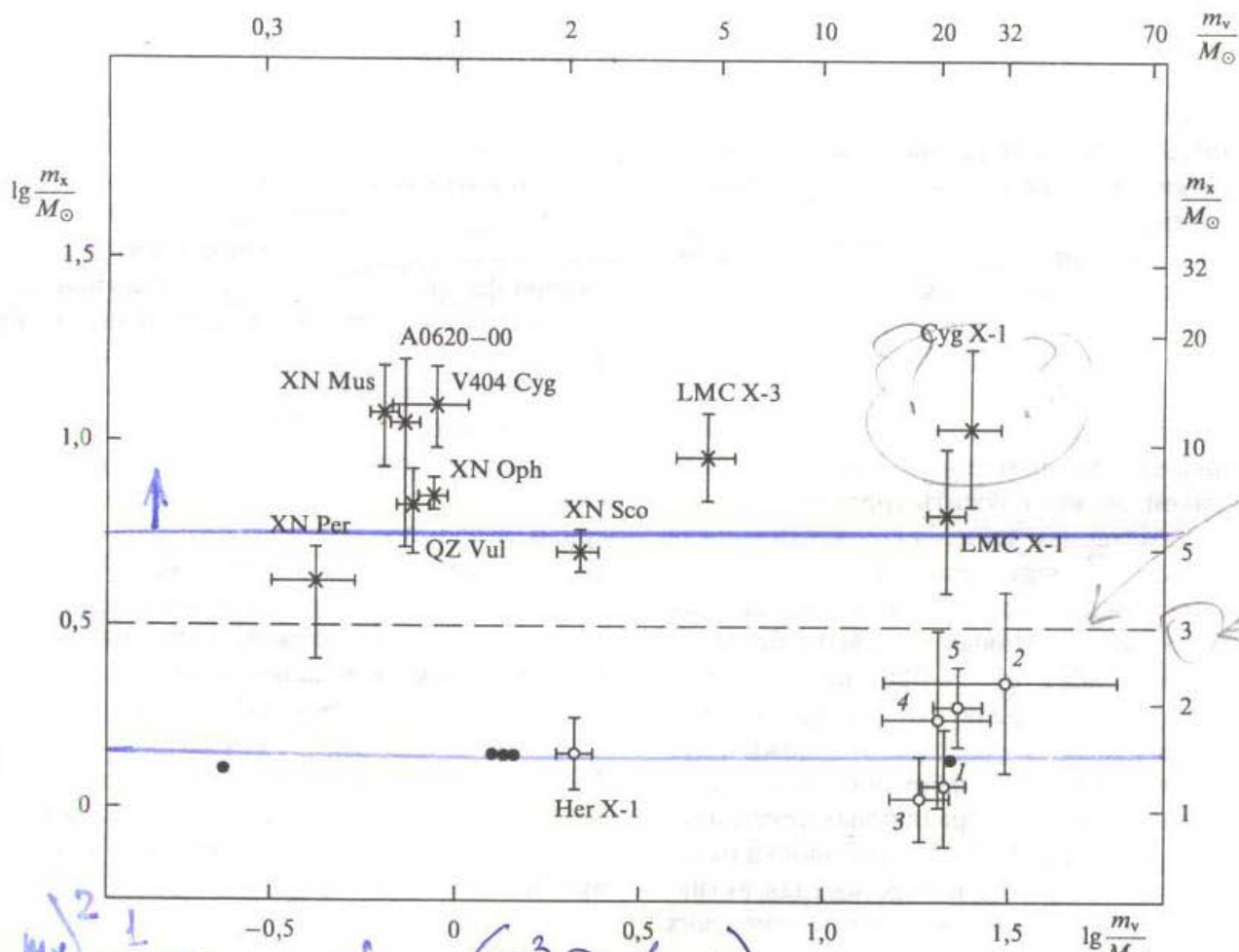
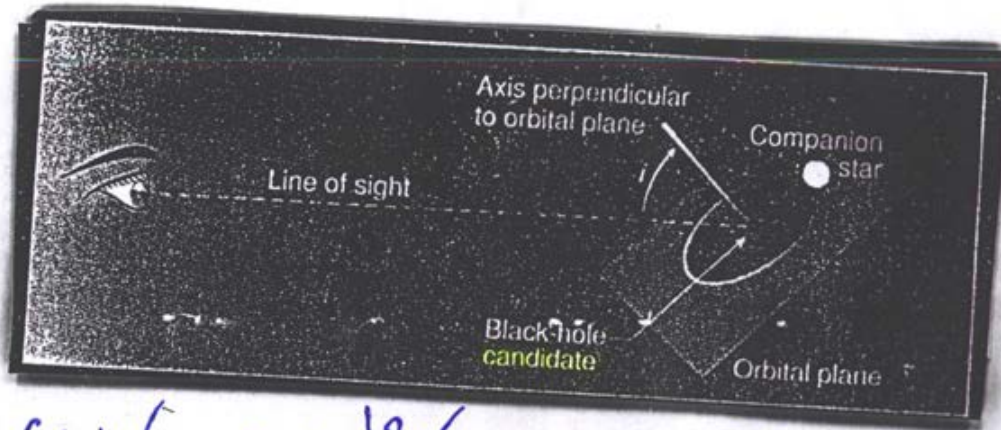


Рис. 20. Зависимость масс нейтронных звезд m_x (точки темные и светлые) и черных дыр (крестики) от масс спутников m_v в тесных двойных системах. Цифровые обозначения: 1 — система Сен X-3, 2 — LMC X-4, 3 — SMC X-1, 4 — 4U1538-52, 5 — 4U0900-40. Указаны ошибки определения масс у рентгеновских пульсаров (светлые точки). Ошибки определения масс радиопульсаров (темные точки) пренебрежимо малы. Ни один из массивных ($m_x > 3 M_\odot$) рентгеновских источников не является ни рентгеновским пульсаром, ни рентгеновским барстером I-го типа, т.е. не обладает признаками характерными для аккрецирующих нейтронных звезд.

см 829стр (37)

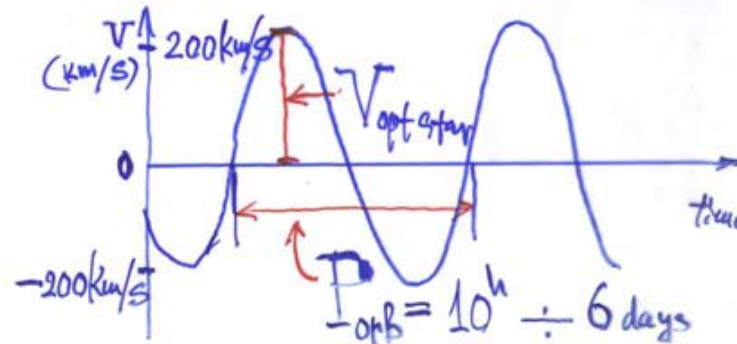


$$M_x = f(M_x) \cdot \left(1 + \frac{m_{\text{opt star}}}{M_x}\right)^2 / 8 \sin^3 i$$

$$f(M_x) = (V_{\text{opt star}}^3 P_{\text{orb}} / 2\pi G)$$

for $m_{\text{opt star}}/M_x \ll 1$ and $i \approx 90^\circ$

$$M_x \geq f(M_x)$$



Из доклада
А.М. Черепащука

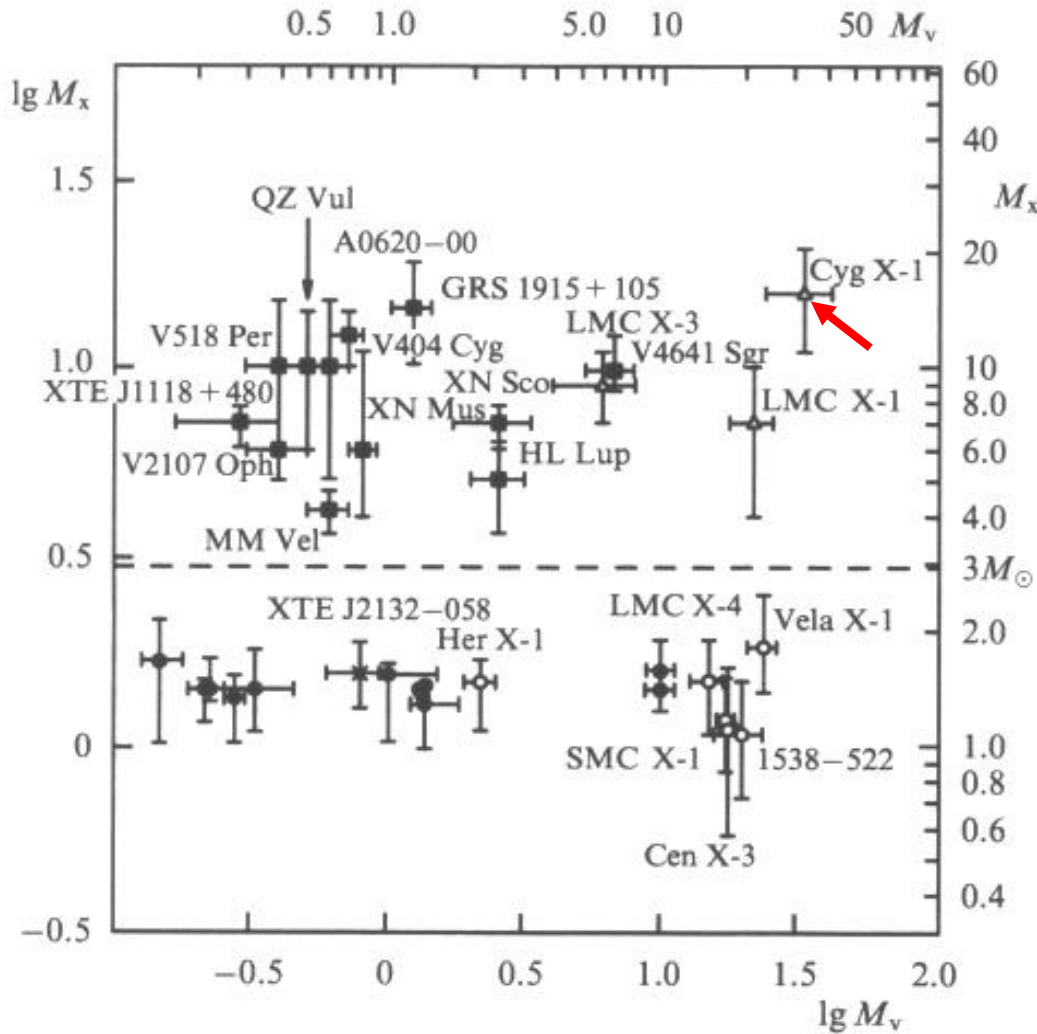


Figure 27. The dependence of masses M_x of NSs (circles and crosses) and BHs (triangles and squares) on the companion masses M_v in binary systems (masses are in solar units M_\odot). The filled circles correspond to radio pulsars, the open circles to X-ray pulsars, and the cross stands for the NS in X-ray nova XTE J2132–058 [324]. The filled squares correspond to BHs in X-ray novae and the open triangles to BHs in quasi-persistent X-ray binaries with massive O–B companions.

Из доклада
А.М. Черепашку

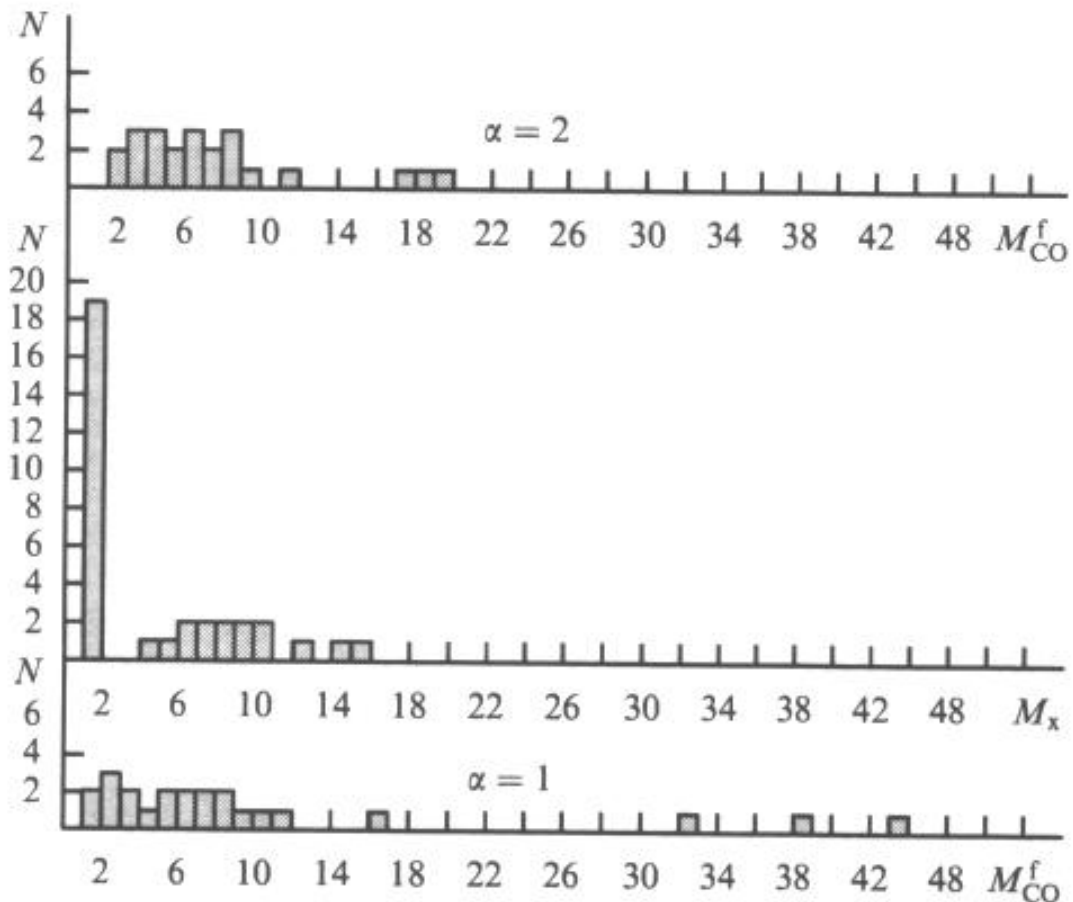
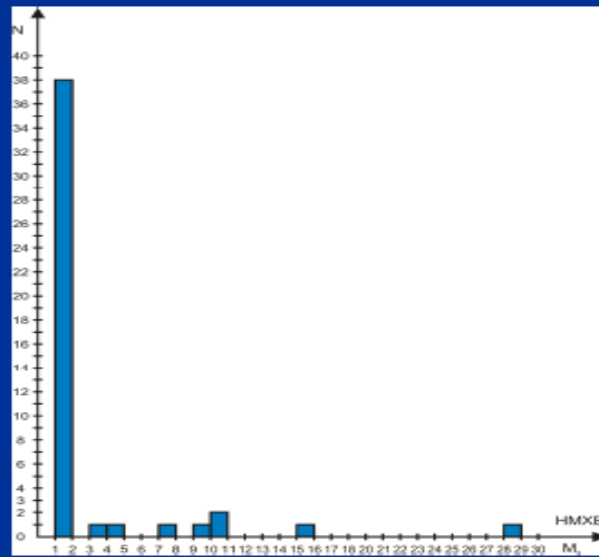
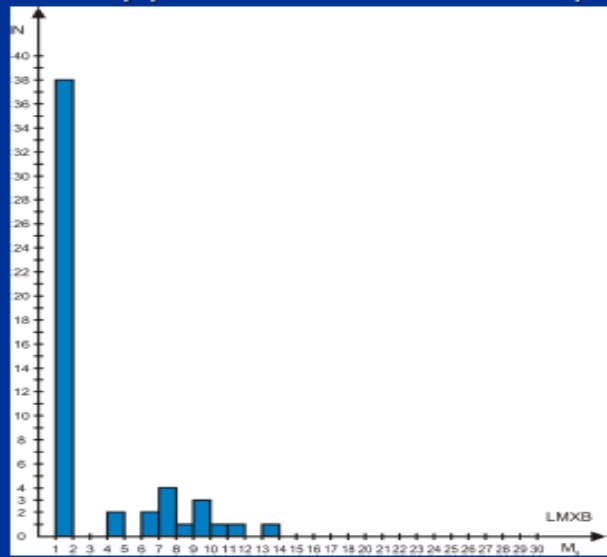


Figure 30. Histograms of distributions of the final masses of carbon-oxygen cores M_{CO}^{f} for 23 WR stars with known masses (the bottom plot corresponds to the case $\alpha = 1$ in $\dot{M}_{\text{WR}} = k M_{\text{WR}}^{\alpha}$, the upper plot to the case $\alpha = 2$). In the middle, the histogram of the M_x mass distribution for 34 relativistic objects in binary systems is shown. (Masses M_{CO}^{f} and M_x are in solar units M_{\odot}). The high peak at $(1-2)M_{\odot}$ corresponds to a NS. The distributions of M_{CO}^{f} are continuous, while the distribution for M_x is bimodal with a gap at $M_x = (2-4)M_{\odot}$ (from Refs [377, 378]).

- 2. Намечается провал в распределении масс н.з. и ч.д. в интервале масс $2-4 M_{\text{Sun}}$. В этом интервале масс число открытых н.з. и ч.д. в двойных системах близко к нулю. И в этом случае можно показать, что наличие провала в интервале $2-4 M_{\text{Sun}}$, скорее всего, не связано с эффектами наблюдательной селекции.



В работе Постнова и Черепашку (2003) выдвинута гипотеза, что плоское распределение ч.д. по массам и провал в этом распределении в районе $2-4 M_{\text{Sun}}$ могут быть связаны с усиленным квантовым испарением ч.д., которое следует из некоторых многомерных моделей гравитации с макроскопическими дополнительными измерениями (см., например, Randall and Sundrum, 1999).

.... **старые работы** из

1401.3032 (Tsing-Wai Wong, Christopher L. Fryer et al.,
«The Fall-back Mechanisms in Core-Collapse SNe.»):

The masses of compact remnants in a binary systems:

The mass distribution studies of compact remnants in a binary systems проводятся уже давно:

e.g. **Bailyn et al. 1998**; **Finn 1994**;

Thorsett & Chakrabarty 1999;

Kaper et al. 2006; **Nice et al. 2008**;

“Ozel et al. 2010, 2012; Schwab et al. 2010;,”

в 1401.3032 много слов и ссылок, см. на стр.3.

- Тут главное – осознание проблемы профессионалами!

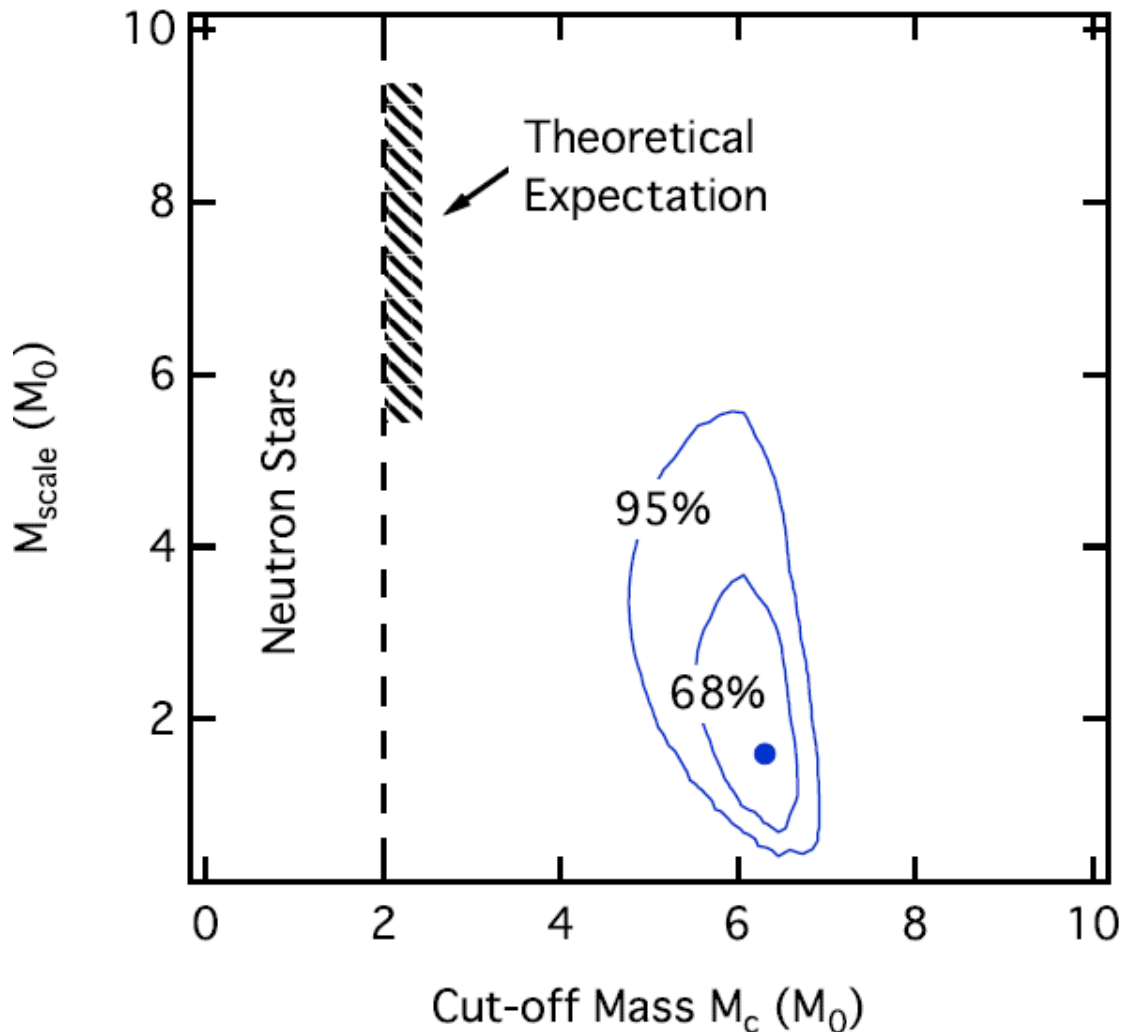


Such a gap is puzzling in light of
theoretical studies

that **predict a continuous distribution** of
compact object SN remnant
masses with a **smooth transition** from
NSs to BHs

(Fryer & Kalogera 2001).





exponentially decaying mass distribution with a
cut-off

$$P(M; M_{\text{scale}}, M_c) = \frac{\exp(M_c/M_{\text{scale}})}{M_{\text{scale}}} \\ \times \begin{cases} \exp(-M/M_{\text{scale}}) , & M > M_c \\ 0 , & M \leq M_c \end{cases}$$



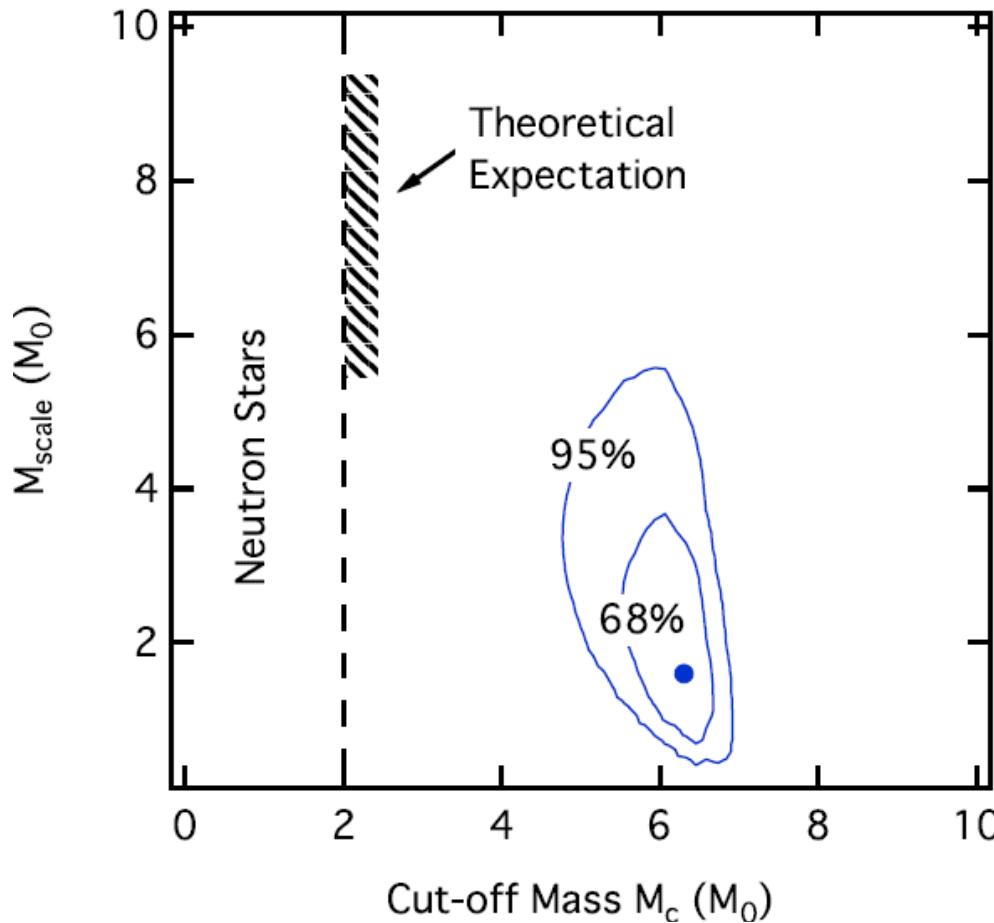


Figure 3. Parameters of an exponential black hole mass distribution with a low-mass cutoff. The cutoff mass is well above theoretical expectations, indicating a sizable gap between neutron-star and black hole masses. Furthermore, the mass scale in the exponential is significantly smaller than theoretical expectations.



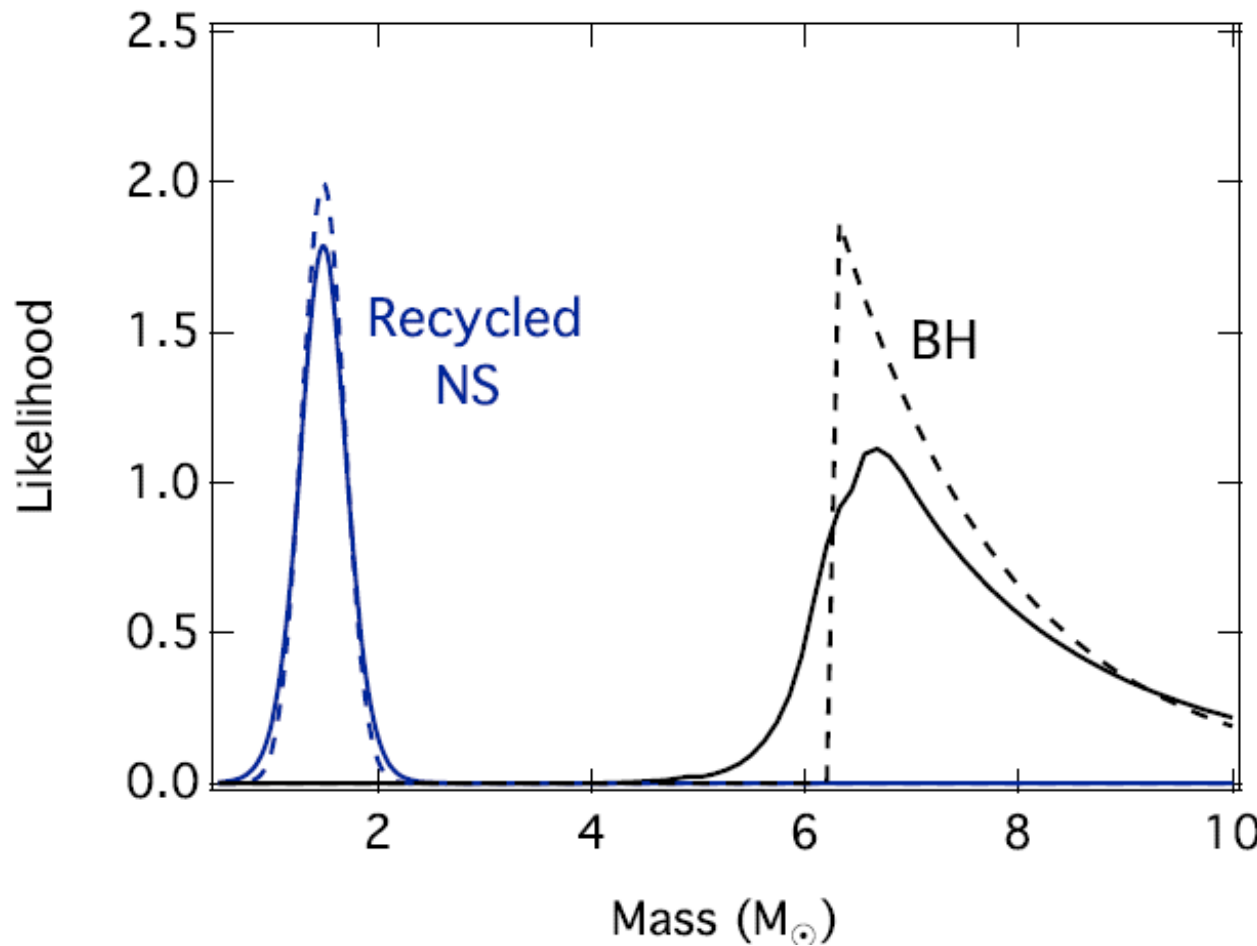


Fig. 15.— For the case of black holes, we used the exponential distribution with a low mass cut-off at $M_c = 6.32 M_{\odot}$ and a scale of $M_{scale} = 1.61 M_{\odot}$ obtained in "Ozel et al. (2010a). The solid lines represent the weighted mass distributions for each population, for which appropriate fitting formulae are given in the Appendix. The distributions for the case of black holes have been scaled up by a factor of three for clarity.

exponentially decaying mass distribution with a
cut-off

$$P(M; M_{\text{scale}}, M_c) = \frac{\exp(M_c/M_{\text{scale}})}{M_{\text{scale}}} \\ \times \begin{cases} \exp(-M/M_{\text{scale}}) , & M > M_c \\ 0 , & M \leq M_c \end{cases}$$



Ozel et al, 2010

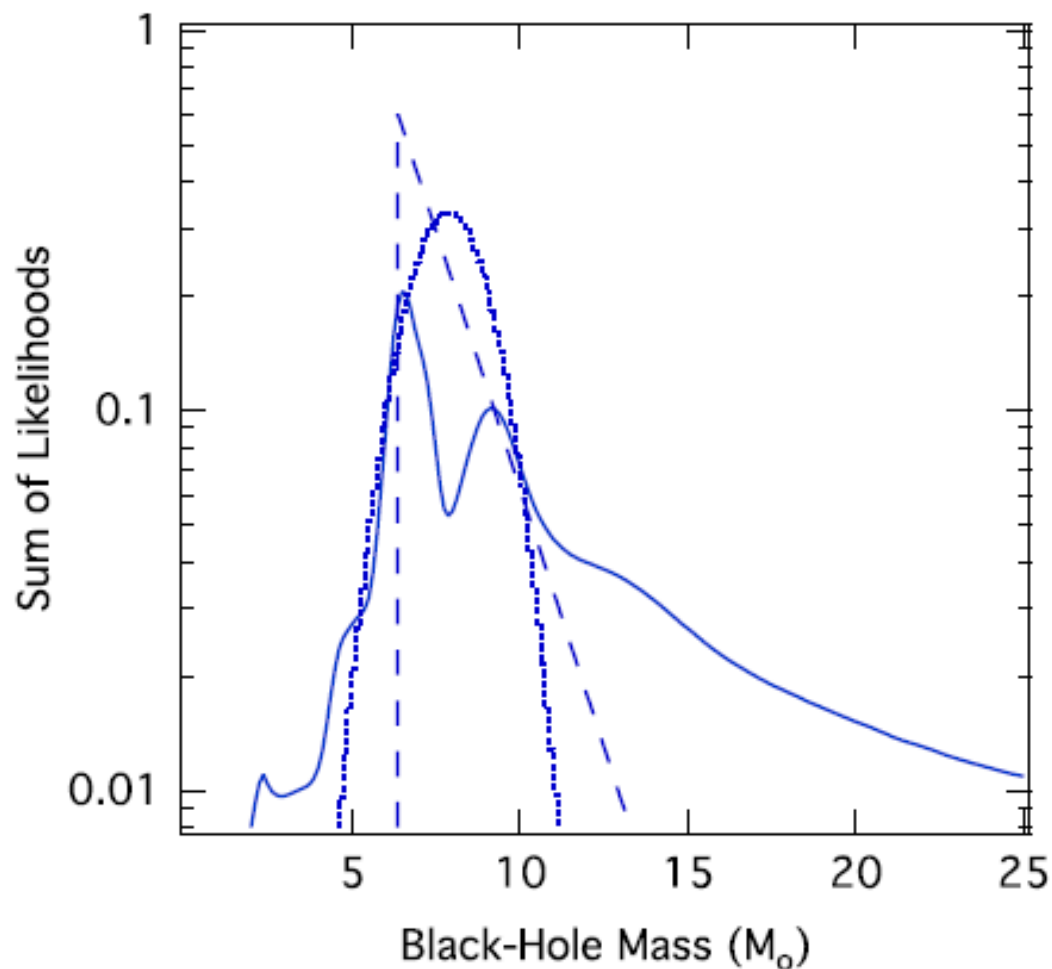


Figure 2. Solid line shows the sum of likelihoods for the mass measurements of the 16 black holes in low-mass X-ray binaries. Note that because of the high-mass wings of the individual likelihoods, the shape of their sum is artificial at the high-mass end. The dashed and dotted lines show the exponential and Gaussian distributions, respectively, with parameters that best fit the data (see Section 4).

the probability distribution can be described as a Gaussian

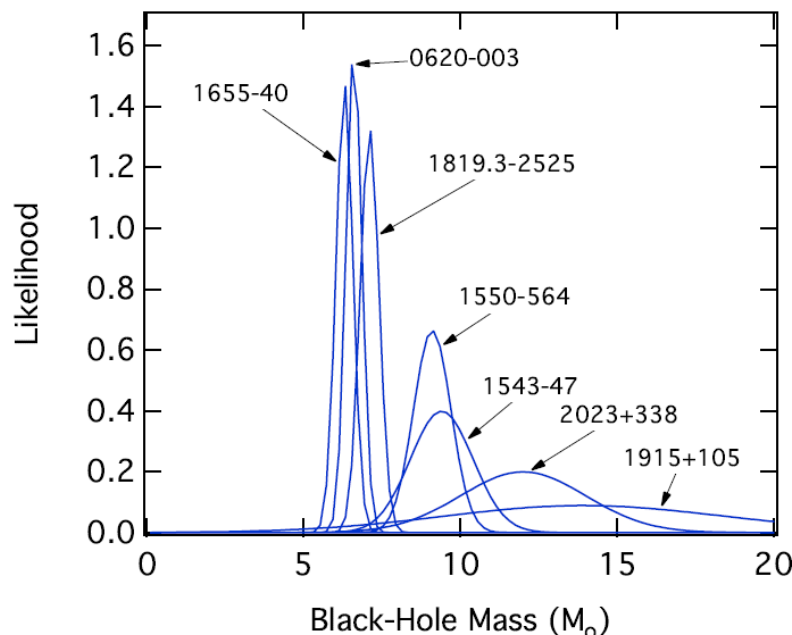
$$P_i(\text{data}|M) = C_i \exp \left[\frac{-(M - M_{0,i})^2}{2\sigma_{M,i}^2} \right]$$

with a mean $M_{0,i}$ and a standard deviation $\sigma_{M,i}$.

C_i is a proper normalization constant such that

$$\int_0^\infty P_i(\text{data}|M)dM = 1$$

For six sources
well-determined black hole
masses



Orbital Parameters for 16 Black Hole Binaries

X-Ray Name	Optical Counterpart	Spectral Type	$f(M_{\odot})$	q	i (deg)	i_{\min} (deg)	i_{\max} (deg)
4U 1543–47	IL Lup	A2 V	$N(0.25, 0.01)$	$U(0.25, 0.31)$	$I(24.0, 36.0)$	19.8	73.4
A0620–00	V616 Mon	K5 V	$N(3.1, 0.04)$	$N(0.060, 0.004)$	$N(51.0, 0.9)$	36.5	79.8
GRO J0422+32	V518 Per	M2 +2/-1 V	$N(1.19, 0.02)$	$N(0.116, 0.08)$	$N(63.7, 5.2)$	0.0	90.0
GRO J1655–40	V1033 Sco	F6 III	$N(2.73, 0.09)$	$N(0.38, 0.05)$	$N(69.0, 3.0)$	0.0	90.0
GRS 1009–45	MM Vel	G5–K7 V	$N(3.17, 0.12)$	$N(0.137, 0.015)$	$N(62.0, 5.1)$	42.3	76.9
GRS 1124–683	GU Mus	K3–K4 V	$N(3.01, 0.15)$	$N(0.128, 0.04)$	$I(54.0, 65.0)$	33.2	80.1
GRS 1915+105	V1487 Aql	K0-7 III	$N(9.5, 3.0)$	$N(0.058, 0.033)$	$N(70.0, 2.0)$	0.0	90.0
GS 1354–64	BW Cir	G0-5 III	$N(5.73, 0.29)$	$N(0.12, 0.04)$	$I(27.2, 80.8)$	27.2	80.8
GS 2000+25	QZ Vul	K3-6 V	$N(5.01, 0.12)$	$N(0.042, 0.012)$	$I(55.0, 65.0)$	28.3	86.7
GS 2023+338	V404 Cyg	K0 IV	$N(6.08, 0.06)$	$N(0.060, 0.005)$	$N(80.1, 5.1)$	35.4	80.0
H1705–250	V2107 Oph	K5 ± 2 V	$N(4.86, 0.13)$	$U(0, 0.053)$	$I(48.0, 90.0)$	0.0	90.0
SAX J1819.3–2525	V4641 Sag	B9 III	$N(2.74, 0.12)$	$N(0.67, 0.04)$	$I(80.0, 90.0)$	44.8	69.6
XTE J1118+480	KV UMa	K5 V	$N(6.27, 0.04)$	$N(0.024, 0.009)$	$I(68.0, 82.0)$	21.8	89.4
XTE J1550–564	V381 Nor	K3 ± 1 III	$N(7.65, 0.38)$	$U(0.031, 0.037)$	$I(57.7, 77.1)$	26.5	82.0
XTE J1650–500	...	G5–K4 III	$N(2.73, 0.56)$	$U(0, 0.5)$	$N(75.2, 5.9)$	0.0	90.0
XTE J1859+226	V406 Vul	K5–7 V	$N(4.5, 0.6)$	$U(0, 0.5)$	$N(60.0, 3.0)$	0.0	90.0

... проверка на дорогах:

Farr et al. 2011,

Kreidberg et al. 2012;

Kiziltan et al. 2013,

+ статья команды ГАИШ (Петров В.С., Черепащук А.М., Антохина Э.А., 2014)

Kreidberg et al. 2012

(Particularly) о массах компактных объектов

In systems with a faint companion star

$$q = M_{\text{opt}} / M_x \approx 0.1$$

Для таких систем оптическая звезда – пробное тело:



THE MASS DISTRIBUTION OF STELLAR-MASS BLACK HOLES

WILL M. FARR¹, NIHARIKA SRAVAN¹, ANDREW CANTRELL², LAURA KREIDBERG², CHARLES D. BAILY²,
ILYA MANDEL^{3,4}, AND VICKY KALOGERA¹

¹ Northwestern University Center for Interdisciplinary Exploration and Research in Astrophysics, 2145 Sheridan Rd.,
Evanston, IL 60208, USA; w-farr@northwestern.edu, niharika.sravan@gmail.com, vicky@northwestern.edu

² Department of Astrophysics, Yale University, P. O. Box 208101, New Haven, CT 06520,
USA; andrew.cantrell@yale.edu, laura.kreidberg@yale.edu, charles.bailyn@yale.edu

³ Kavli Institute, Massachusetts Institute of Technology, Cambridge, MA 02139,
USA; ilyamandel@chgtk.info

**We conclude that our sample of BH
masses provides strong evidence of
a gap between the maximum NS mass
and the lower bound on BH masses.**



THE ASTROPHYSICAL JOURNAL, 757:36 (17pp), 2012

MASS MEASUREMENTS OF BLACK HOLES IN X-RAY TRANSIENTS: IS THERE A MASS GAP?

LAURA KREIDBERG^{1,2}, CHARLES D. BAILY¹, WILL M. FARR^{3,4}, AND VICKY KALOGERA³

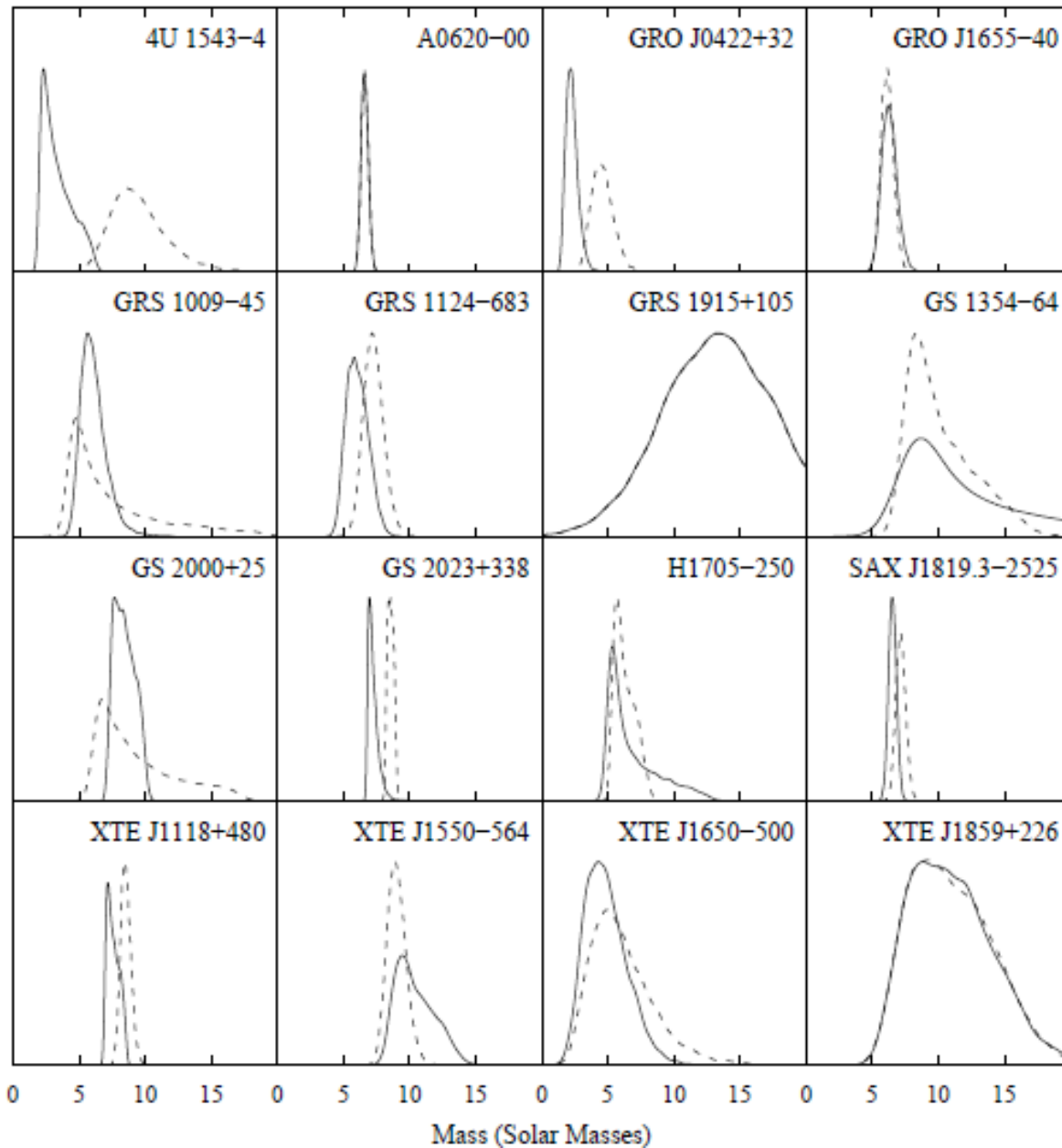
¹ Department of Astronomy, Yale University, New Haven, CT 06520, USA

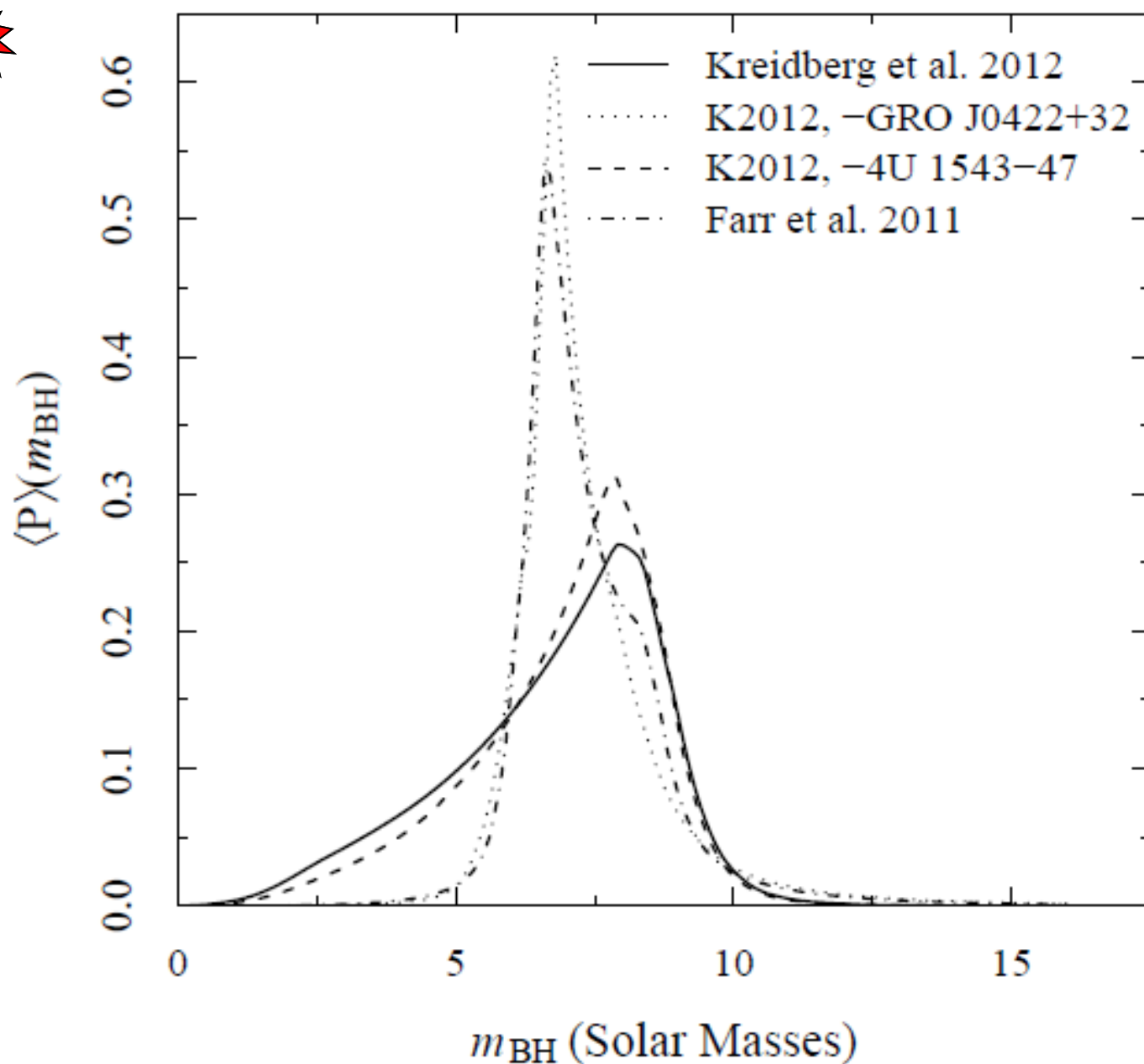
IS THERE A MASS GAP?



Kreidberg et al. 2012

No	Name	$M_{\text{comp}} [M_{\odot}]^{\text{b}}$	$M_{\text{BH}} [M_{\odot}]$
1	XTEJ1118+480	0.22 ± 0.07	$6.9 \div 8.2$
2	XTEJ1550-564	0.3 ± 0.07	10.5 ± 1.0
3	GS2000+25	$0.16 \div 0.47(0.315)$	~ 6.55
4	GROJ0422+32	~ 0.45	~ 10.4
5	GRS1009-45 (Nova Vel 1993)	~ 0.5	~ 8.5
6	GROJ1716-249 (Nova Oph 1993)	$\sim 0.5^{\text{c}}$	$\gtrsim 4.9$
7	GX339-4	$0.3 \div 1.1(0.54)$	> 7
8	H1705-25 (Nova Oph 1977)	$0.15 \div 1.0$	$4.9 \div 7.9$
9	A0620-00 (V616 Mon)	0.68 ± 0.18	9.2 ± 1.9
10	XTEJ1650-50(0)	0.7^{c}	~ 5.1
11	XTEJ1859+226	0.7^{c}	7.7 ± 1.3
12	GS2023+338 (V404 Cyg)	$0.5 \div 1.0(0.7)$	> 6.08
13	GRS 1124-68 (Nova Mus)	$0.3 \div 2.5(0.8)$	6.95 ± 0.6
14	GRS1915+105	0.8 ± 0.5	12.9 ± 2.4
15	GS 1354-64 (BW Cir)	1.03^{c}	7.6 ± 0.7
16	GROJ1655-40	1.45 ± 0.35	6.3 ± 0.5
17	4U1543-47	$2.3 \div 2.6(2.45)$	$2.7 \div 7.5$
18	XTEJ1819-254 (V4641 Sgr)	$5.49 \div 8.14(6.81)$	$8.73 \div 11.70$
19	CygX-1 persistent ^a	19.2 ± 1.9	14.8 ± 0.1





- The first study of the mass distribution of stellar-mass BHs, in **Bailyn et al. (1998)**, examined a sample of seven low-mass X-ray binaries thought to contain a BH,
- concluding in a Bayesian analysis that the **mass function was strongly peaked around 7Θ** .



Ozel et al, 2010

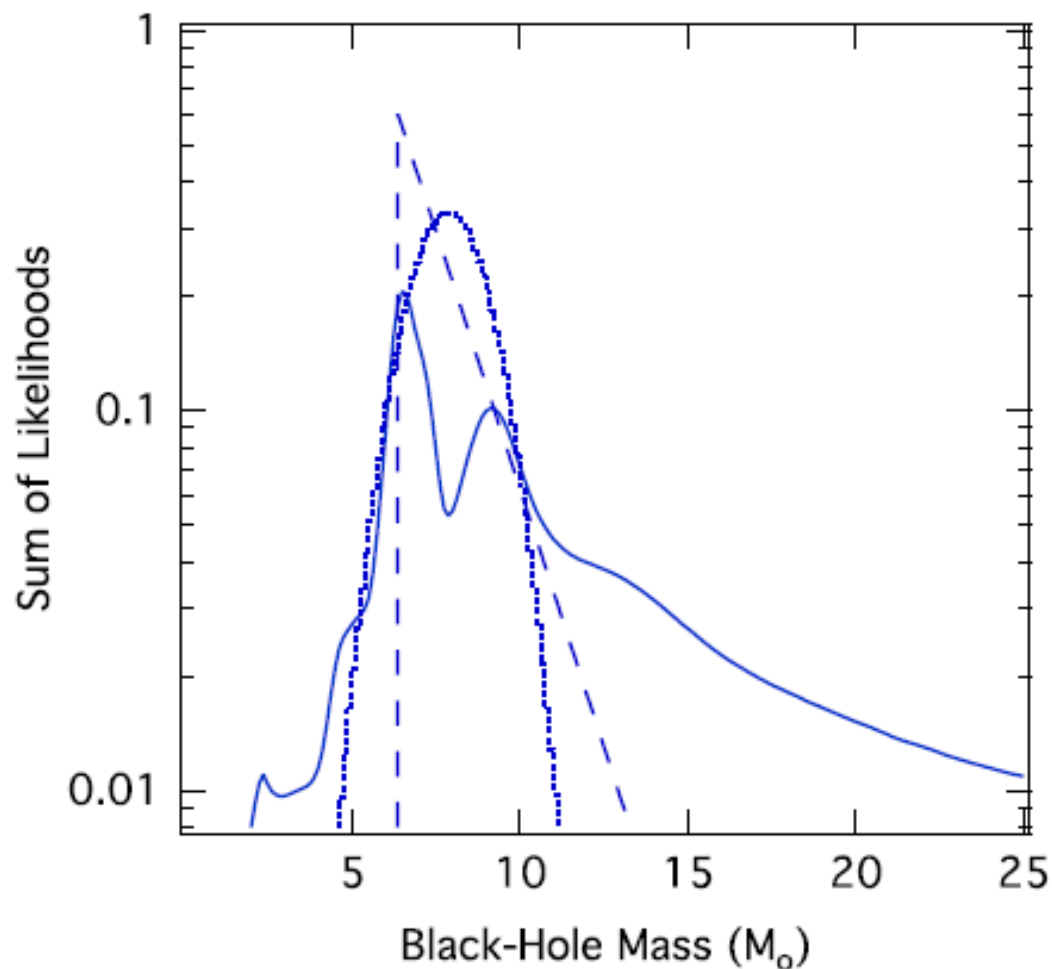


Figure 2. Solid line shows the sum of likelihoods for the mass measurements of the 16 black holes in low-mass X-ray binaries. Note that because of the high-mass wings of the individual likelihoods, the shape of their sum is artificial at the high-mass end. The dashed and dotted lines show the exponential and Gaussian distributions, respectively, with parameters that best fit the data (see Section 4).

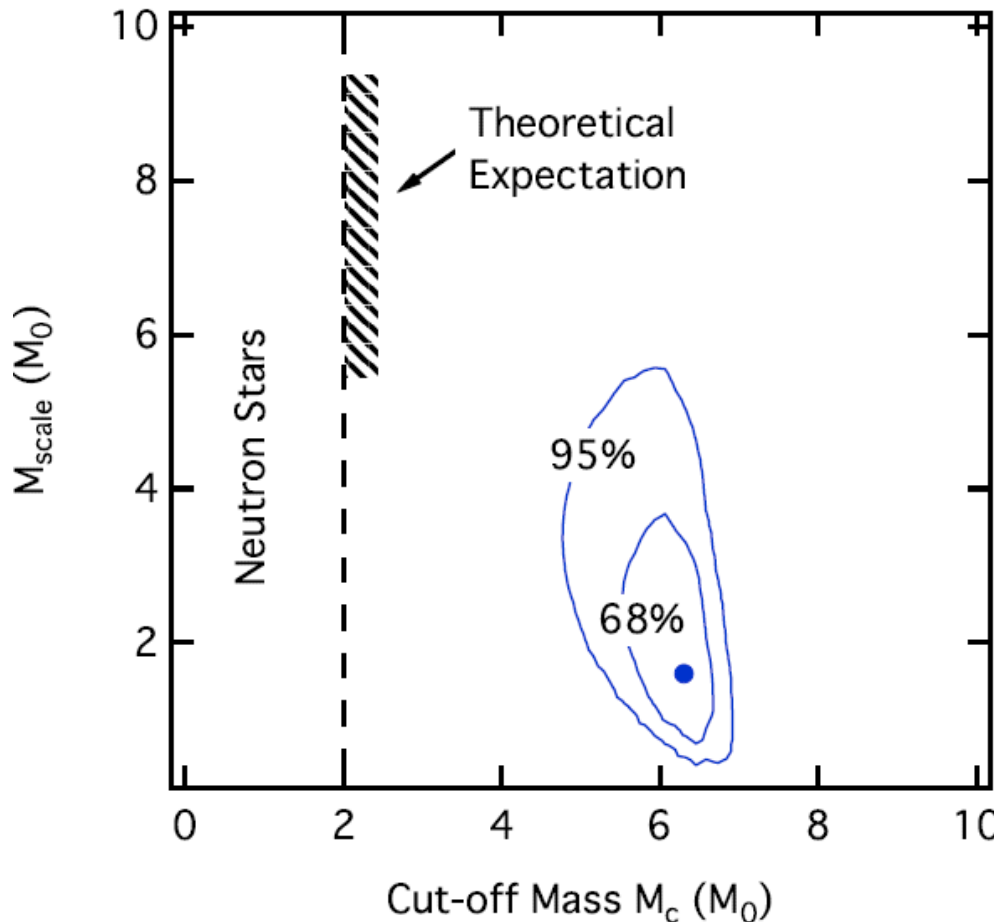


Figure 3. Parameters of an exponential black hole mass distribution with a low-mass cutoff. The cutoff mass is well above theoretical expectations, indicating a sizable gap between neutron-star and black hole masses. Furthermore, the mass scale in the exponential is significantly smaller than theoretical expectations.

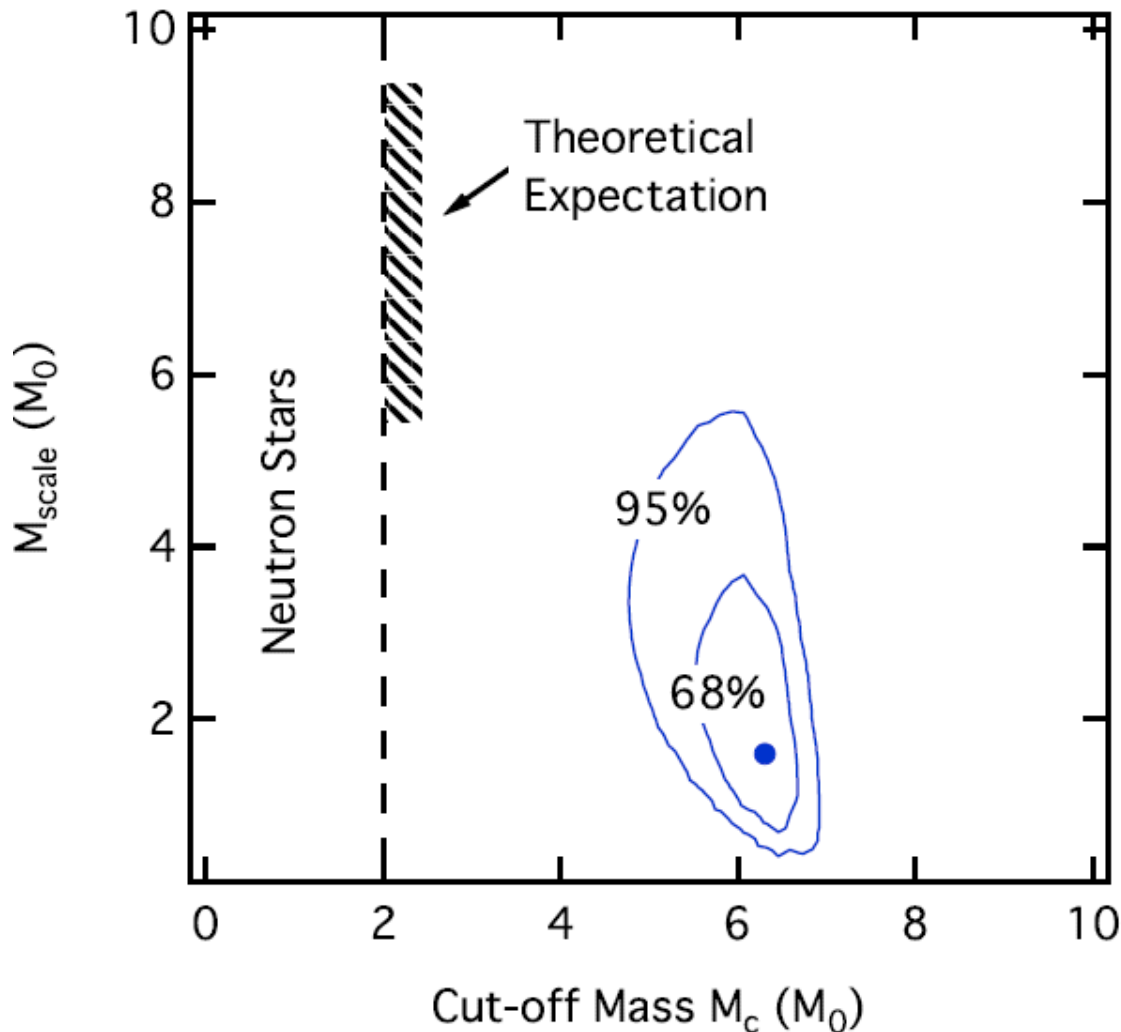


Table 1
The Source Parameters for the 20 X-ray Binaries Used in This Work

Source	$f(M_\odot)$	q	i (deg)	References
GRS 1915	$N(9.5, 3.0)$	$N(0.0857, 0.0284)$	$N(70, 2)$	Greiner et al. (2001)
XTE J1118	$N(6.44, 0.08)$	$N(0.0264, 0.004)$	$N(68, 2)$	Gelino et al. (2008)
XTE J1650	$N(2.73, 0.56)$	$U(0, 0.5)$	$I(50, 80)$	Harlaftis & Filippenko (2005)
GRS 1009	$N(3.17, 0.12)$	$N(0.137, 0.015)$	$I(37, 80)$	Filippenko et al. (1999)
A0620	$N(2.76, 0.036)$	$N(0.06, 0.004)$	$N(50.98, 0.87)$	Cantrell et al. (2010)
				Neilsen et al. (2008)
GRO J0422	$N(1.13, 0.09)$	$U(0.076, 0.31)$	$N(45, 2)$	Gelino & Harrison (2003)
Nova Mus 1991	$N(3.01, 0.15)$	$N(0.128, 0.04)$	$N(54, 1.5)$	Gelino et al. (2001)
GRO J1655	$N(2.73, 0.09)$	$N(0.3663, 0.04025)$	$N(70.2, 1.9)$	Greene et al. (2001)
4U 1543	$N(0.25, 0.01)$	$U(0.25, 0.31)$	$N(20.7, 1.5)$	Orosz (2003)
XTE J1550	$N(7.73, 0.4)$	$U(0, 0.04)$	$N(74.7, 3.8)$	Orosz et al. (2011)
V4641 Sgr	$N(3.13, 0.13)$	$U(0.42, 0.45)$	$N(75, 2)$	Orosz (2003)
GS 2023	$N(6.08, 0.06)$	$U(0.056, 0.063)$	$I(66, 70)$	Charles & Coe (2006)
				Khargharia et al. (2010)
GS 1354	$N(5.73, 0.29)$	$N(0.12, 0.04)$	$I(50, 80)$	Casares et al. (2009)
Nova Oph 77	$N(4.86, 0.13)$	$U(0, 0.053)$	$I(60, 80)$	Charles & Coe (2006)
GS 2000	$N(5.01, 0.12)$	$U(0.035, 0.053)$	$I(43, 74)$	Charles & Coe (2006)
Cyg X1	$N(0.251, 0.007)$	$N(2.778, 0.386)$	$I(23, 38)$	Gies et al. (2003)
M33 X7	$N(0.46, 0.08)$	$N(4.47, 0.61)$	$N(74.6, 1)$	Orosz et al. (2007)
NGC 300 X1	$N(2.6, 0.3)$	$U(1.05, 1.65)$	$I(60, 75)$	Crowther et al. (2010)
LMC X1	$N(0.148, 0.004)$	$N(2.91, 0.49)$	$N(36.38, 2.02)$	Orosz et al. (2009)
IC 10 X1	$N(7.64, 1.26)$	$U(0.7, 1.7)$	$I(75, 90)$	Prestwich et al. (2007)
				Silverman & Filippenko (2008)

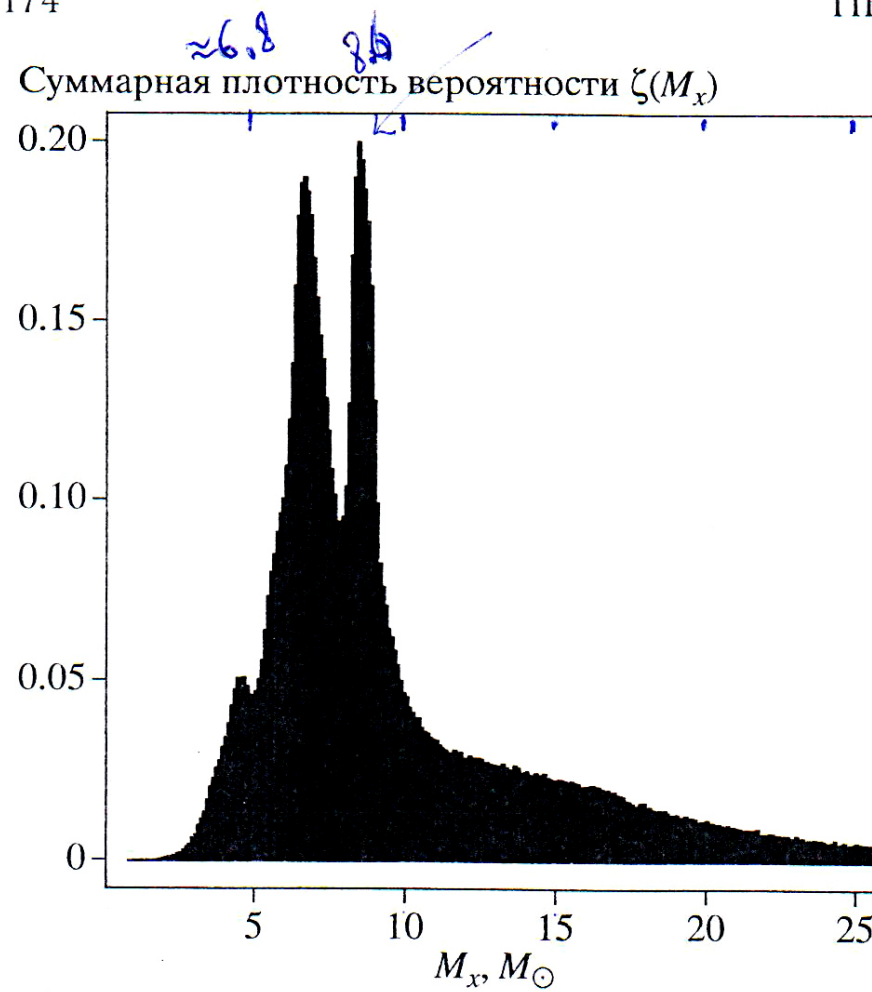


Рис. 6. Суммарная плотность вероятности $\zeta(M_x)$ распределения масс компактных объектов M_x в 20 рентгеновских двойных системах (табл. 1).

Ozel et al, 2010

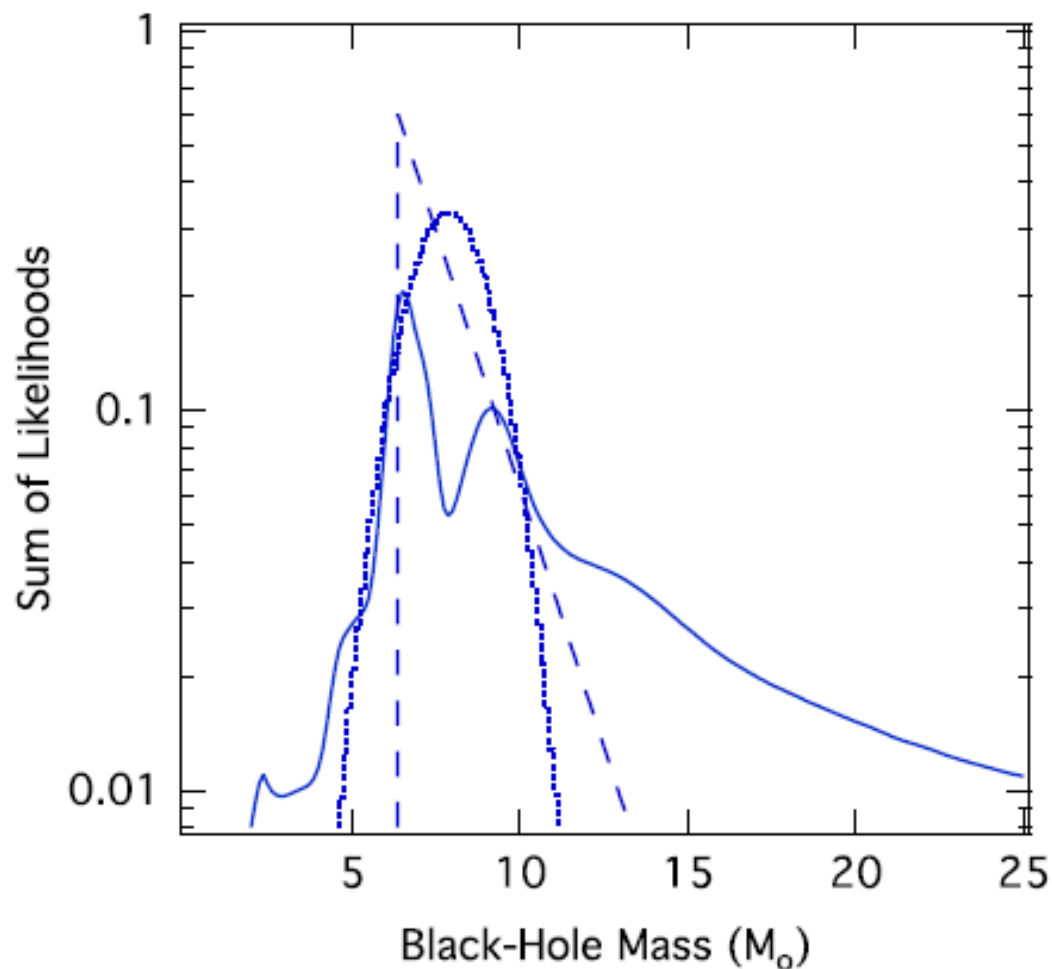
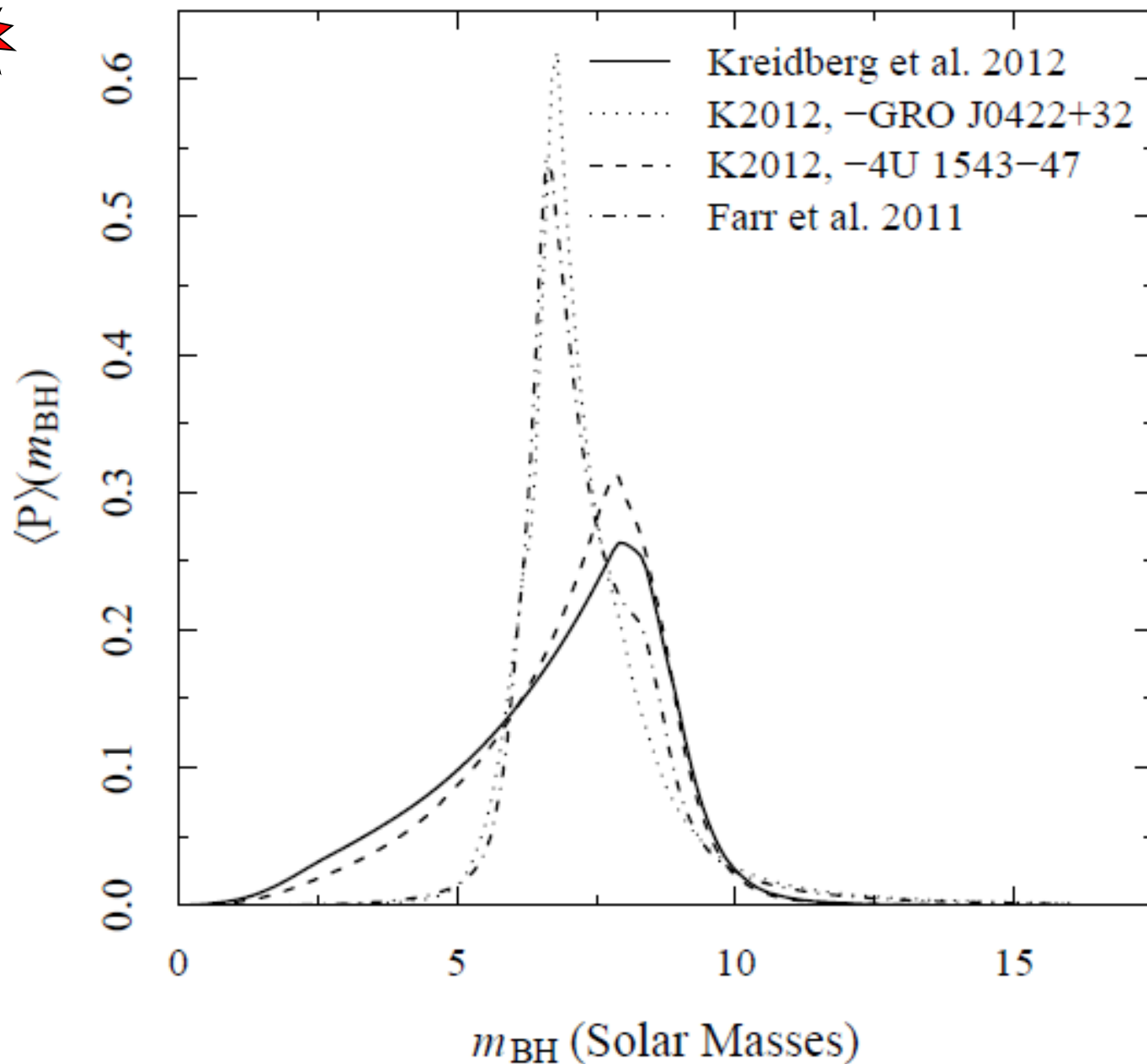
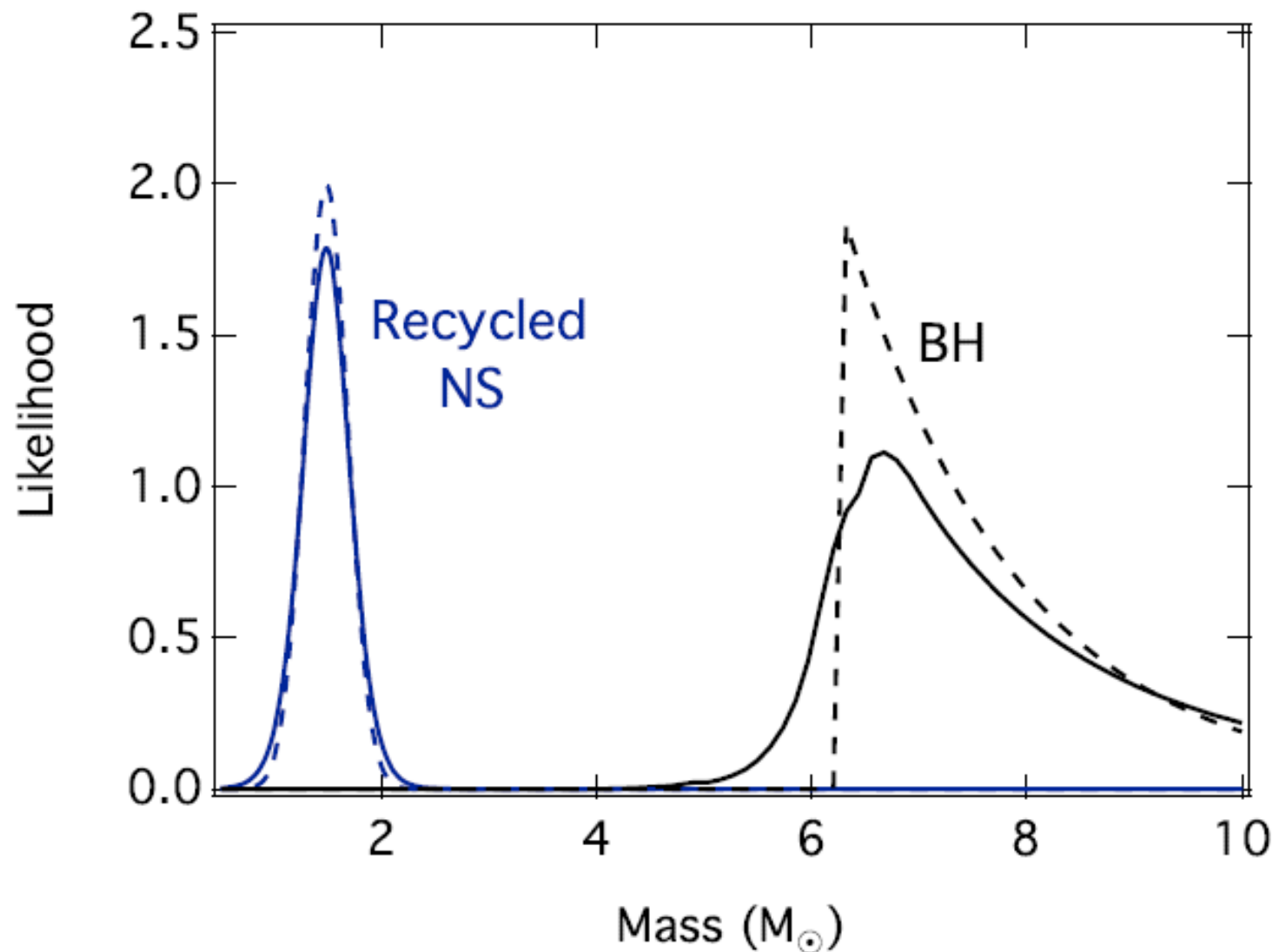


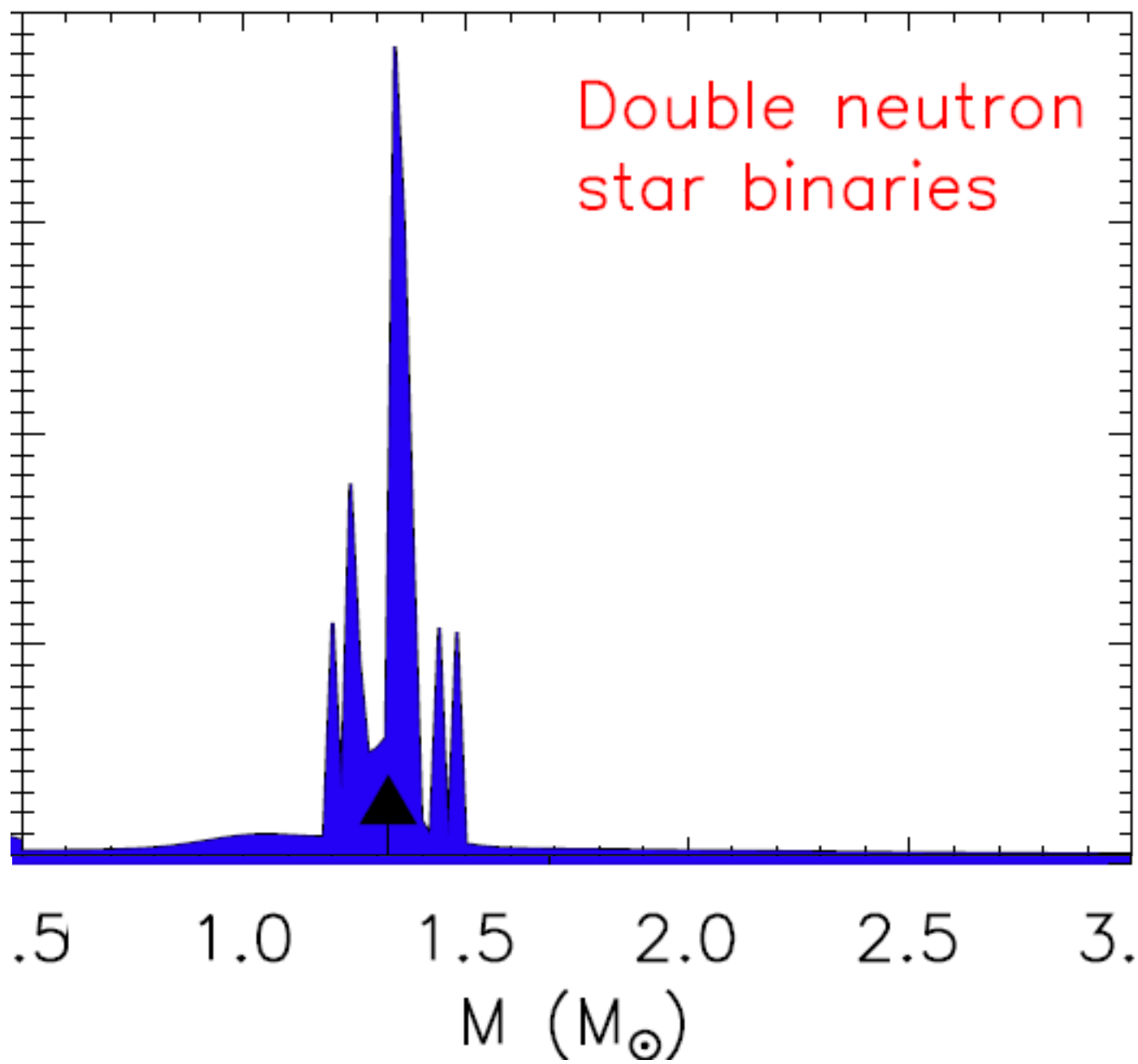
Figure 2. Solid line shows the sum of likelihoods for the mass measurements of the 16 black holes in low-mass X-ray binaries. Note that because of the high-mass wings of the individual likelihoods, the shape of their sum is artificial at the high-mass end. The dashed and dotted lines show the exponential and Gaussian distributions, respectively, with parameters that best fit the data (see Section 4).





2.

*Пики в распределении масс
нейтронных зезд...*



ON THE MASS DISTRIBUTION AND BIRTH MASSES OF NEUTRON STARS

FERYAL ÖZEL¹, DIMITRIOS PSALTIS¹, RAMESH NARAYAN², ANTONIO SANTOS VILLARREAL¹

¹Department of Astronomy, University of Arizona, 933 N. Cherry Ave., Tucson, AZ 85721 and

² Harvard-Smithsonian Center for Astrophysics, 60 Garden St., Cambridge, MA 02138

Draft version September 10, 2012



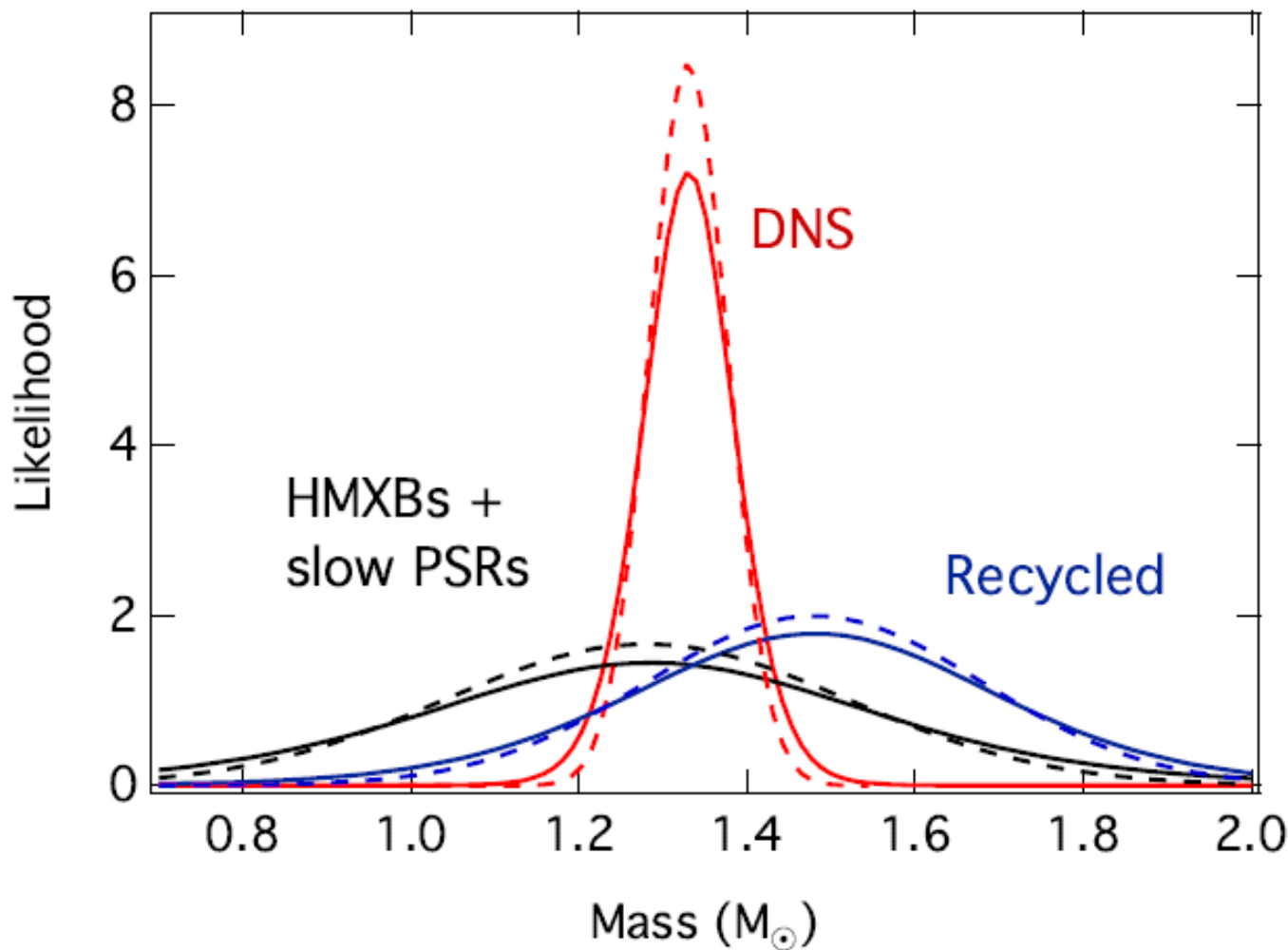
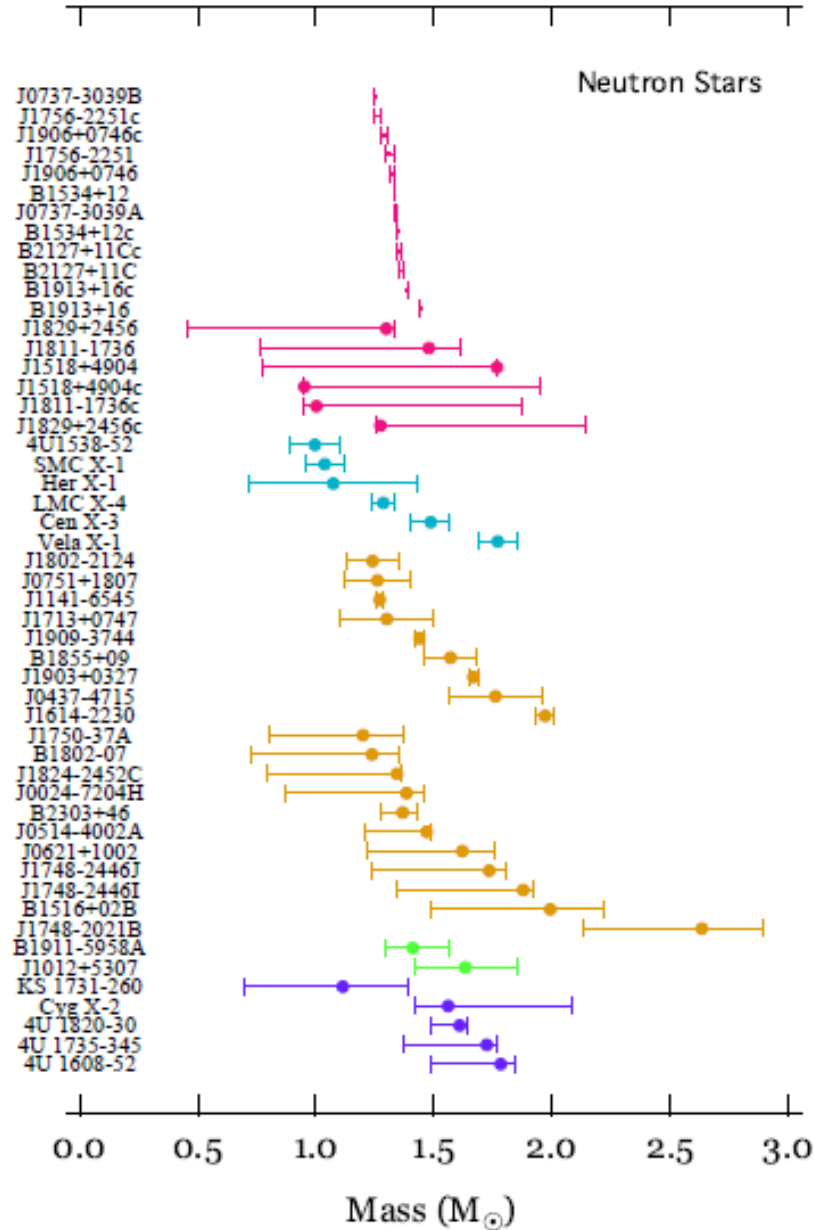
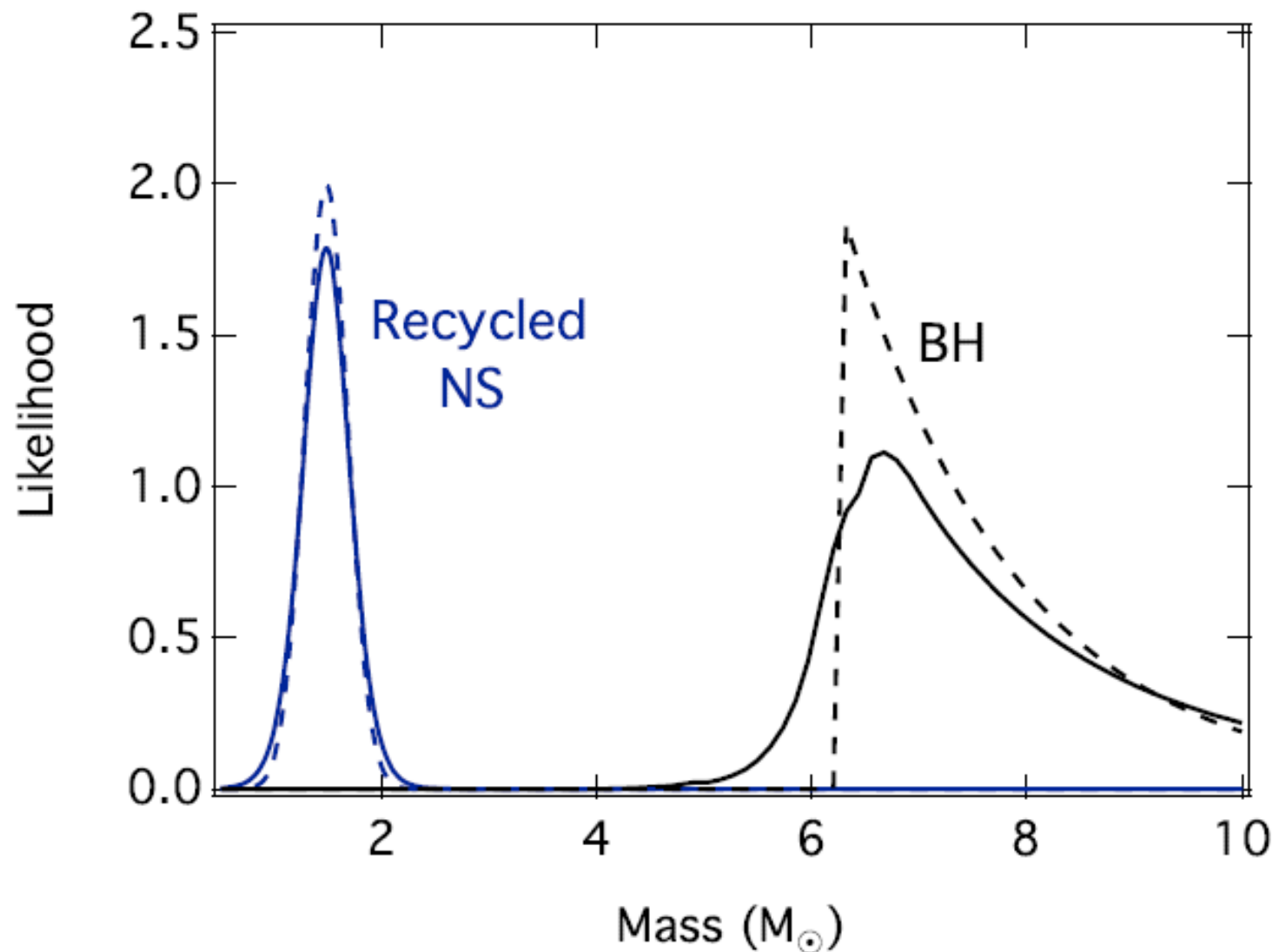
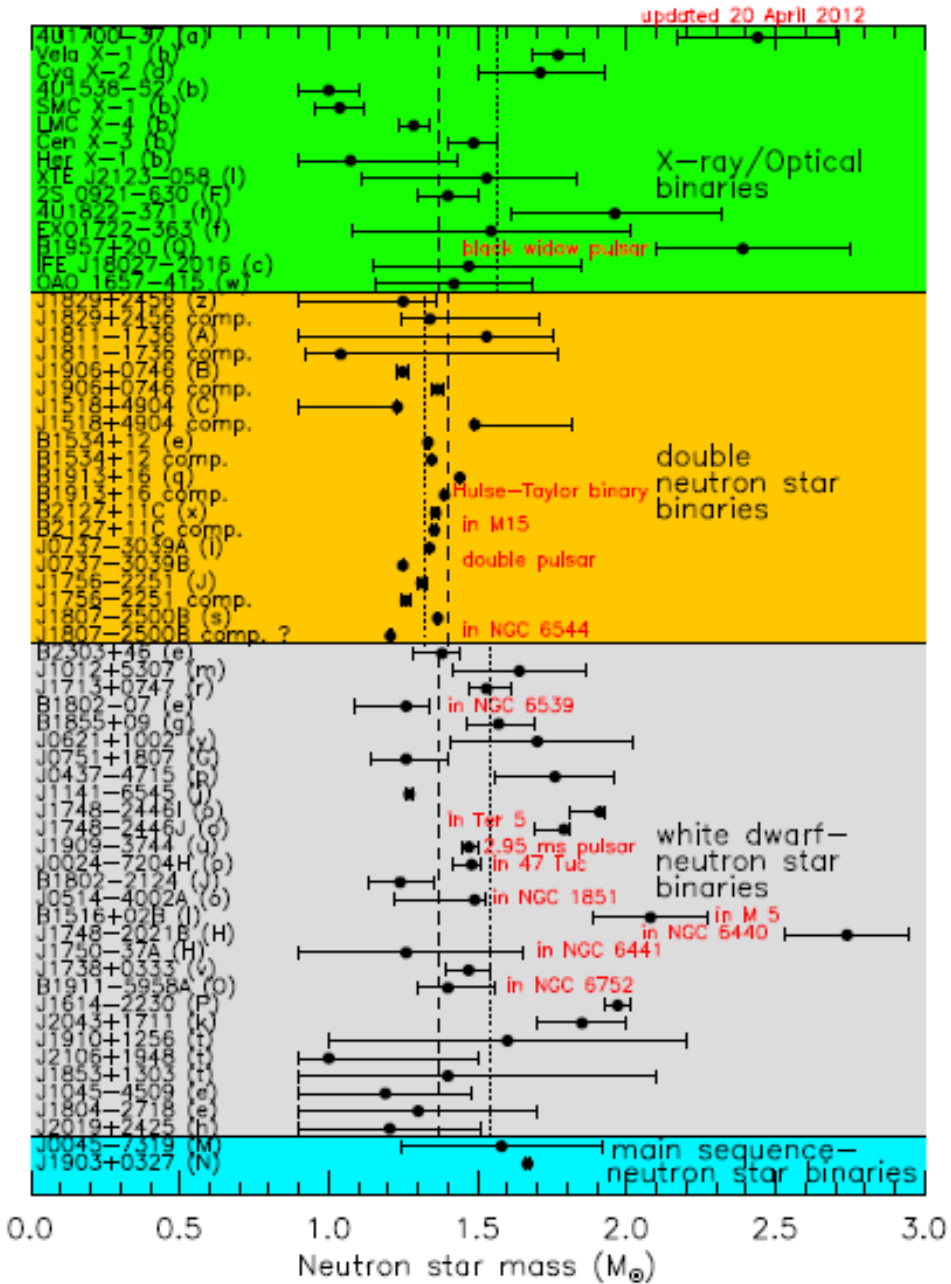
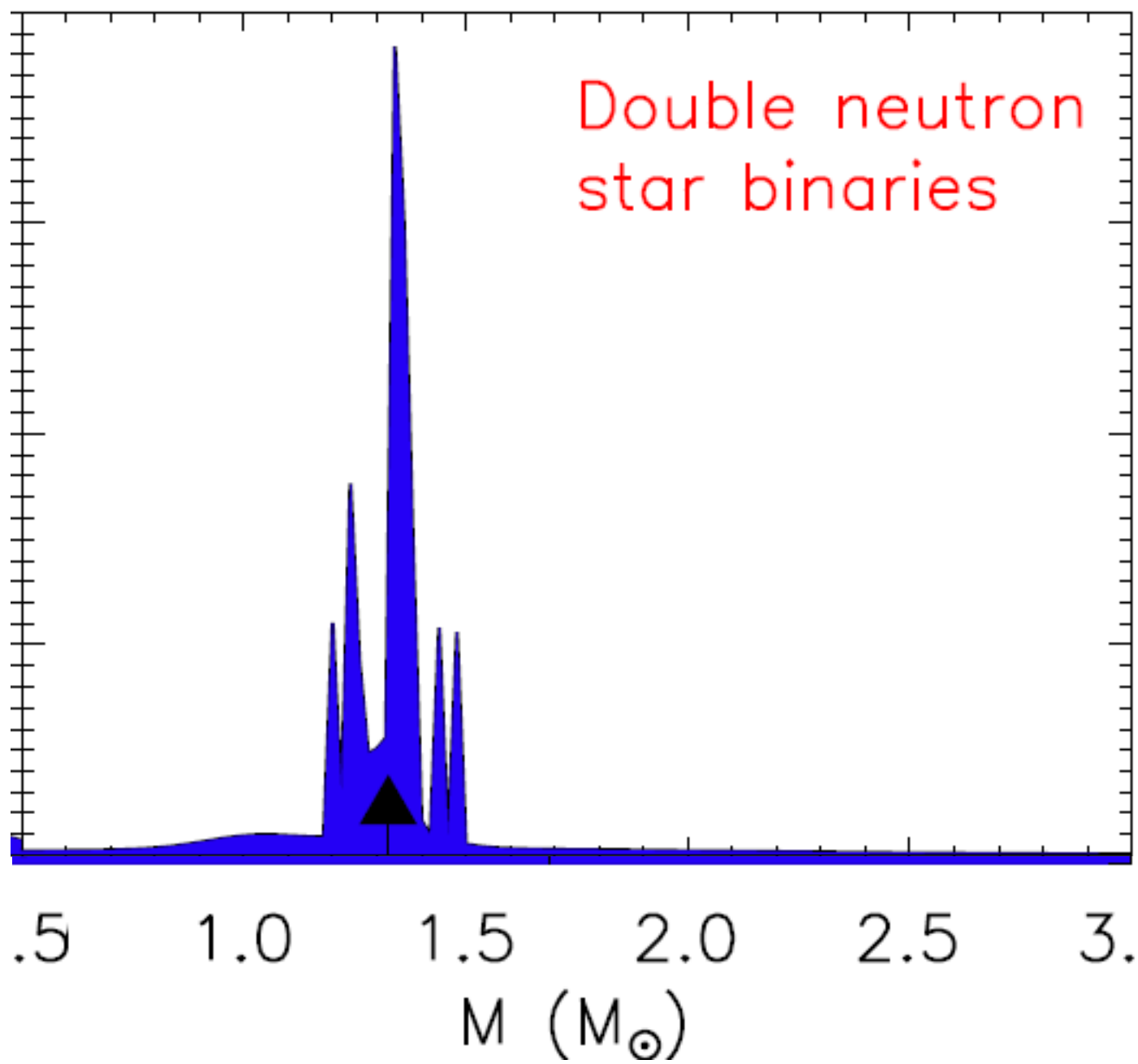


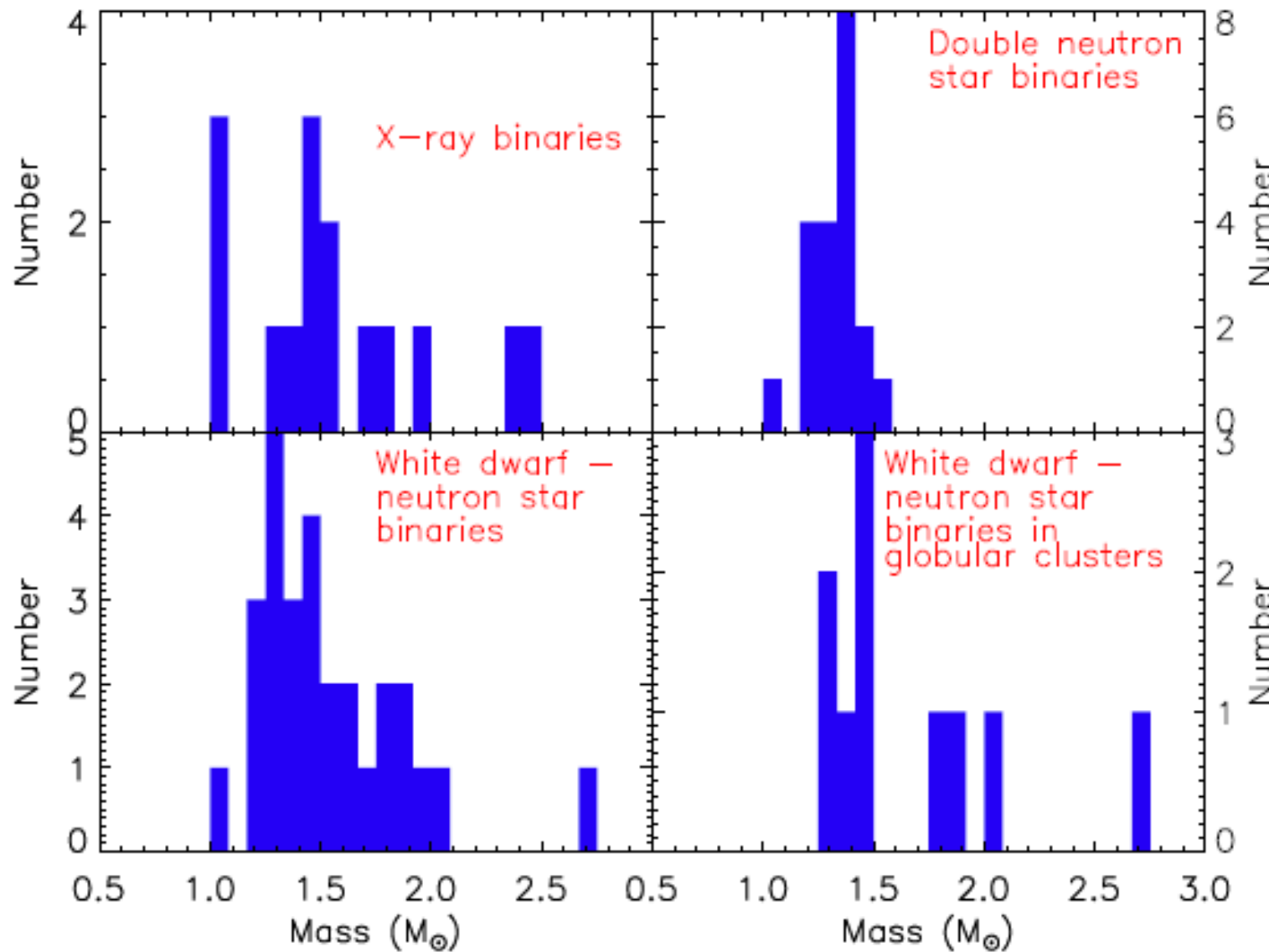
Fig. 15.— The inferred mass distributions for the different populations of NSs. The dashed lines correspond to the most likely values of the parameters. For the different NS populations these are: $M_0 = 1.33M_\odot$ and $\sigma = 0.05M_\odot$ for the double NSs (DNS), $M_0 = 1.28M_\odot$ and $\sigma = 0.24M_\odot$ for the other NSs near their birth masses, and $M_0 = 1.48M_\odot$ and $\sigma = 0.20M_\odot$ for the recycled NSs.

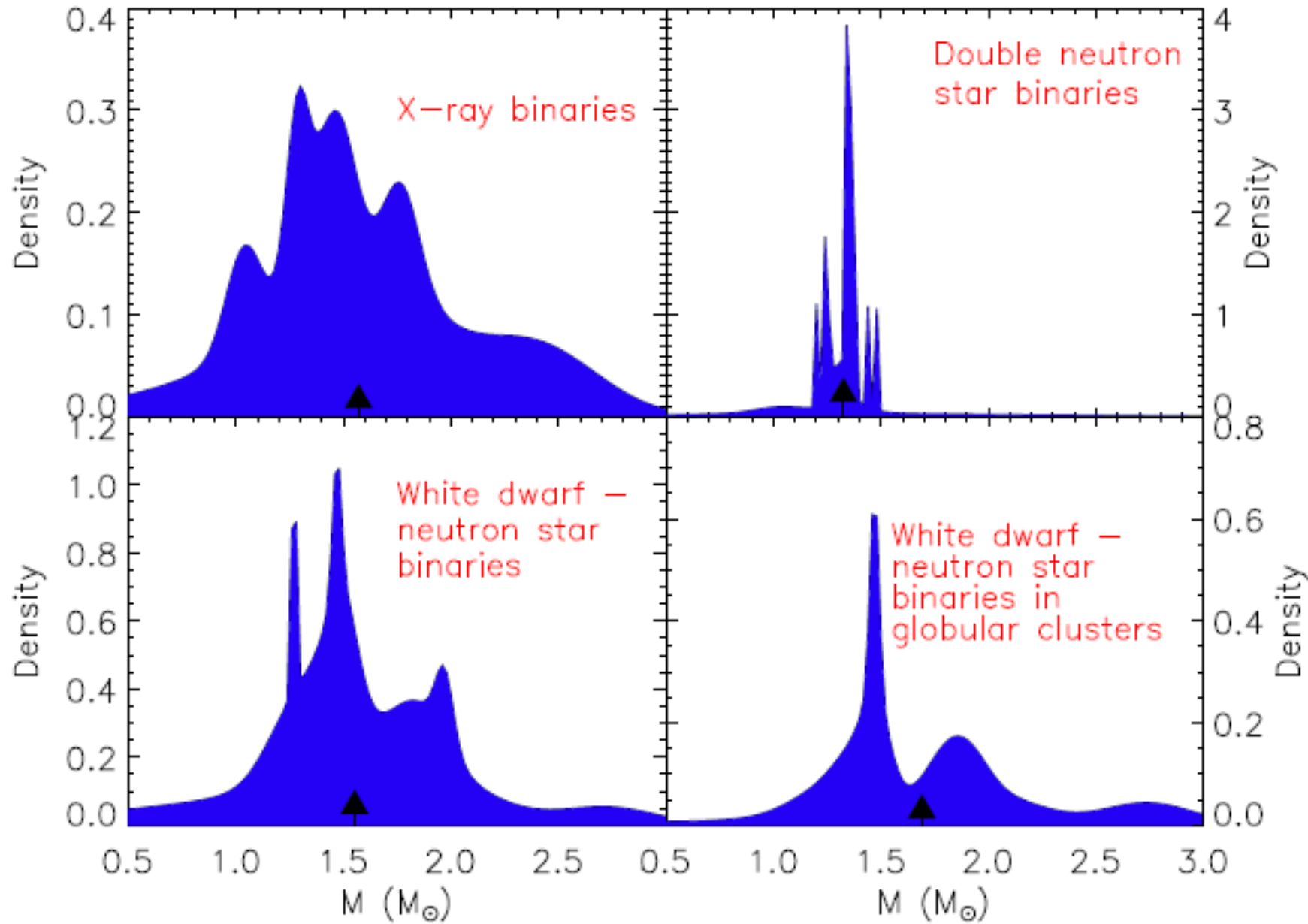








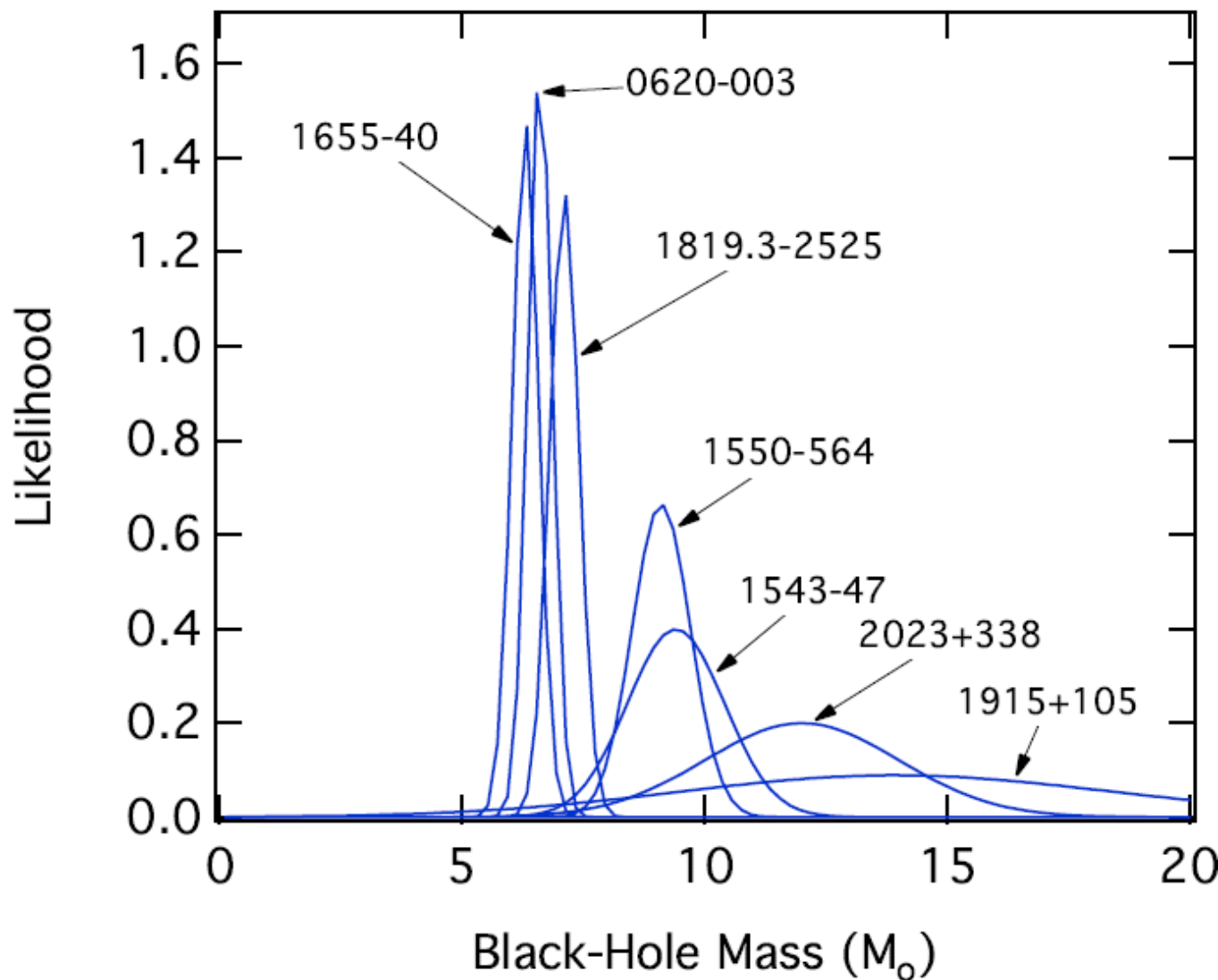




- [arXiv:1305.3510v1](https://arxiv.org/abs/1305.3510v1),
- статья в Annu. Rev. Nucl. Part. Sci. 62, 485 (2012) : The Nuclear **Equation of State** and **Neutron Star Masses**, [James M. Lattimer](#)



Ozel et al., 1006.2834



Ozel et al, 2010

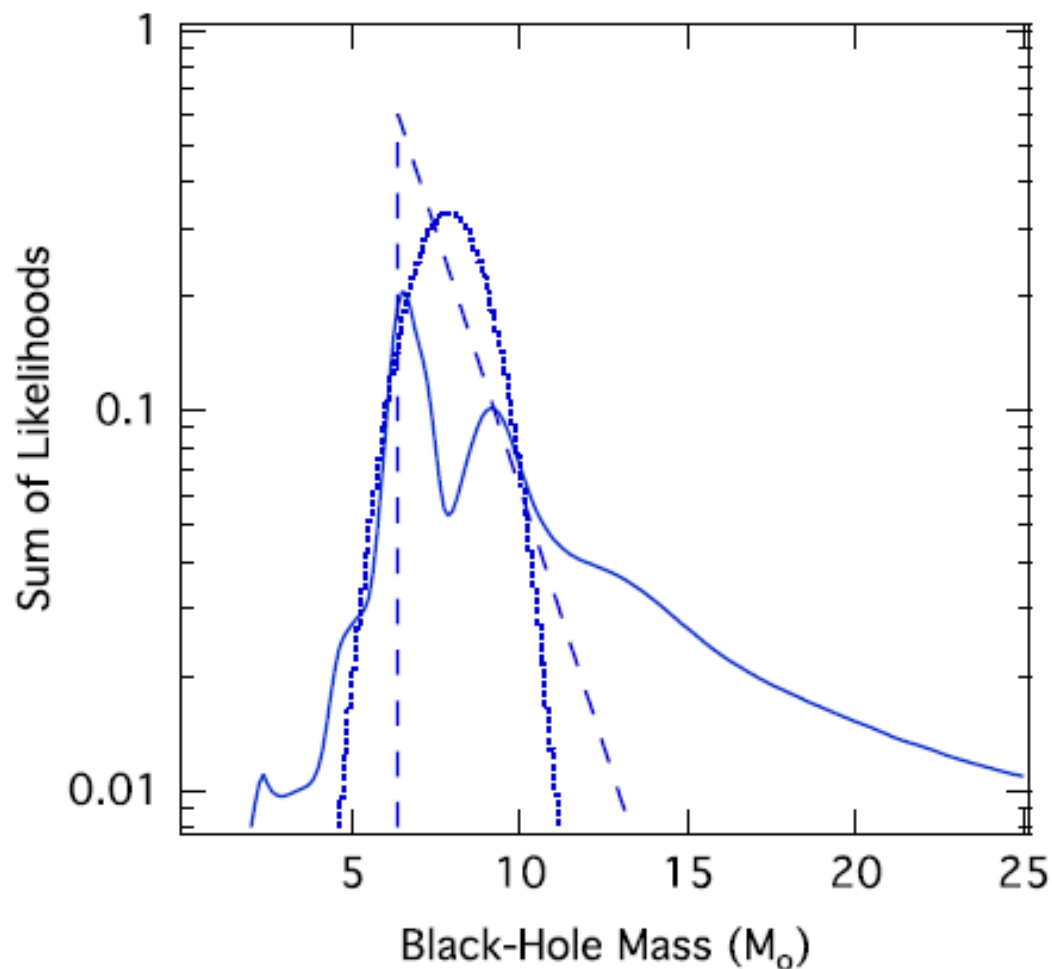
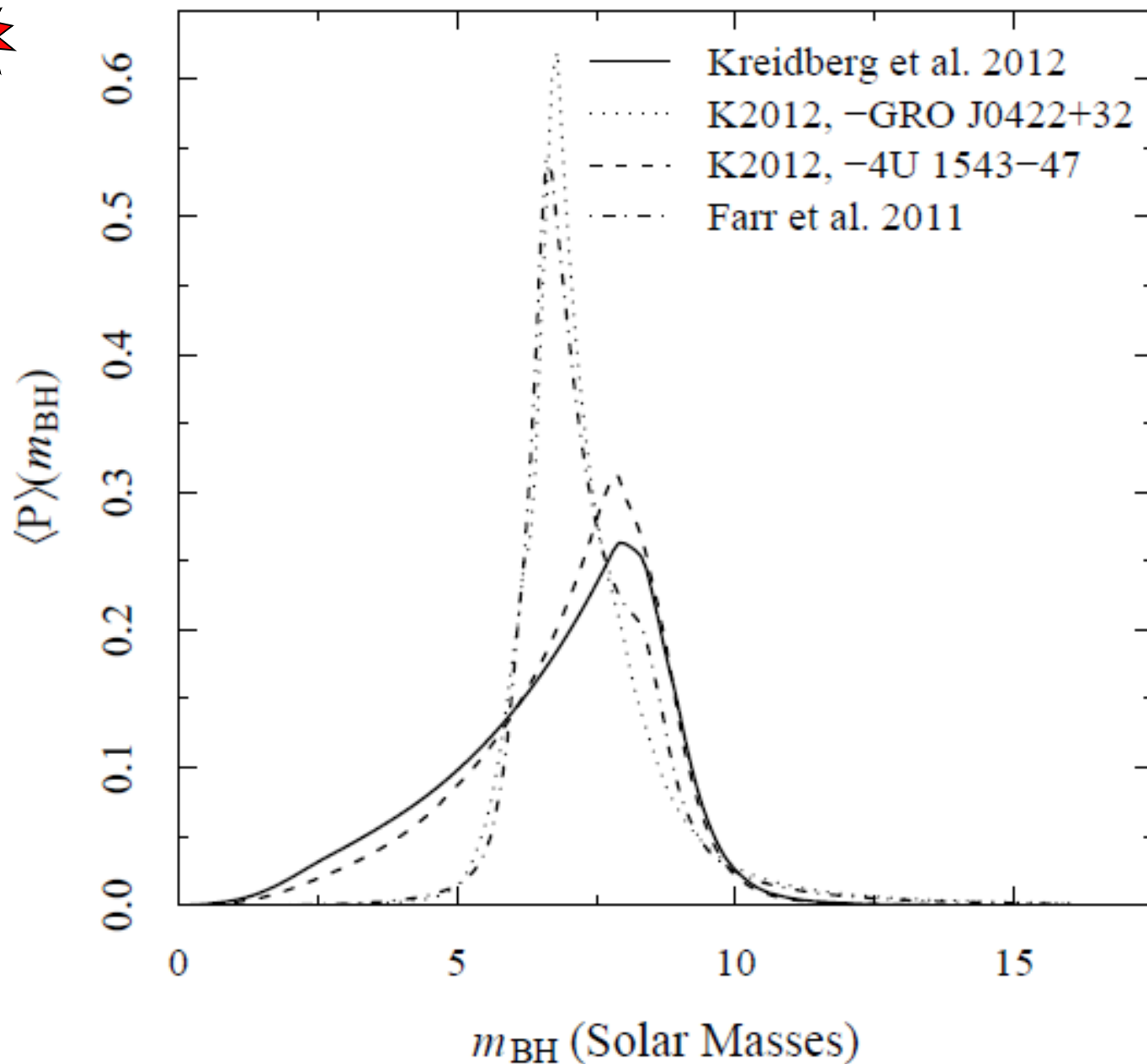


Figure 2. Solid line shows the sum of likelihoods for the mass measurements of the 16 black holes in low-mass X-ray binaries. Note that because of the high-mass wings of the individual likelihoods, the shape of their sum is artificial at the high-mass end. The dashed and dotted lines show the exponential and Gaussian distributions, respectively, with parameters that best fit the data (see Section 4).



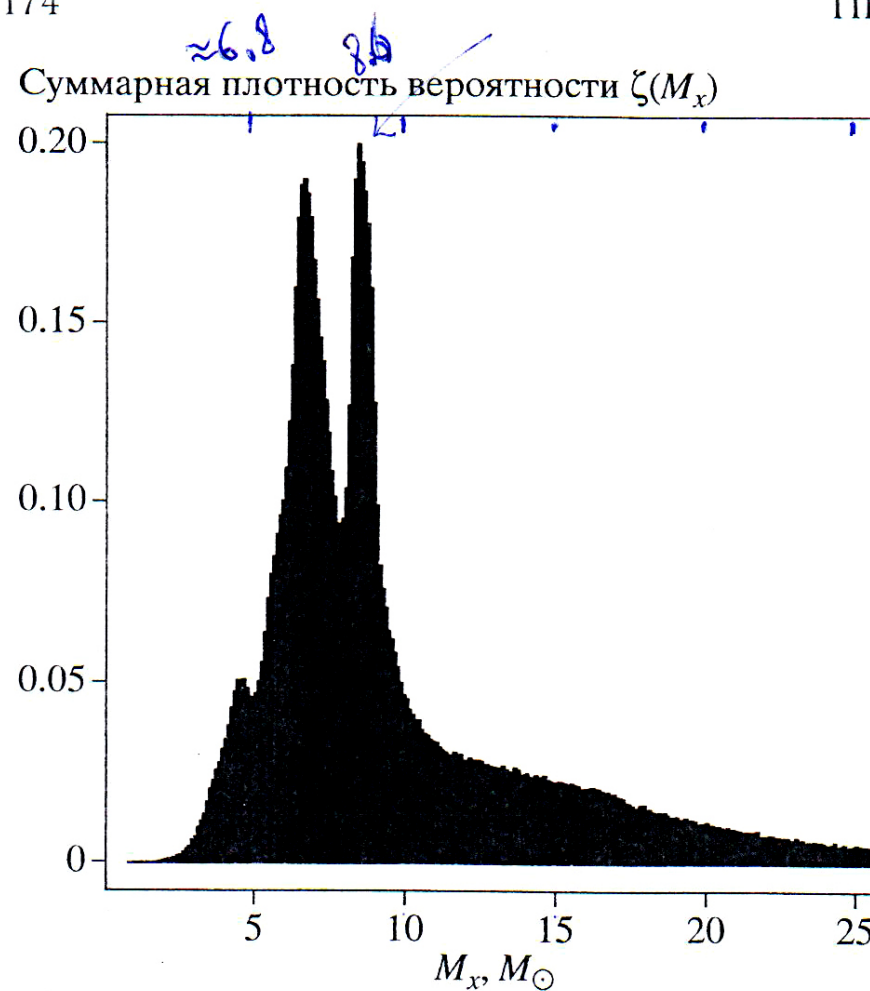
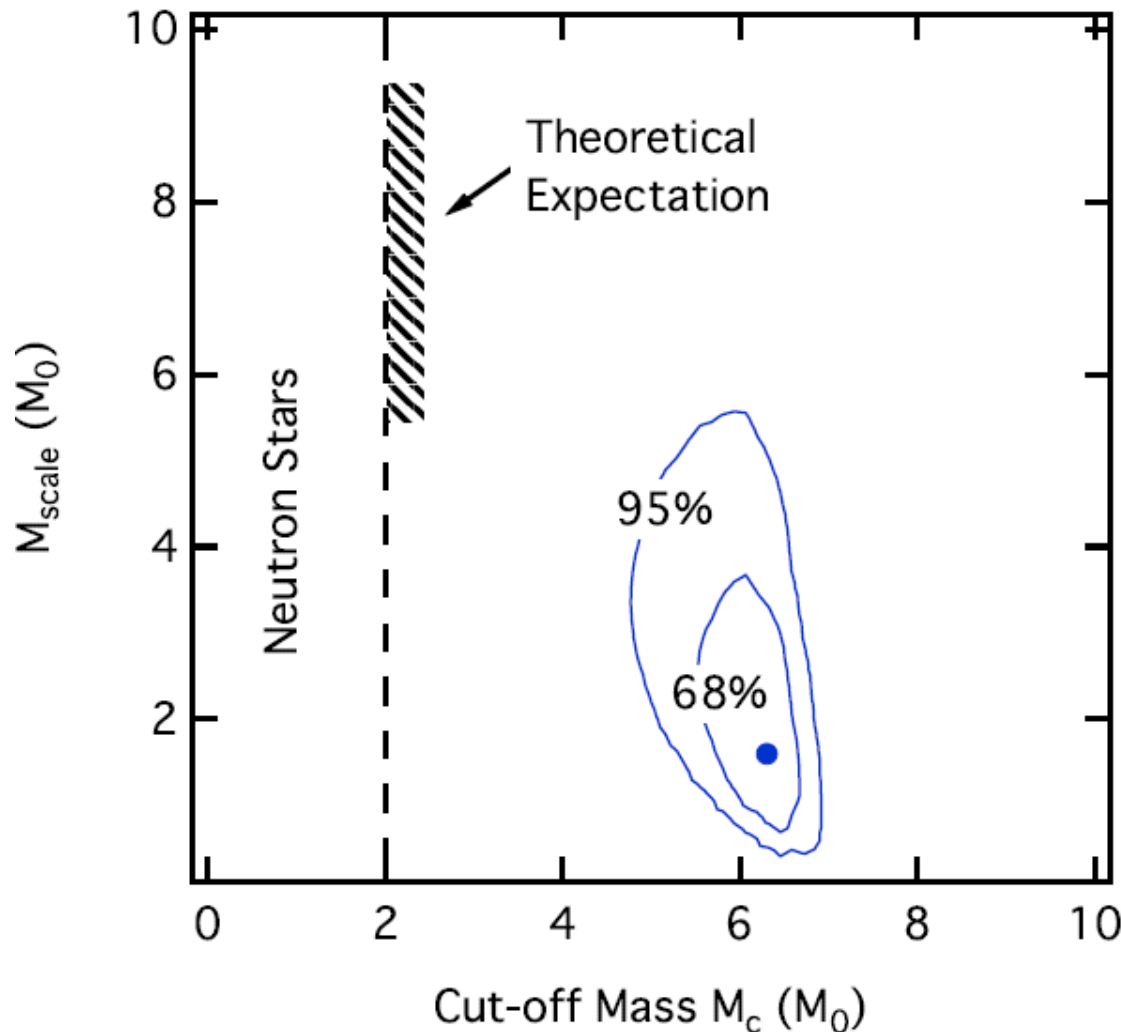
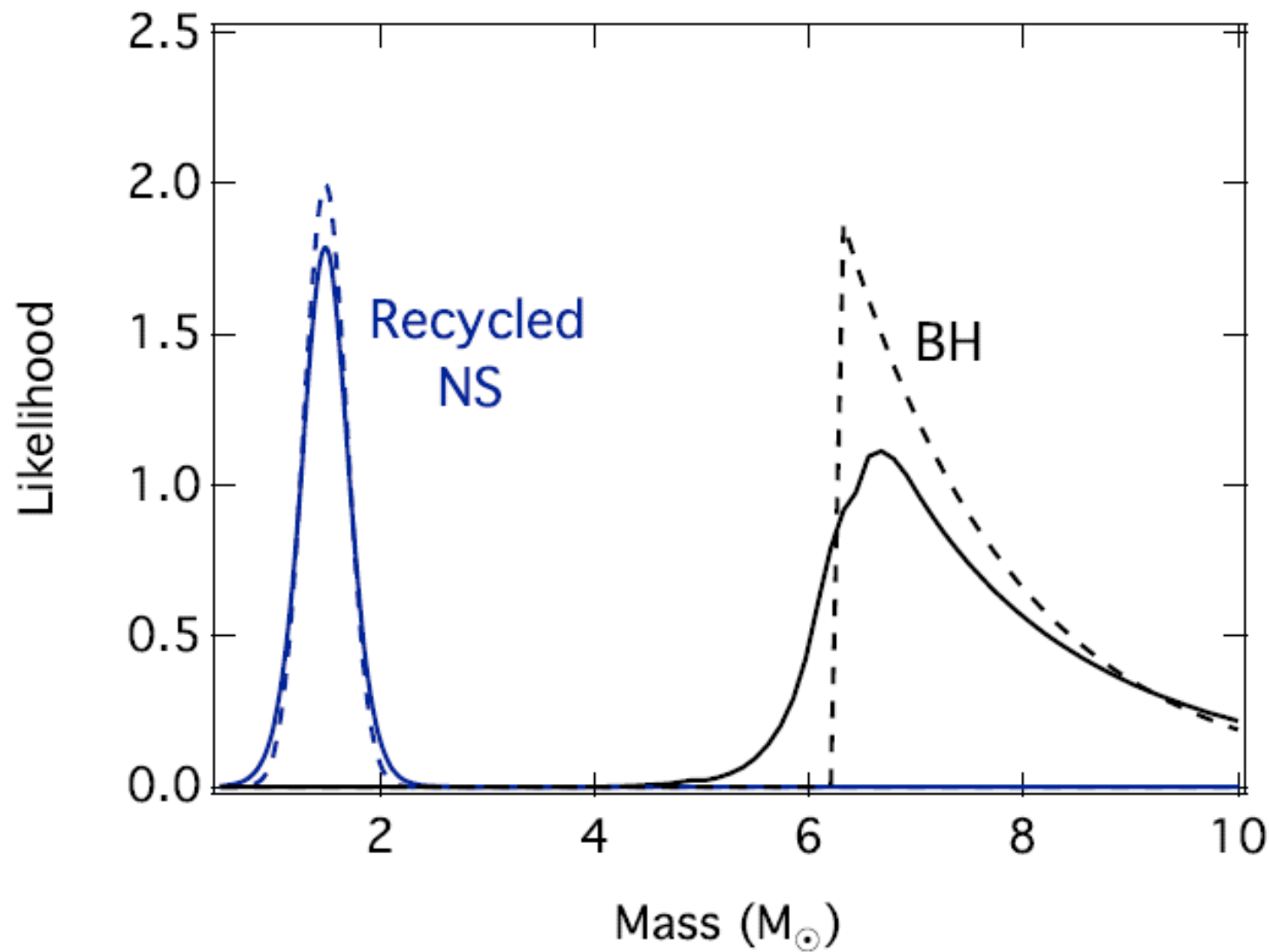


Рис. 6. Суммарная плотность вероятности $\zeta(M_x)$ распределения масс компактных объектов M_x в 20 рентгеновских двойных системах (табл. 1).





3.

Проблема максимальной массы NS, предельно жесткое уравнение состояния и кварковые звезды (QSs)

On the Maximum Mass of Neutron Stars -

см. обзор 1307.3995

	BHF (N)	BHF (NH)	DBHF (N)	VCS (N)	pQCD (NQ)	RMF (N)	RMF/NJL (NQ)	RMF/MBM (NQ)
M_{\max}/M_{\odot}	2.0-2.5	1.3-1.6	2.0-2.5	2.0-2.2	2.0	2.1-2.8	2.0-2.3	2.0-2.2

EMMI Rapid Reaction Task Force Meeting on “Quark Matter in Compact Star”

A task force meeting was held from October 7-10, 2013 at the Frankfurt Institute for Advanced Studies to address the presence of quark matter in these massive stars.

The recent measurement of 20 pulsars has initiated an intense discussion on its impact on our understanding of the high-density matter in the cores of NSs.

During this meeting, the recent observational astrophysical data was reviewed.

The possibility of pure **quark** stars, **hybrid** stars and the nature of the **QCD phase transition** were discussed and their observational signals delineated. + **SNe & GRBs**



Уравнения состояния:

$$1) P = 1/3 \cdot \varepsilon, \quad M_{OV} < 2 M_\odot$$

$$2) P = \varepsilon, \quad ? \quad M_{OV} \approx 3.2 M_\odot$$

Пересмотр предела OV неизбежен, а также возможны другие наблюдательные следствия существования **кварковых звезд** в Природе

$$3) P = -\varepsilon, \quad \text{для Темной Энергии?}$$

($P = \varepsilon$, за это уравнение Л.Д.Ландау назвал его автора)



К докладу Д.Г. Яковлева «Странные звезды»

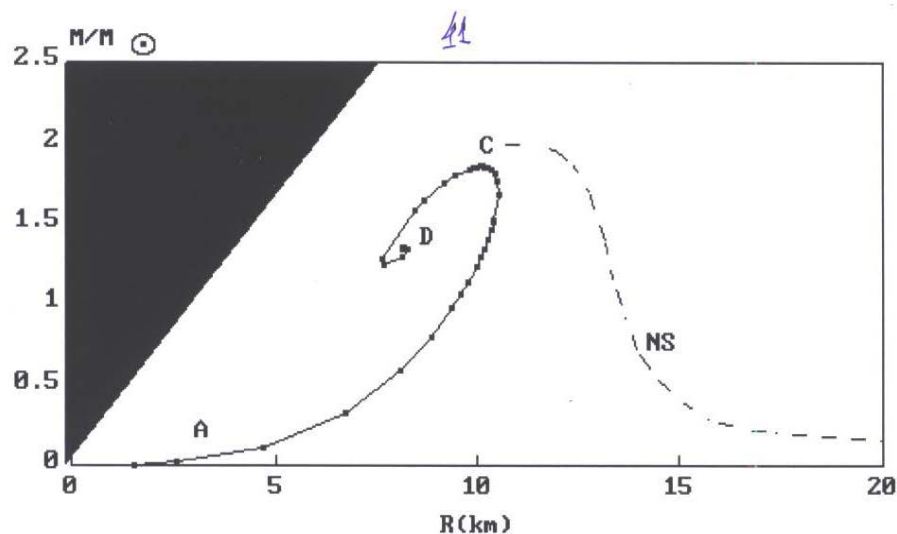


Рисунок 1: Зависимость масса - радиус для кварковых странных звезд с уравнением состояния (1). Прерывистой линией показана зависимость масса - радиус для нейтронных звезд, описываемых уравнением состояния Бете - Джонсона, в рамках Общей теории Относительности. Точка С соответствует пределу ОВ, точкой D отмечено положение предельно неоднородной кварковой конфигурации в ОТО. Заштрихована область, соответствующая черным дырам. $B = 67 \text{ MeV}/\text{fm}^3$.

$$\rho = \frac{1}{3} (\rho c^2 - 4B)$$

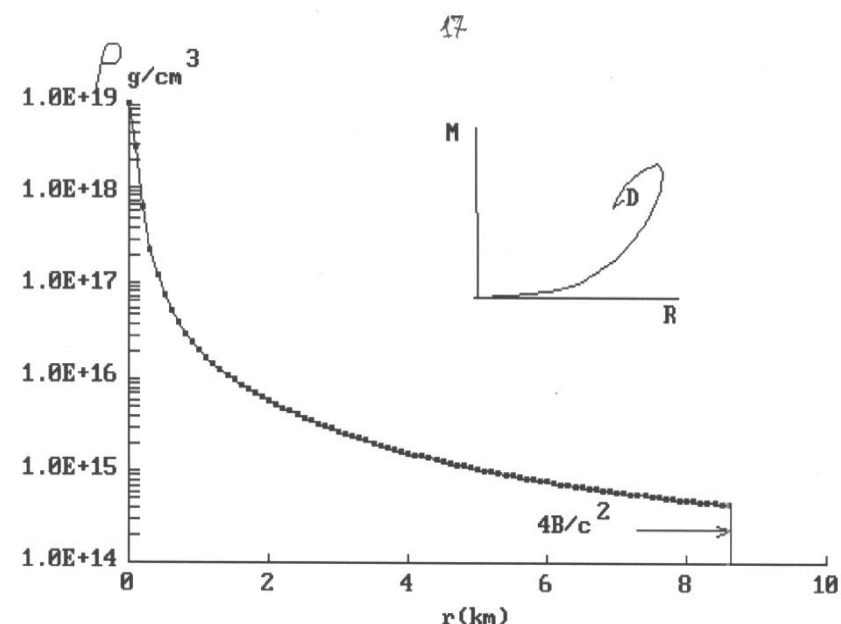
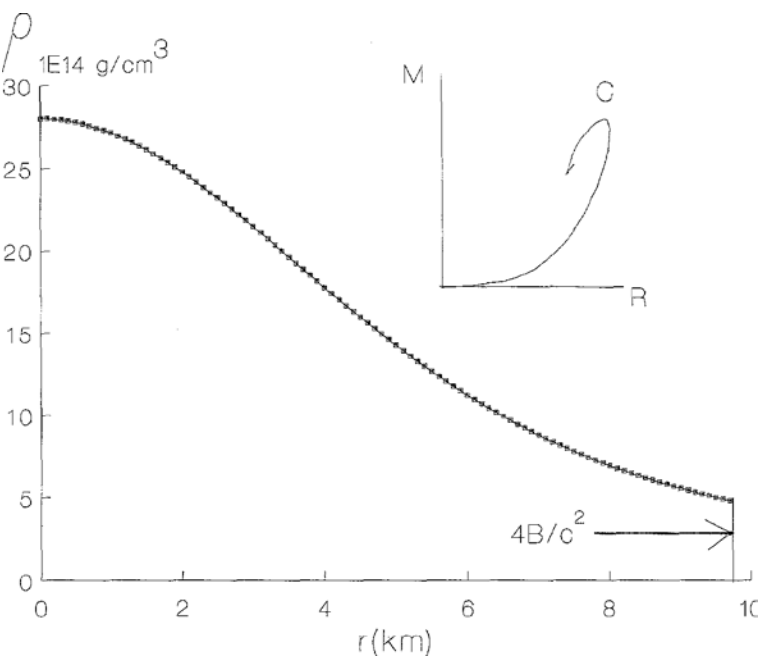
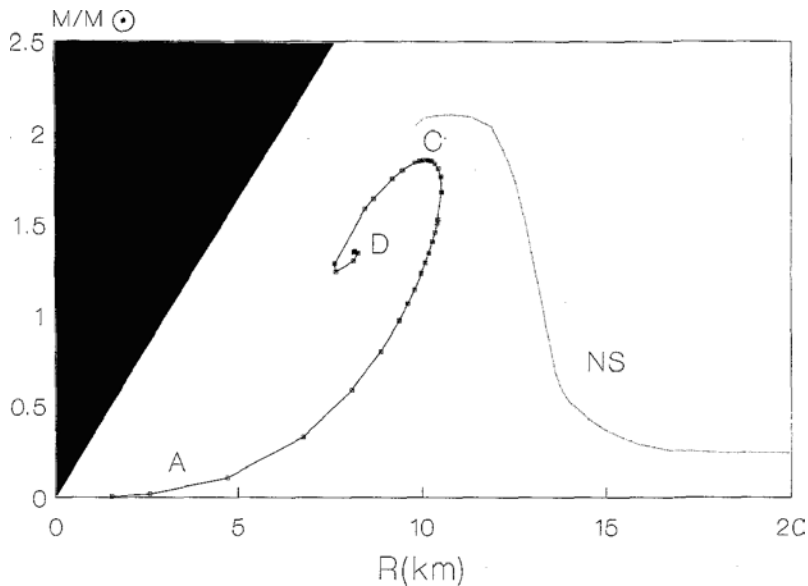


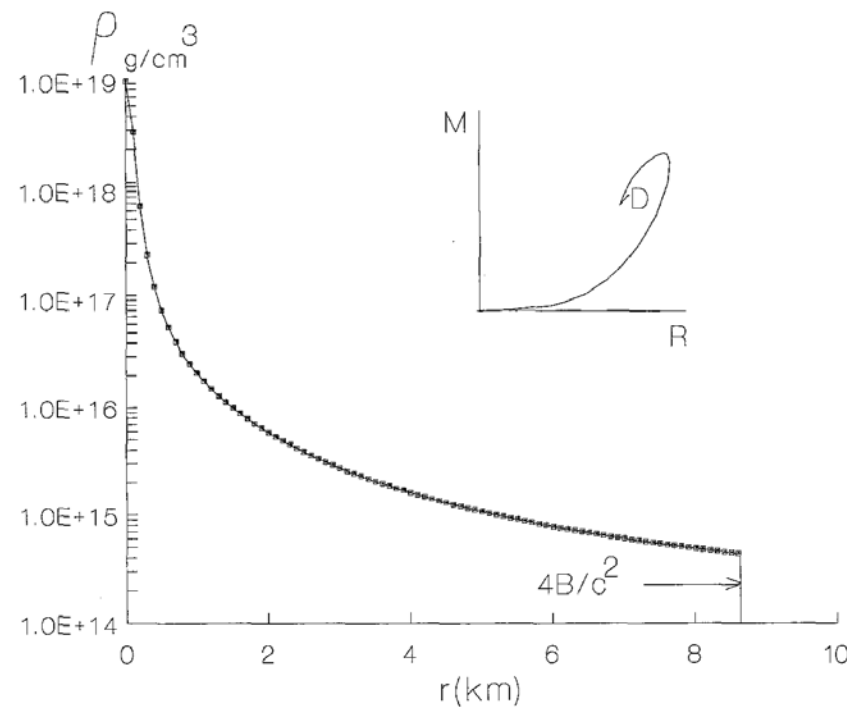
Рисунок 4: Профиль плотности энергии для предельно неоднородной гидростатически устойчивой кварковой звездной конфигурации с уравнением состояния (1) вычисленной в рамках ОТО. $B = 67 \text{ MeV}/\text{fm}^3$.



$P_Q = 1/3 (\varepsilon - 4B)$

$B = 67 \text{ MeV fm}^{-3}$. $P_Q = 0$,
 $\rho_{\text{QGP}} \approx 1.7 \rho_{\text{nuclei}}$
 $(\rho_{\text{nuclei}} = 2.8 \times 10^{14} \text{ g cm}^{-3})$.

$$M_{\max}(C) \approx 1.85 \left(\frac{67 \text{ MeV fm}^{-3}}{B} \right)^{1/2} M_\odot$$



4.

Коллапсар в гравидинамике

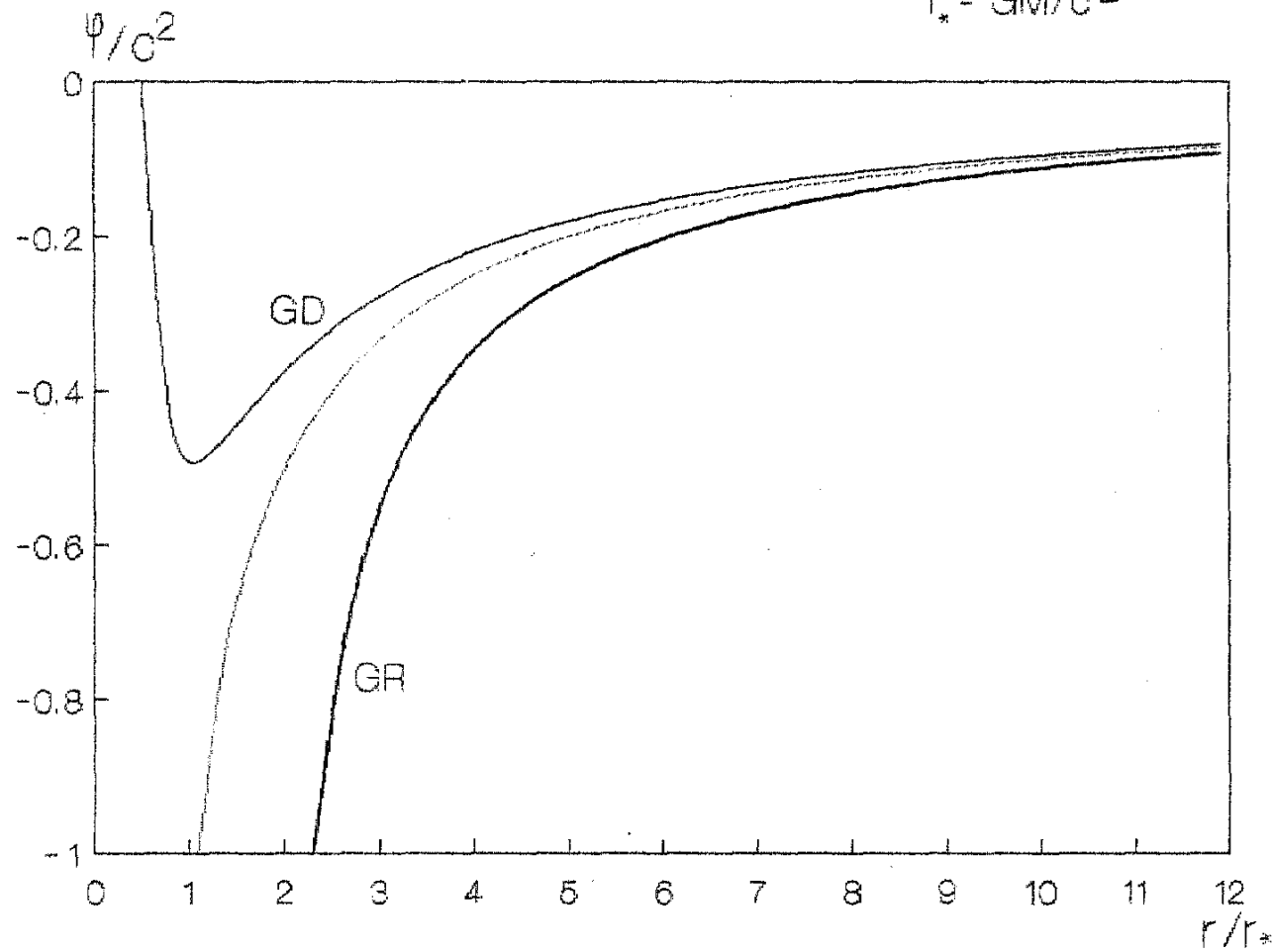
(См. V.V.Sokolov, and S.V.Zharikov, Astrophysics and Space Science, 1993, 201, p.303 + ссылки там)

1. Гравидинамика: в этой модели грав.взаимодействия (как и в электродинамике) полю приписывается энергия = совершенно определенная часть массы любого гравитирующего объекта (как электромагнитная масса у электрона).
2. Все известные эффекты **слабого** поля объяснены (как и в ОТО), поскольку поле в этих случаях в основном только тензорное = гравитация.
3. Но в **сильном** поле компактного объекта все большую роль начинает играть скалярная компонента поля – отталкивание (антигравитация/левитация).
4. Полная масса (**6.7 М_⊙**) такого объекта уже наполовину состоит из одного только поля – скалярно-тензорной смеси...

А до каких плотностей энергия поля нелокализуема?



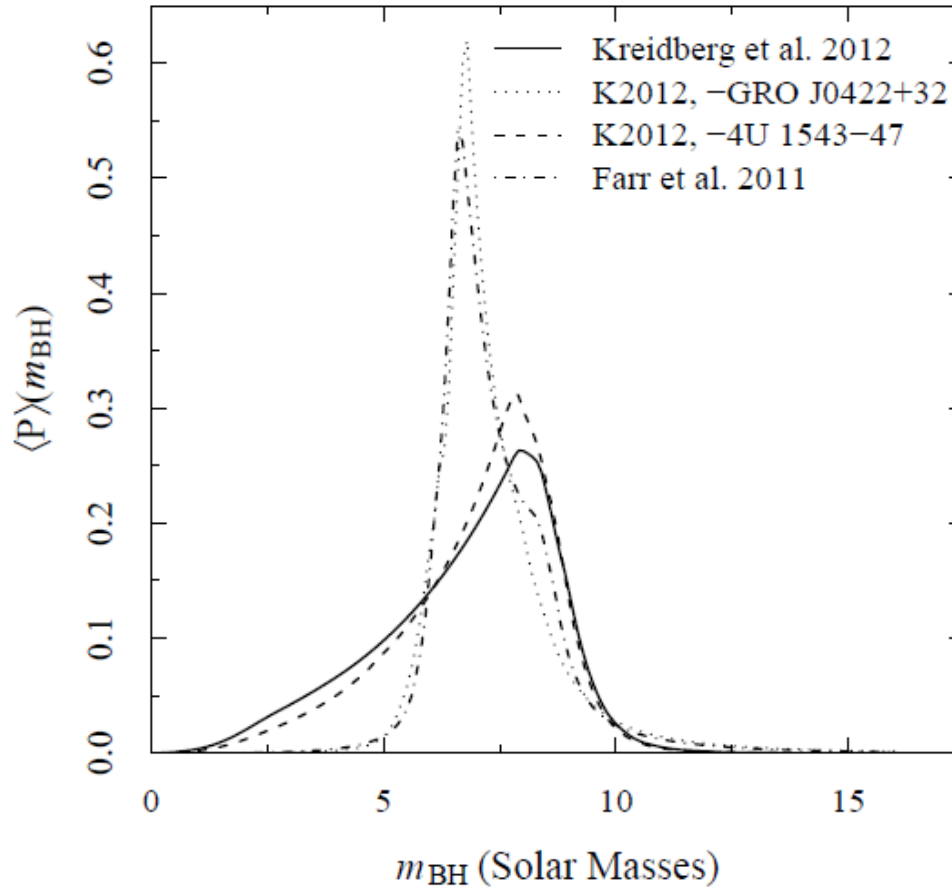
$$r_* = GM/c^2$$

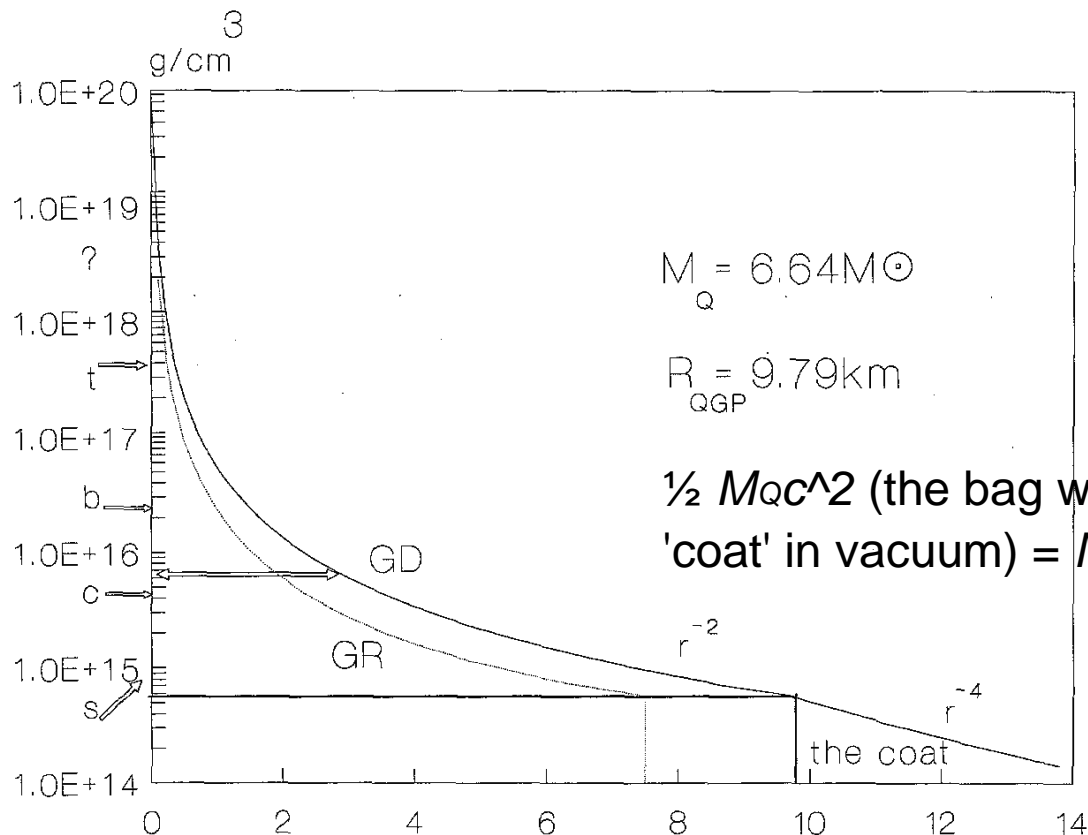


$$\varphi_{GD} \equiv -f\psi_{00}(r) = -\frac{GM}{r}\left(1 - \frac{1}{2}\frac{r_*}{r}\right)$$



ПИК в распределении массы релятивистского объекта близок к **6.7 \odot**



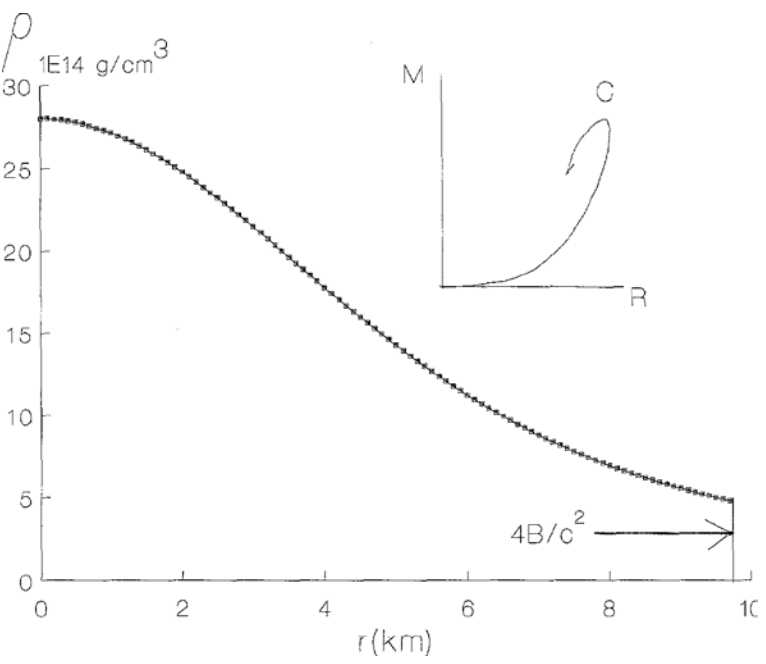
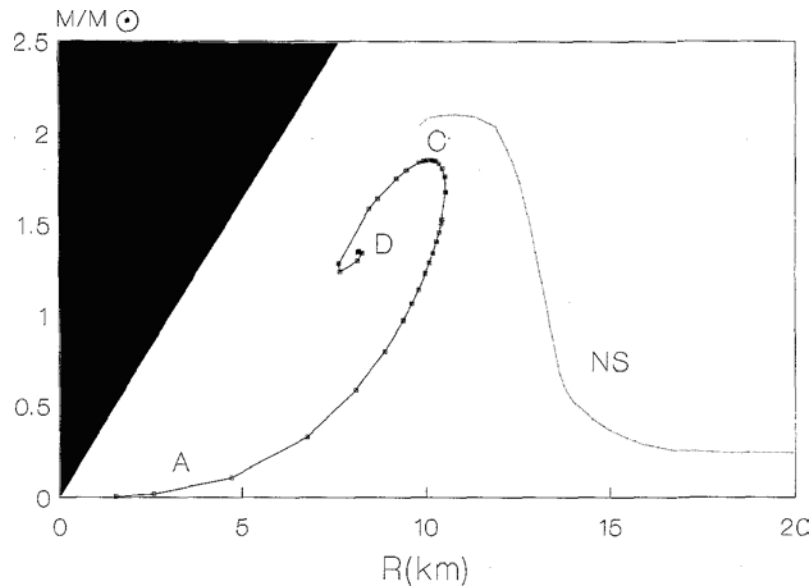


$$P_Q = 1/3 (\varepsilon - 4B)$$

$$M_Q = 6.64M_\odot \left(\frac{2\rho_{nucl}}{4B/c^2} \right)^{1/2}$$

$\frac{1}{2} M_Q c^2$ (the bag with $R = R_{QGP}$) + $\frac{1}{2} M_Q c^2$ (the 'coat' in vacuum) = $M_Q c^2$

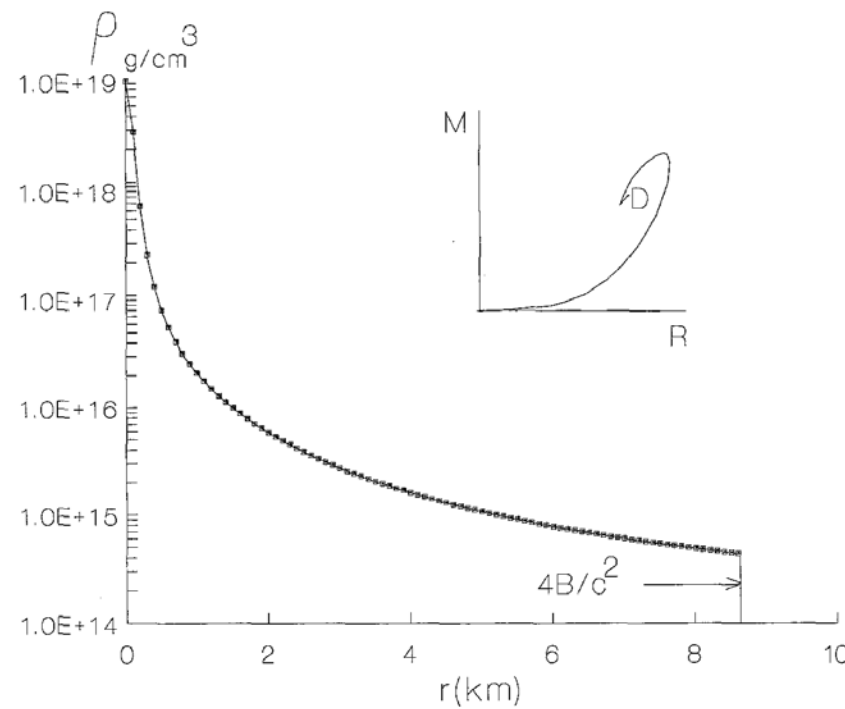
Density profile for a quark star in GD (solid line). Fat rectangle shows 'the background' created by gluons (see the text) distributed homogeneously (?) in the bag with $R_{QGP} \approx 10$ km. 'Vacuum' around the bag is filled by a 'gas' of virtual gravitons (the fur-coat) with energy density $\theta_{00}(r)$. The densities are indicated at which 'the defreezing' of s, c, b, t, \dots quarks occurs. The arrow indicates the density at which the perturbative QCD vacuum must be totally restored ($a_{cm} \approx 0.7$). The dotted line represents the density profile of analogous quark configuration in GR for $4B: c^2 = 2\rho_{nucl}$ ($B = 78.5$ MeV fm -3).

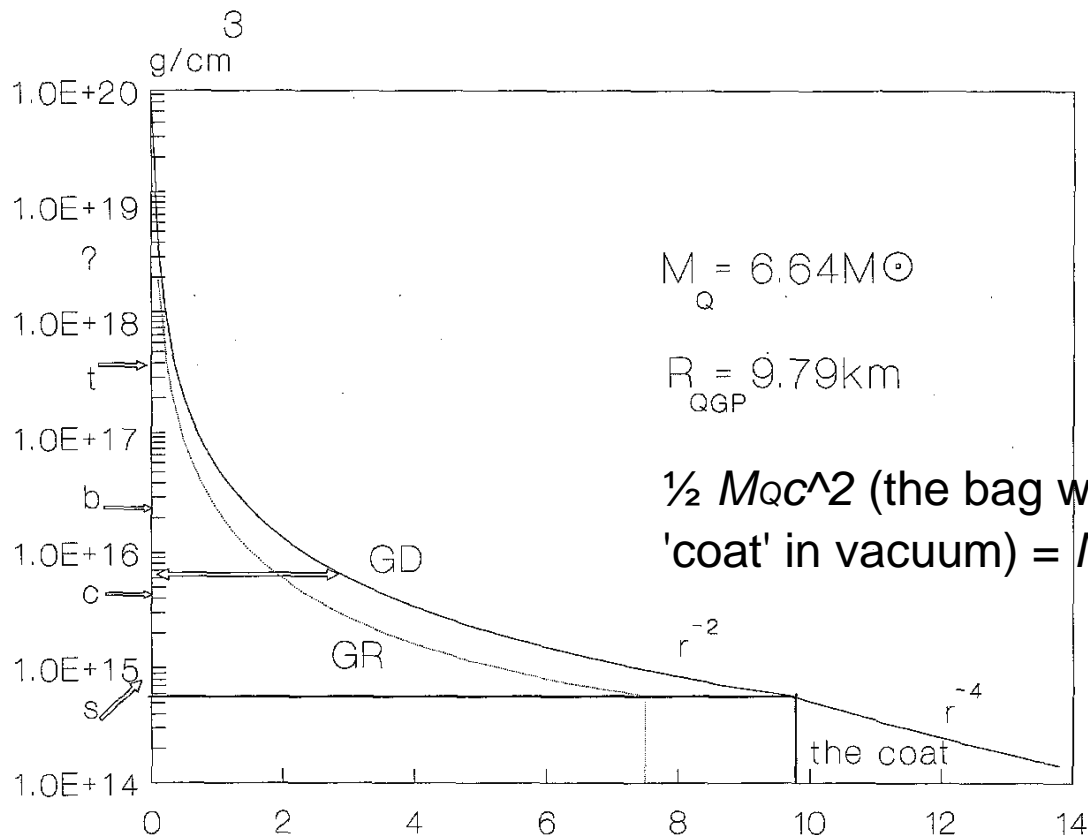


$P_Q = 1/3 (\varepsilon - 4B)$

$B = 67 \text{ MeV fm}^{-3}$. $P_Q = 0$,
 $\rho_{\text{QGP}} \approx 1.7 \rho_{\text{nuclei}}$
 $(\rho_{\text{nuclei}} = 2.8 \times 10^{14} \text{ g cm}^{-3})$.

$$M_{\max}(C) \approx 1.85 \left(\frac{67 \text{ MeV fm}^{-3}}{B} \right)^{1/2} M_\odot$$





$$P_Q = 1/3 (\varepsilon - 4B)$$

$$M_Q = 6.64M_\odot \left(\frac{2\rho_{nucl}}{4B/c^2} \right)^{1/2}$$

$$\frac{1}{2} M_Q c^2 \text{ (the bag with } R = R_{QGP}) + \frac{1}{2} M_Q c^2 \text{ (the 'coat' in vacuum)} = M_Q c^2$$

Density profile for a quark star in GD (solid line). Fat rectangle shows 'the background' created by gluons (see the text) distributed homogeneously (?) in the bag with $R_{QGP} \approx 10 \text{ km}$. 'Vacuum' around the bag is filled by a 'gas' of virtual gravitons (the fur-coat) with energy density $\theta_{00}(r)$. The densities are indicated at which 'the defreezing' of s, c, b, t, \dots quarks occurs. The arrow indicates the density at which the perturbative QCD vacuum must be totally restored ($a_{cm} \approx 0.7$). The dotted line represents the density profile of analogous quark configuration in GR for $4B$: $c^2 = 2\rho_{nucl}$ ($B = 78.5 \text{ MeV fm}^{-3}$).

!



К докладу Д.Г. Яковлева «Странные звезды»

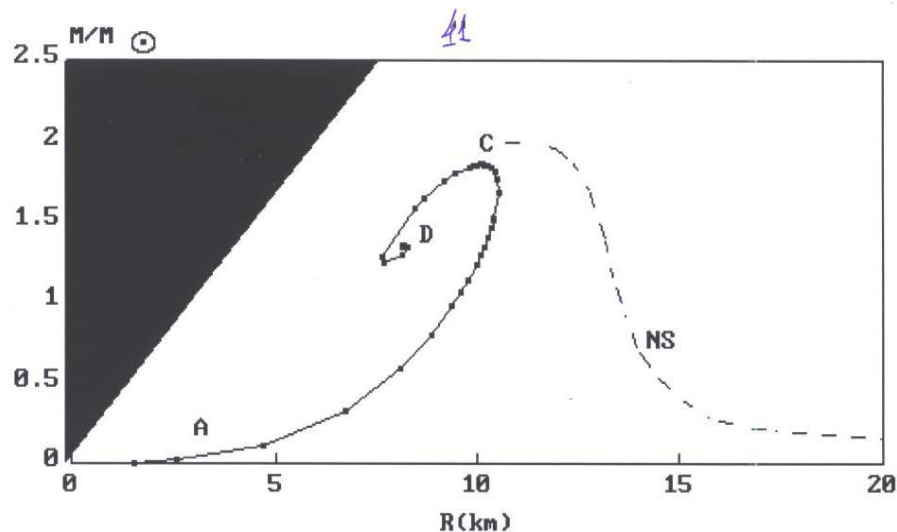


Рисунок 1: Зависимость масса - радиус для кварковых странных звезд с уравнением состояния (1). Прерывистой линией показана зависимость масса - радиус для нейтронных звезд, описываемых уравнением состояния Бете - Джонсона, в рамках Общей теории Относительности. Точка С соответствует пределу ОВ, точкой D отмечено положение предельно неоднородной кварковой конфигурации в ОТО. Заштрихована область, соответствующая черным дырам. $B = 67 \text{ MeV}/\text{fm}^3$.

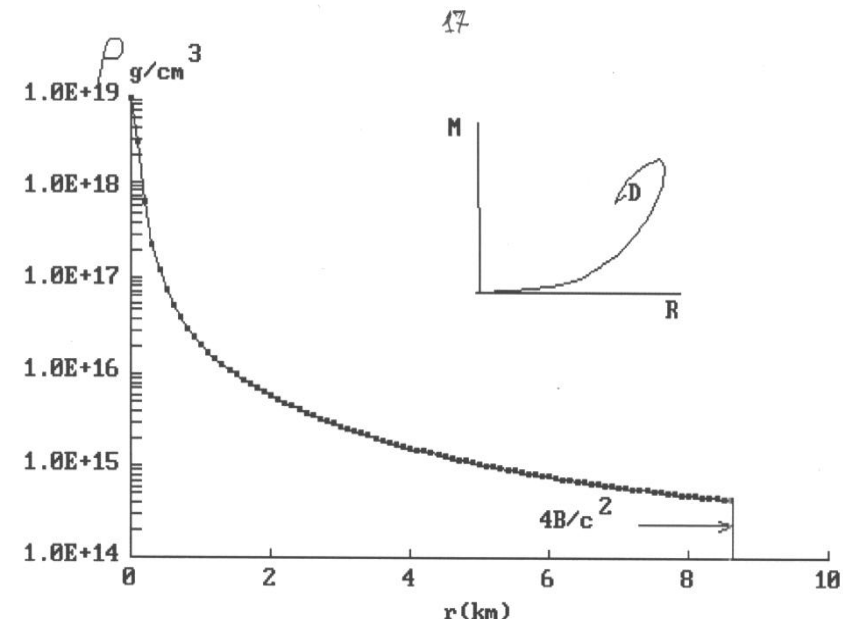
$$\rho = \frac{1}{3} (\rho c^2 - 4B)$$


Рисунок 4: Профиль плотности энергии для предельно неоднородной гидростатически устойчивой кварковой звездной конфигурации с уравнением состояния (1) вычисленной в рамках ОТО. $B = 67 \text{ MeV}/\text{fm}^3$.

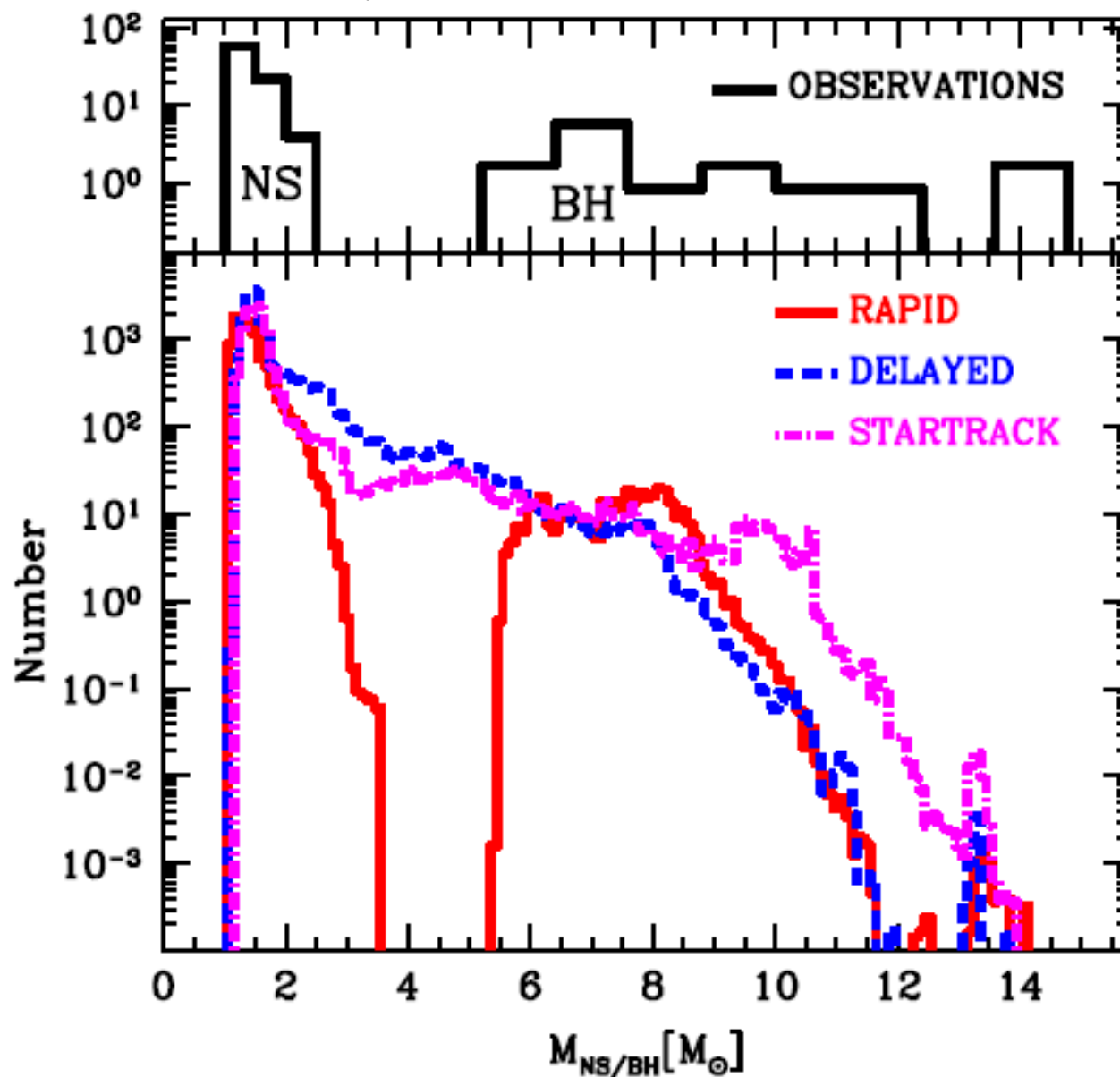
5.

mass gap + SNe & GRBs

GRB – начало взрыва CC-SNe

MISSING BLACK HOLES UNVEIL THE SUPERNOVA EXPLOSION MECHANISM

Belczynski et al, [arXiv:1110.1635v2](https://arxiv.org/abs/1110.1635v2)



EMMI Rapid Reaction Task Force Meeting on
“Quark Matter in Compact Star”

The possibility of pure **quark** stars, **hybrid** stars and the nature of the **QCD phase transition** were discussed and their observational signals delineated. + **GRBs**



1402.6911

EMMI Rapid Reaction Task Force Meeting on “Quark Matter in Compact Star”

[27, 28]. The time-delay between the moment of the SN explosion and the moment of the quark phase transition could explain a few observed features of Gamma-Ray Bursts, as e.g. the existence of very long quiescent times seen in a few bursts [29] and the possible existence of Gamma-Ray Bursts for which no associated SN explosion is observed [30].



Модель асимметричного взрыва GRB/SN прапорителя

...a strongly non-spherical explosion may be a generic feature of core-collapse supernovae of all types.

...Though while it is not clear that the same mechanism that generates the GRB is also responsible for exploding the star.

astro-ph/0603297
Leonard, Filippenko et al.

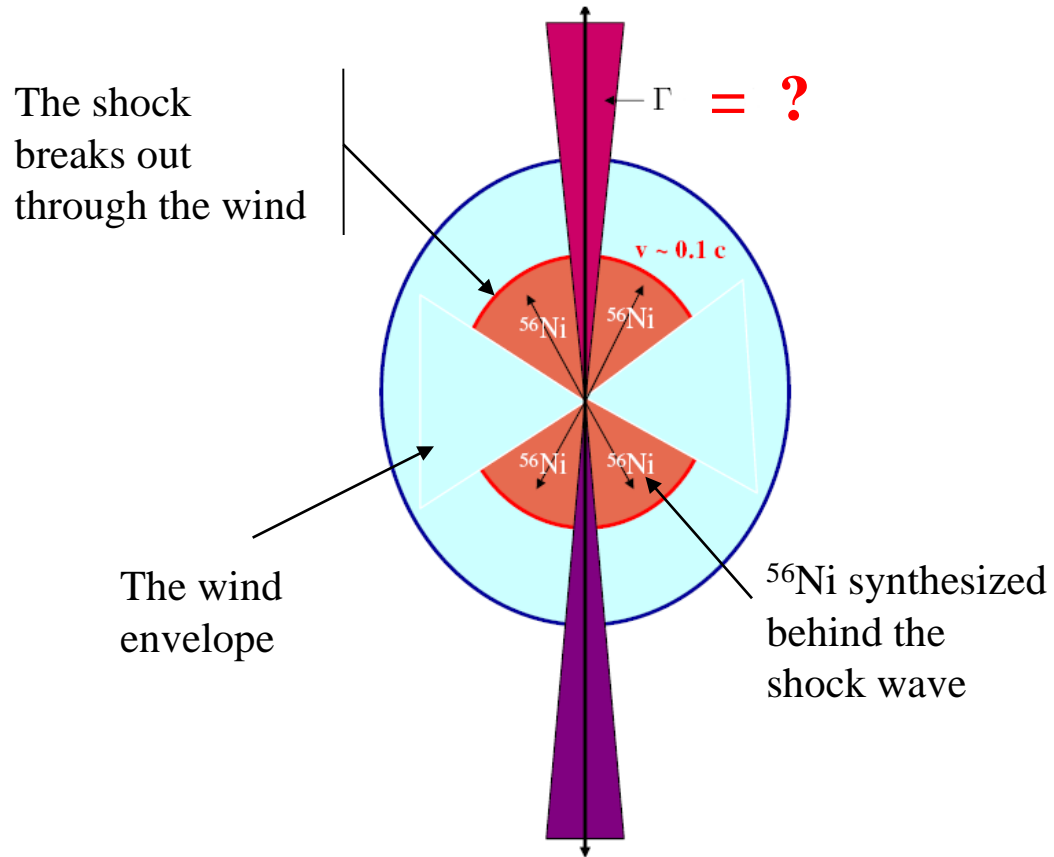


Fig. from Astro-ph/0604131, Woosley and Heger

Хотя само явление необычное, но объект-источник не так уж и уникален !/? Чем ближе GRB-вспышка, тем больше признаков СН.

Astro-

ph/0405427

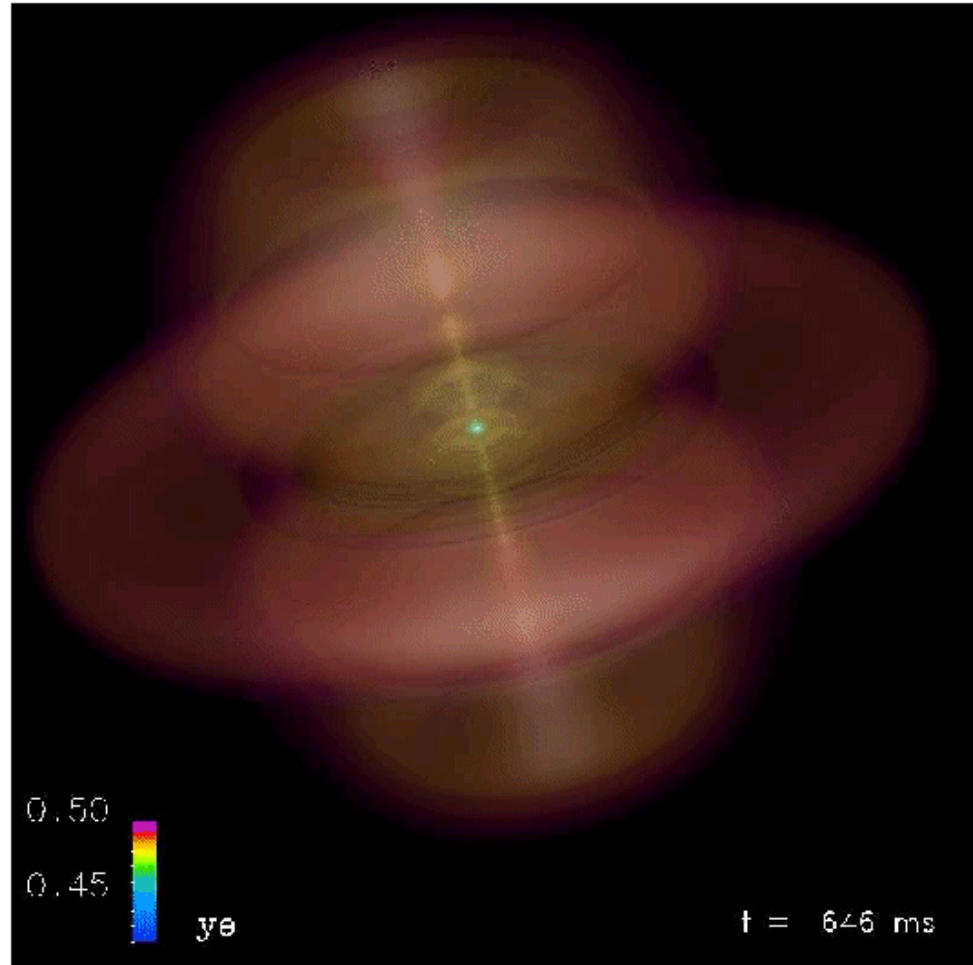
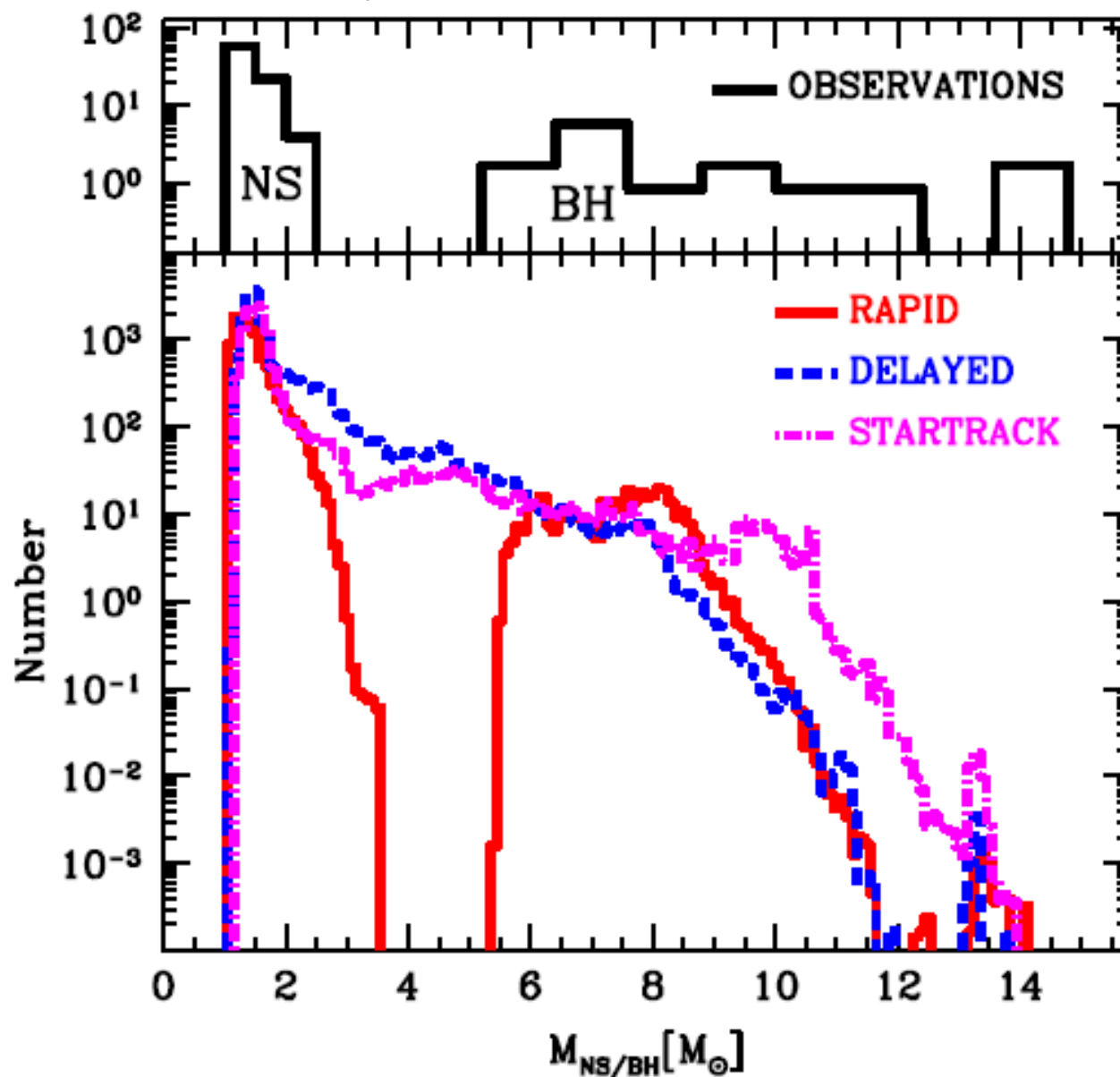
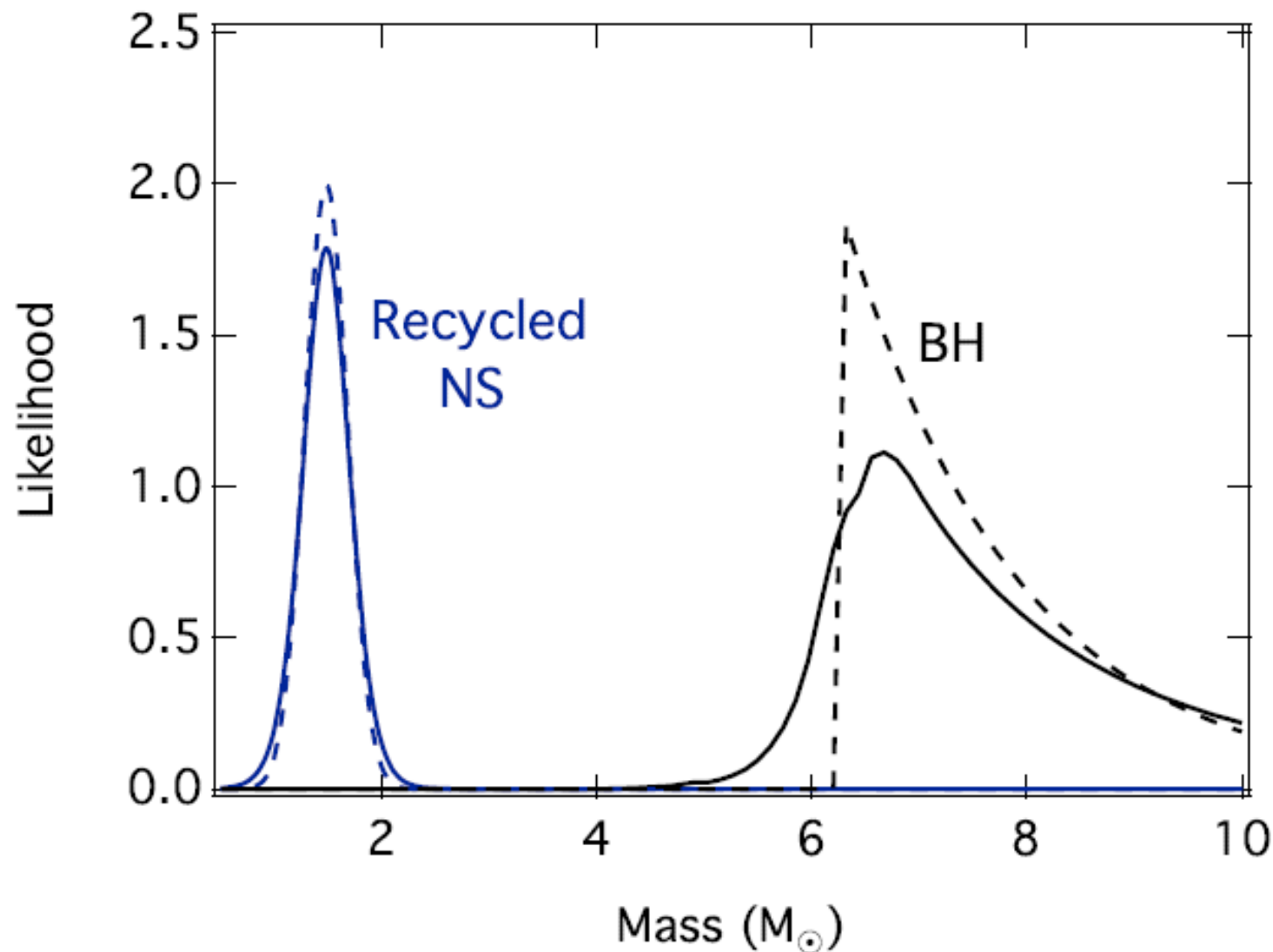


Figure 2: A snapshot after bounce of a calculation of a $20 M_{\odot}$ model with rotation. The surfaces are nested isodensity shells and the approximate scale is 600 kilometers. Funnels due to an emerging centrifugal barrier are clearly seen along the poles, as is an equatorial bulge. (Obtained in collaboration with C. Ott and R. Walder.)

MISSING BLACK HOLES UNVEIL THE SUPERNOVA EXPLOSION MECHANISM

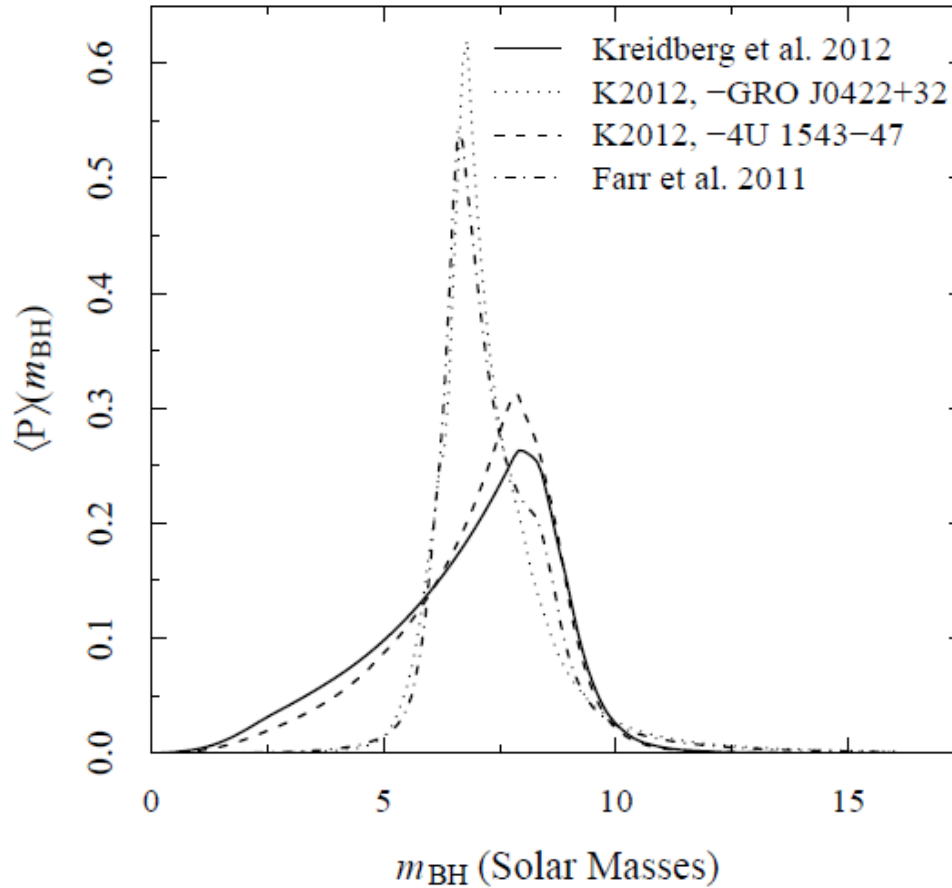
Belczynski et al, [arXiv:1110.1635v2](https://arxiv.org/abs/1110.1635v2)







ПИК в распределении массы релятивистского объекта близок к **6.7 \odot**



6. *On the compact GRB model*

Gamma-ray bursts (GRBs) are the brief (~0.01-100s), intense flashes of γ -rays (mostly sub-MeV) with enormous electromagnetic energy release up to $\sim 10^{51}$ - 10^{54} ergs. The rapid temporal variability, $\delta T < 10$ msec, observed in GRBs implies *compact* sources with a size smaller than $c\delta T < 3000$ km.



Модель асимметричного взрыва GRB/SN прадителя

...a strongly non-spherical explosion may be a generic feature of core-collapse supernovae of all types.

...Though while it is not clear that the same mechanism that generates the GRB is also responsible for exploding the star.

astro-ph/0603297
Leonard, Filippenko et al.

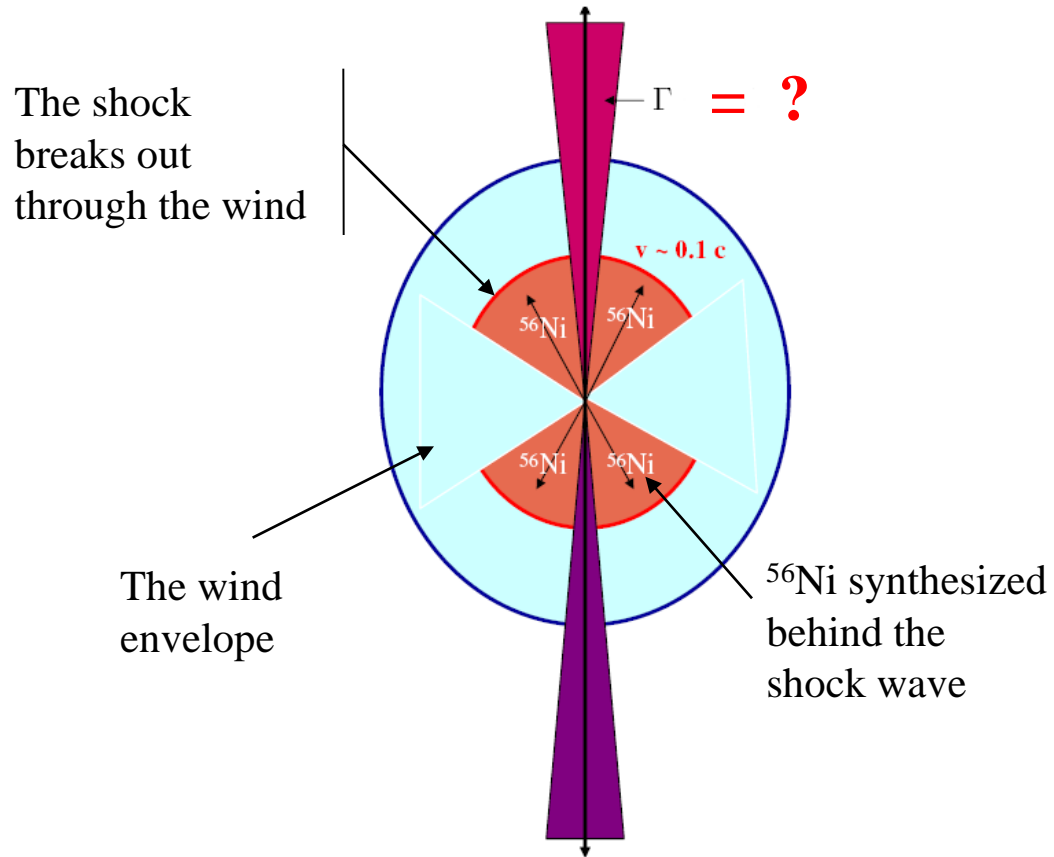
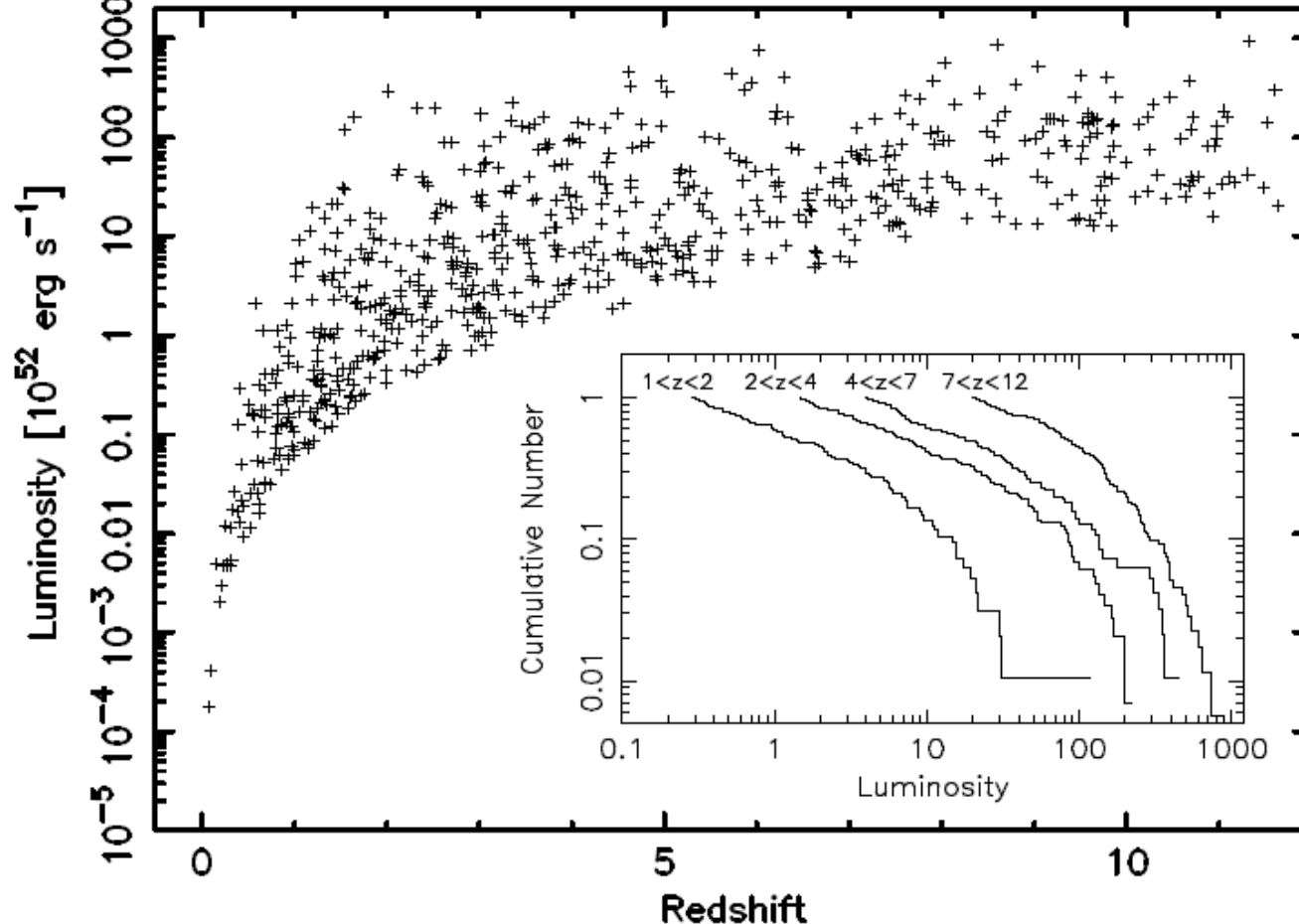
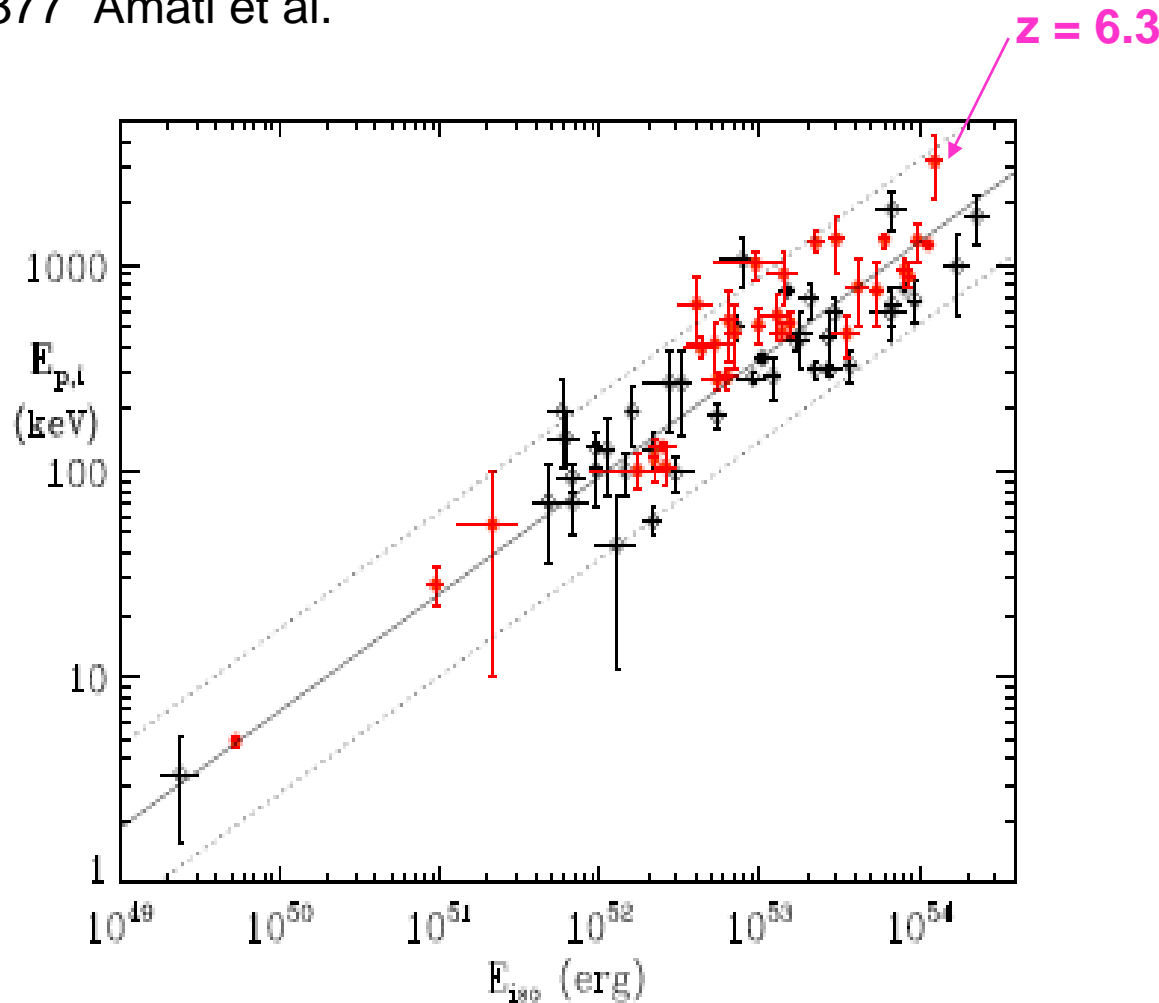


Fig. from Astro-ph/0604131, Woosley and Heger

Хотя само явление необычное, но объект-источник не так уж и уникален !/? Чем ближе GRB-вспышка, тем больше признаков СН.



The distribution of luminosity vs. redshift derived from the Ep-luminosity relation. The truncation(усечение) of the lower end of the luminosity is caused by the flux limit of $F_{\text{limit}} = 1 \times 10^{-7} \text{ erg cm}^{-2}\text{s}^{-1}$. The inserted figure is the cumulative luminosity function in the several redshift ranges. The luminosity evolution exists because the break-luminosity increase toward the higher redshift.



One can see that at least **the sufficient condition** of our description of the $E_{\text{peak}}\text{-}E_{\text{iso}}$ correlation is fulfilled: the most distant GRB 050904 with $z=6.29$ has the largest $E_{\text{p},i} = 3178$ keV (just the highest point in this figure).

В компактной модели GRB эта связь (закон Амати) может быть "простым" следствием как формулы для $E_{th} = \sqrt{E_1 E_2}$, так и анизотропии излучения, связанной (скорее всего) с магнитным полем на или вблизи поверхности компактного объекта.

Анизотропия, может быть связана с переносом излучения в среде с сильным (регулярным, $\sim 10^{14} - 10^{16}$ Гс) магнитным полем, когда поглощение для фотонов, поляризованных поперек магнитного поля (необыкновенная волна), оказывается очень маленьким (B. Paczyński, 1992; V.G. Bezchastnov, G.G. Pavlov, Yu.A. Shibanov, V.E. Zavlin, 1996).

Тогда наблюдение сильной линейной поляризации излучения GRB должно быть еще одним следствием компактной модели.

Evidence of polarisation in the prompt gamma-ray emission from GRB 930131 and GRB 960924.

D.R. Willis^{1,2,3 *}, E.J. Barlow¹, A.J. Bird¹, D.J. Clark¹, A.J. Dean¹, M.L. McConnell⁴, L. Moran¹, S.E. Shaw^{1,3}, and V. Sguera¹

¹ School of Physics and Astronomy, University of Southampton, SO17 1BJ, UK

² Max-Planck-Institut für extraterrestrische Physik, MPI, Garching, Munich, Germany

³ INTEGRAL Science Data Centre, CH-1290 Versoix, Switzerland

⁴ Space Science Center, University of New Hampshire, Durham, NH 03824, USA

Received now / Accepted then

Abstract. The true nature of the progenitor to GRBs remains elusive; one characteristic that would constrain our understanding of the GRB mechanism considerably is gamma-ray polarimetry measurements of the initial burst flux. We present a method that interprets the prompt GRB flux as it Compton scatters off the Earth's atmosphere, based on detailed modelling of both the Earth's atmosphere and the orbiting detectors. The BATSE mission aboard the *CGRO* monitored the whole sky in the 20 keV – 1 MeV energy band continuously from April 1991 until June 2000. We present the BATSE Albedo Polarimetry System (BAPS), and show that GRB 930131 and GRB 960924 provide evidence of polarisation in their prompt flux that is consistent with degrees of polarisation of $\Pi > 35\%$ and $\Pi > 50\%$ respectively. While the evidence of polarisation is strong, the method is unable to strongly constrain the degree of polarization beyond a systematics based estimation. Hence the implications on GRB theory are unclear, and further measurements essential.

Key words. gamma-rays: bursts – Techniques: polarimetric – Methods: data analysis – Polarization



1. Introduction

Whatever the mechanism, polarisation in the prompt gamma-ray flux from GRBs is evidence of strong magnetic fields within the burst. Theories on the GRB production mechanism can be constrained by different degrees of linear polarisation. For large degrees of polarisation, $\Pi \approx 80\%$, either shock accelerated synchrotron emission or a tuned Compton-drag model is the most likely (Lazzati et al. 2004; Coburn & Boggs 2003; Lyutikov et al. 2003). For intermediate degrees of polarisation ($20\% < \Pi < 60\%$) two electromagnetic models have emerged that involve either synchrotron emission as the dominant source of radiation or as the result of viewing the burst from just outside the edge of the jet (Granot 2003; Ghisellini & Lazzati 1999). Low degrees of polarisation can be a result of either a hydrodynamic model or

The high degree of linear polarisation initially reported in the prompt flux of GRB 021206 [degree of polarisation, $\Pi = 80 \pm 20\%$, Coburn & Boggs (2003)] with the *RHESSI* experiment (McConnell et al. 2002) has stimulated much interest in the implications this has on GRB theory. Though GRB astronomy has the advantage of large fluxes, any polarimetric measurements are still dominated by systematic effects that can only be properly quantified by careful modelling. The importance of correctly evaluating the systematic effects is paramount in any measurement of GRB polarisation as was emphasised by Wigger et al. (2004) in the thorough re-analysis of the initial *RHESSI* result (Coburn & Boggs 2003). Wigger et al. (2004) re-analysed the degree of polarisation to be $\Pi = 41^{+57\%}_{-44\%}$. This implies that many of the production mechanism theories are now similarly competitive.

*

Application of Jitter Radiation: Gamma-ray Burst Prompt Polarization

Jirong Mao^{1,2,3} and Jiancheng Wang^{2,3}

jirong.mao@riken.jp

Gamma-ray bursts (GRBs) are the most energetic explosions in the universe. Some polarization detections of GRBs in the prompt γ -ray band were performed. A linear polarization with a degree of $\Pi = 80\% \pm 20\%$ in GRB 021206 was detected by *RHESSI* (Coburn & Boggs 2003). GRB 041219A, observed by the International Gamma-Ray Astrophysics Laboratory, also has a high degree of polarization. Values of $\Pi = 98\% \pm 33\%$ and $\Pi = 63\% \pm 30\%$ were reported by Kalemci et al. (2007) and McGlynn et al. (2007), respectively. Recently, γ -ray prompt polarizations of three GRBs were detected by the GRB polarimeter onboard *IKAROS*: GRB 100826A has an average polarization degree of $27\% \pm 11\%$ (Yonetoku et al. 2011); GRB 110301A and GRB 110721A have high polarization degrees of $70\% \pm 22\%$ and $84^{+16}_{-28}\%$, respectively (Yonetoku et al. 2012). Meanwhile, theoretical models are strongly required to constrain the physical origin of these highly polarized GRB prompt photons and to explore possible magnetic field configurations.



Polarization of GRB Prompt Emission

KENJI TOMA

*Department of Earth and Space Science, Osaka University, Toyonaka 560-0043,
Japan
toma@vega.ess.sci.osaka-u.ac.jp*

We review the recent observational results of the gamma-ray linear polarization of Gamma-Ray Bursts (GRBs), and discuss some theoretical implications for the prompt emission mechanism and the magnetic composition of GRB jets. We also report a strict observational verification of *CPT* invariance in the photon sector as a result of the GRB polarization measurements.

Тогда наблюдение сильной линейной поляризации излучения GRB должно быть еще одним следствием компактной модели.



$z = 2.140$

*A cyclotron
feature
 $E_{\text{rest}} = 21.7$
 $(+1.9/-1.6)\text{keV}$
for magnetic field
 $\sim 10^{12}$ Gauss*

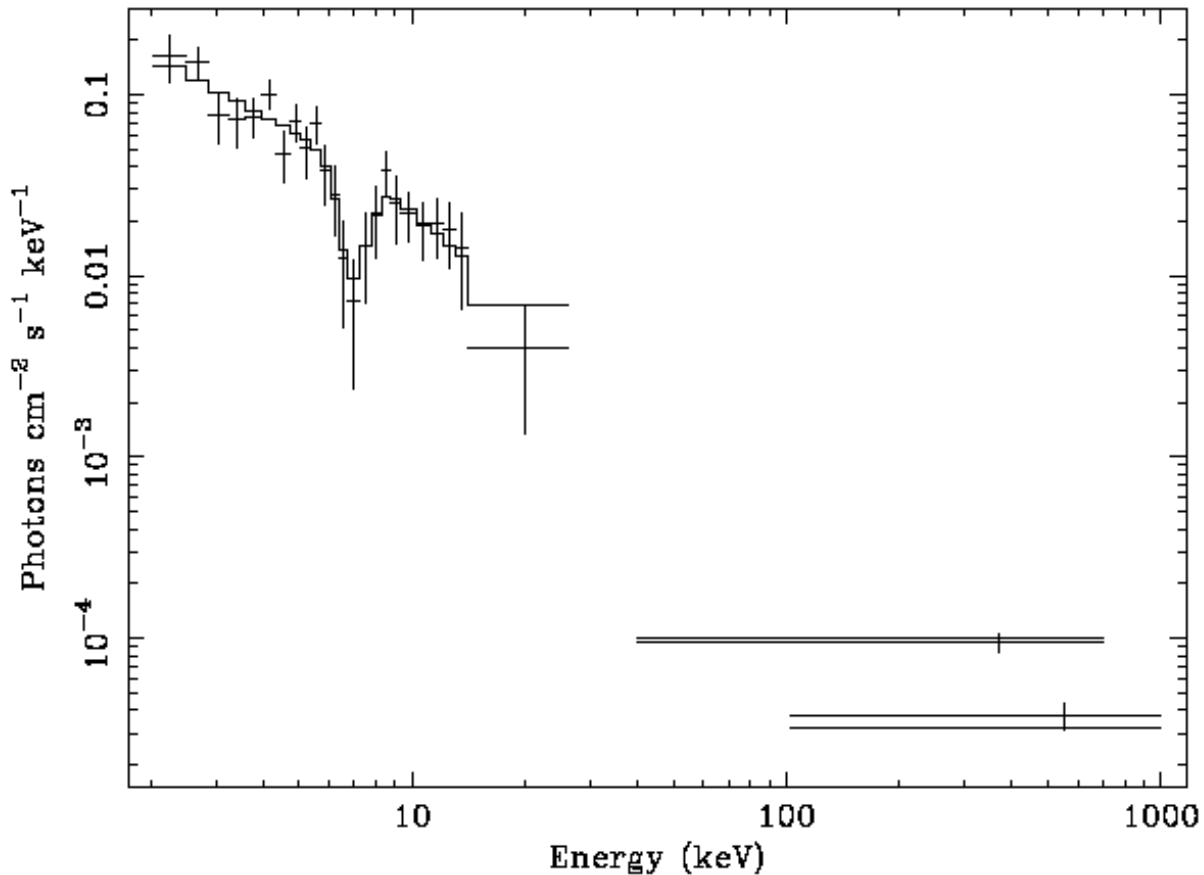


Fig. 6.— *Top:* photon spectrum of GRB011211 in the time interval A. The step-like curve represents the best fit with the model used in Lazzati et al. (2001) (see text).



Если все длинные GRBs действительно связаны с взрывами сверхновых, то длинный всплеск - это коллапс массивной звезды или начало аксиально симметричного взрыва СН,

и **всегда** гамма-всплески должны сопровождаться взрывом СН (Ib/c типа или других типов «массивных» СН). Тогда полное энерговыделение источника всплеска в гамма-лучах во всяком случае может быть не больше, чем вся энергия, излучаемая СН ($<$ или $\sim 10^{49}$ эрг) в электромагнитном диапазоне.

Накопление статистики совпадений GRB + SN будет только подтверждать компактную модель.

СПАСИБО!

Гравидинамика (скалярно-тензорная гравитация) и дискретный спектр масс звездных компактных объектов.

Наблюдаемый спектр масс нейтронных звезд и кандидатов в черные дыры показывает явное отсутствие компактных объектов с массами в интервале 2 - 6 солнечных, а в тесных двойных звездных системах с маломассивными оптическими компаньонами самое вероятное значение (пик в распределении массы кандидатов в черные дыры) близко к 7 массам Солнца.

В полностью неметрической, полевой/скалярно-тензорной модели гравитационного взаимодействия релятивистский компактный объект с предельно сильным гравитационным полем (аналог черных дыр в ОТО) имеет полную массу ≈ 6.7 солнечных масс с радиусом области, занятой веществом (кварк-глюонной плазмой), ≈ 10 км.

Поляризованное излучение гамма-всплесков, чернотельную компоненту в их спектре и другие наблюдательные свойства можно объяснить прямым проявлением поверхности у таких коллапсаров.

... делиться мнениями и сомнениями
(а не убеждениями),
пытаться **предсказать** новые эффекты,
сформулировать наблюдательную
задачу и самому же ее решать.
Рисковать! А не философствовать,
объясняя все, даже и «Вселенную в
целом»...

*The black body radiation
with $kT \sim 100$ keV
for the time-resolved GRB
spectra*

Gamma-ray bursts (GRBs) are the brief (~0.01-100s), intense flashes of γ -rays (mostly sub-MeV) with enormous electromagnetic energy release up to $\sim 10^{51}$ - 10^{54} ergs. The rapid temporal variability, $\delta T < 10$ msec, observed in GRBs implies compact sources with a size smaller than $c\delta T < 3000$ km.

arXiv:0705.1061v1, M. Battelino, F. Ryde, N. Omodei and F. Longo – On
the Black-body component and GeV(?)

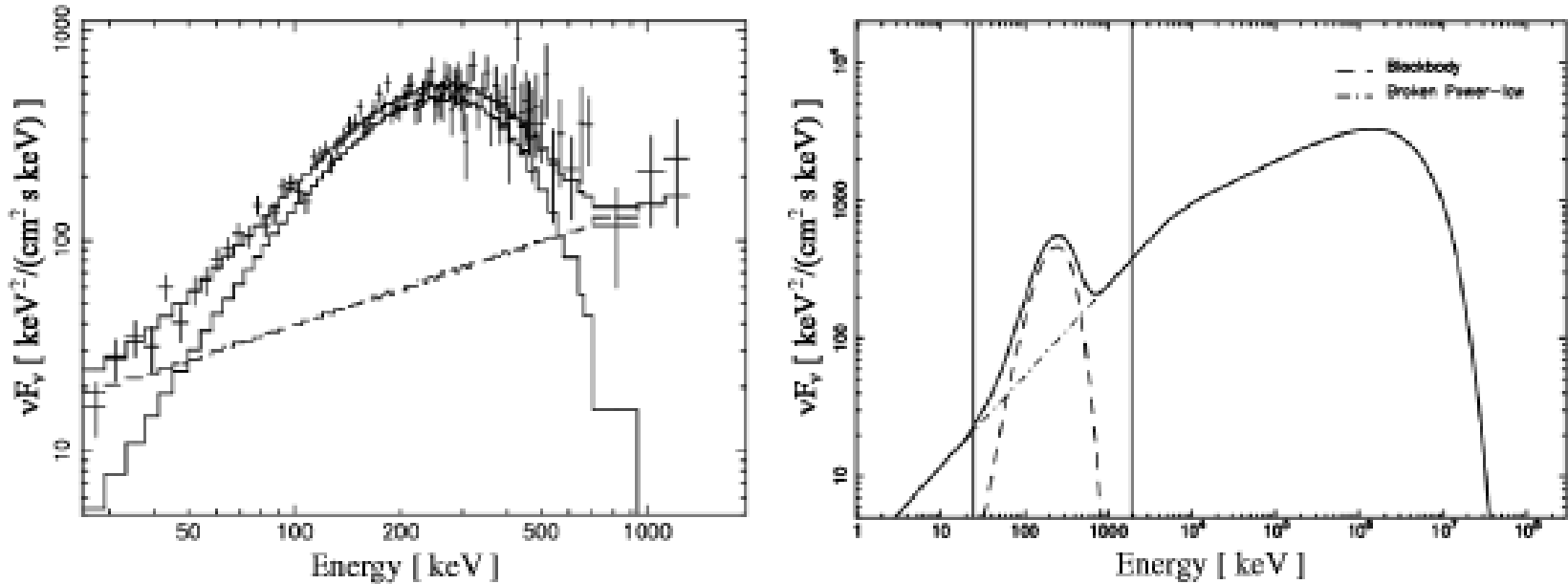


FIGURE 1. Time-resolved vF_v spectra of GRB911016 assumed to have a strong high-energy component in the GeV-domain. See also figure 6. *Left panel:* XSPEC Hybrid model fit in BATSE energy band: 0.704 - 1.280 s. *Right panel:* SBM hybrid model simulation of the same burst extrapolated in the GLAST energy band: 1.0 - 1.1 s. The solid line describes the hybrid model, the dashed line the blackbody component and the dot-dashed line the broken power-law. The two vertical lines in the plot describe the energy range covered by BATSE.

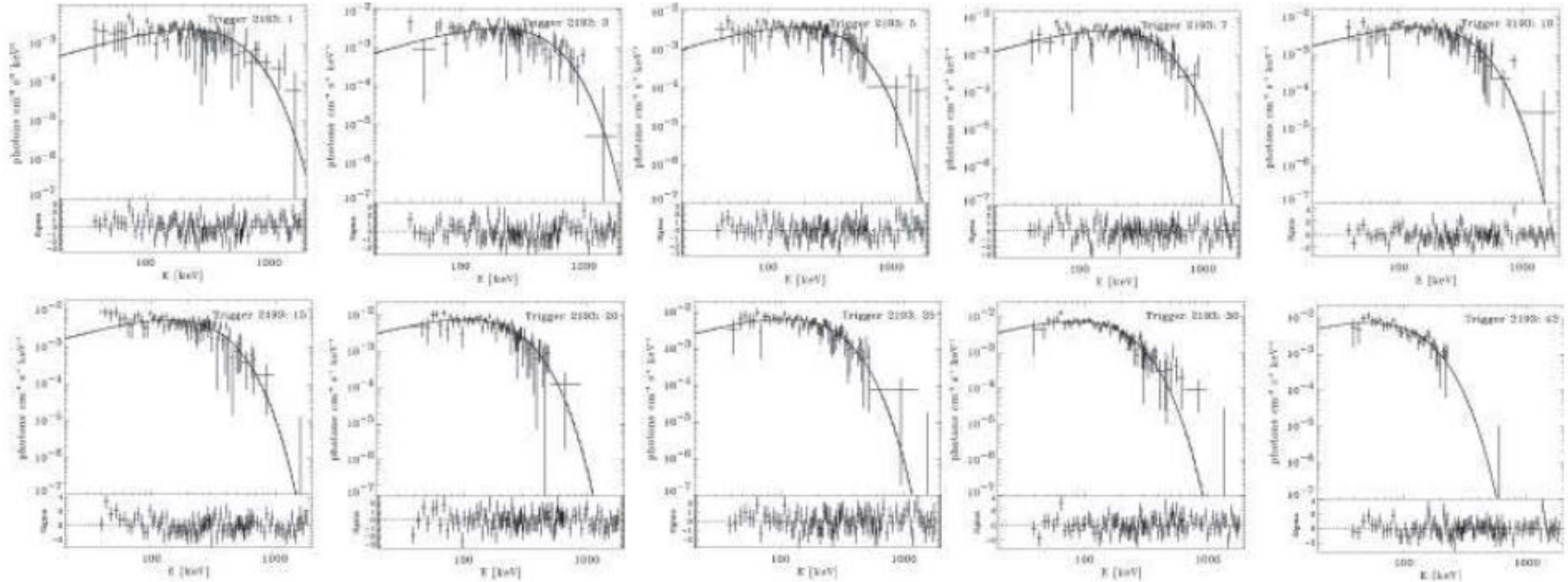


Fig. 4.— Black-body fits to the time-resolved spectra of burst 2193. The spectra correspond to the following time bins (compare fig. [1]), 1: 1.6 – 2.4 s, 3: 3.14 – 3.84 s, 5: 4.5 – 5.3 s, 7: 6.0 – 6.7 s, 10: 8.0 – 8.7 s, 15: 11.3 – 11.9 s, 20: 14.6 – 15.2 s , 25: 18.0 – 18.8 s, 30: 21.6 – 22.9 s, 42: 39.4 – 41 s.

The typical GRB spectra

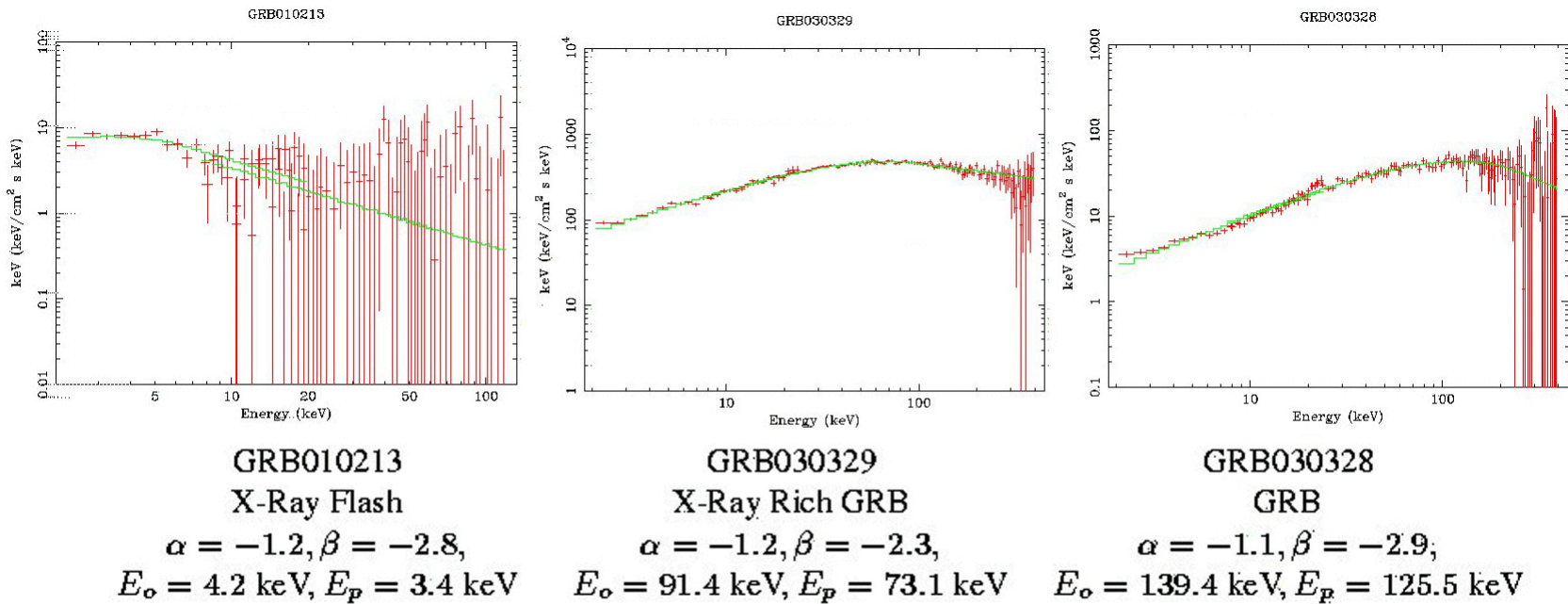


Figure 1. Spectra of the different classes of GRBs: X-Ray Flashe, X-Ray Rich GRB and GRB using both FREGATE and WXM data.

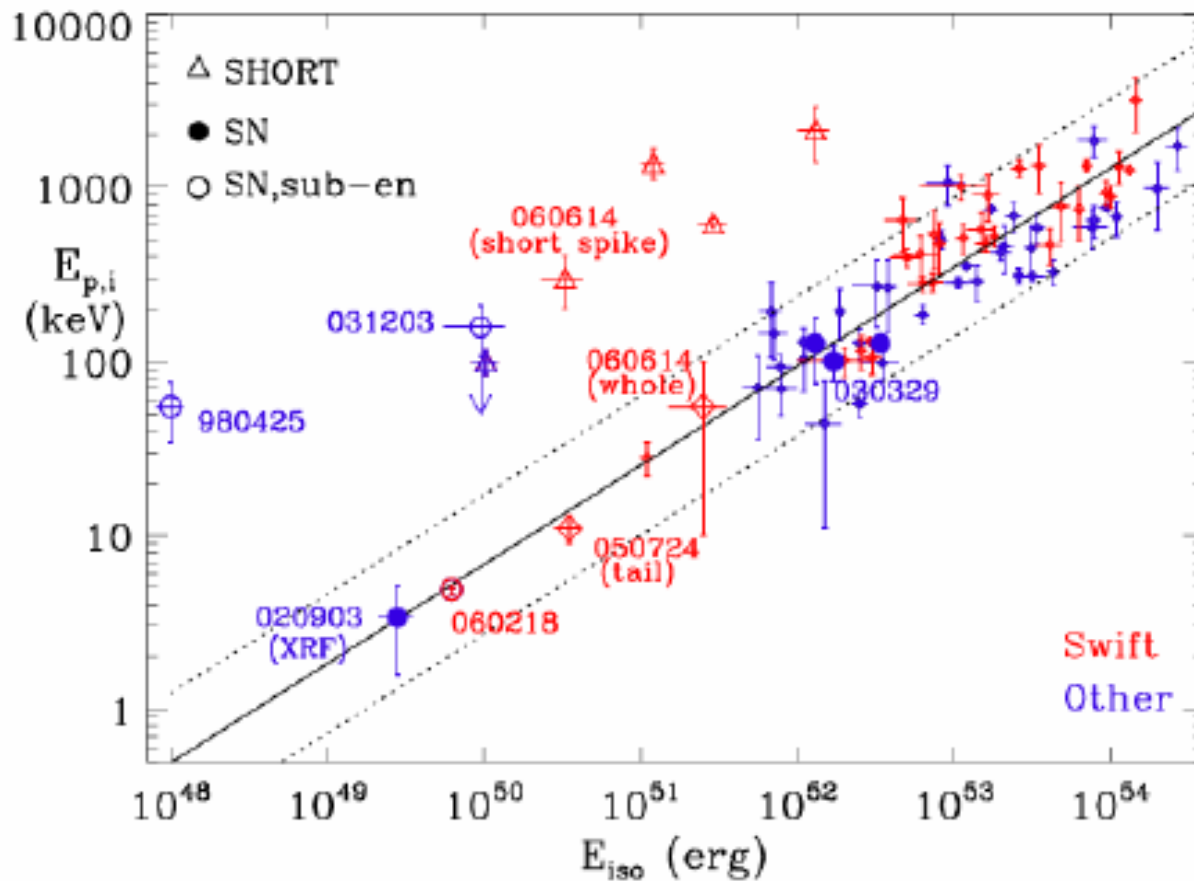


FIGURE 1. Distribution of GRBs with known redshift and measured $E_{p,obs}$, as of April 2008, in the $E_{p,i}$ - E_{iso} plane. Red symbols correspond to *Swift* GRBs, black ones to events detected by other satellites. $E_{p,i}$ and E_{iso} values are taken from [2], [6] and [14]; the continuous and dashed lines indicate the best fit power-law, and the corresponding $\pm 2\sigma$ region, reported by [2]. Short GRBs, GRBs with spectroscopic association with SN, sub-energetic GRBs, XRFs, and other peculiar GRBs are indicated.

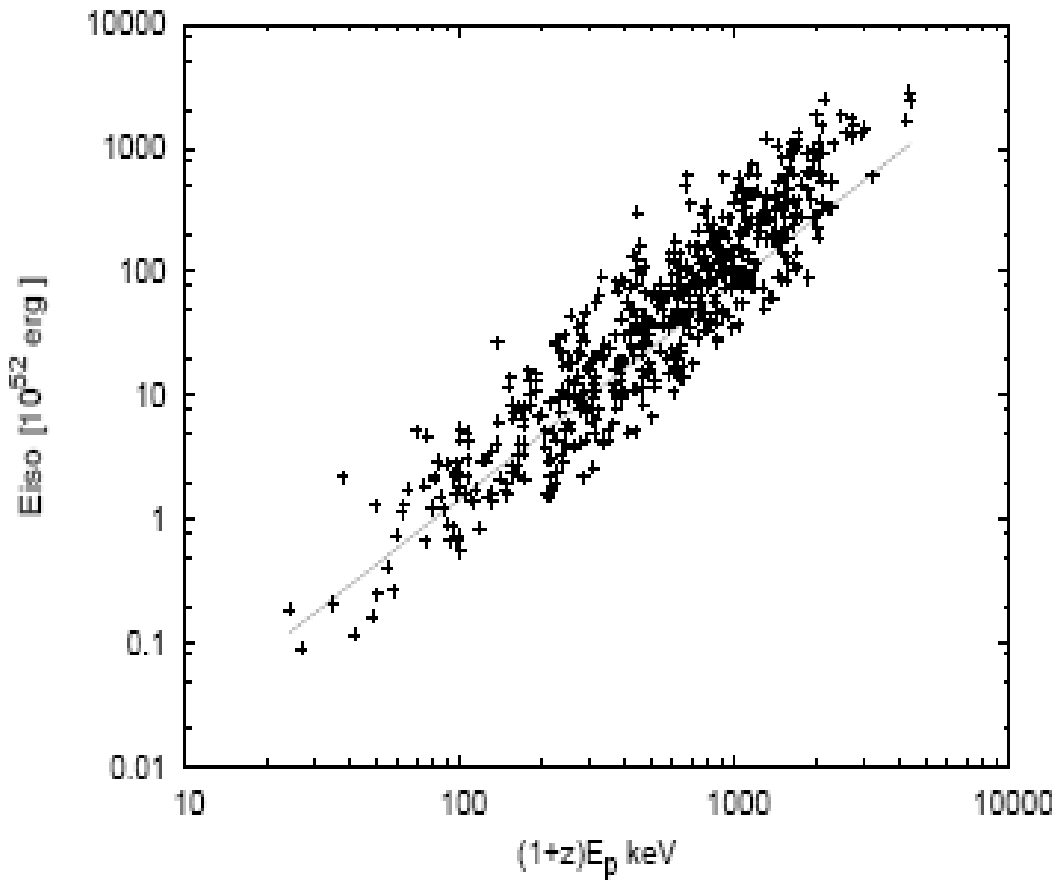


Figure 3. Amati relation in 565 BATSE GRBs. Redshifts derived from Yonetoku relation z_Y is used to estimate E_{iso} and $E_p(1+z)$. The correlation coefficient is 0.92. The chance probability is 5.2×10^{-106} so that the correlation is tight. The solid line is Amati relation (Amati 2006).

1201.15
49v1,

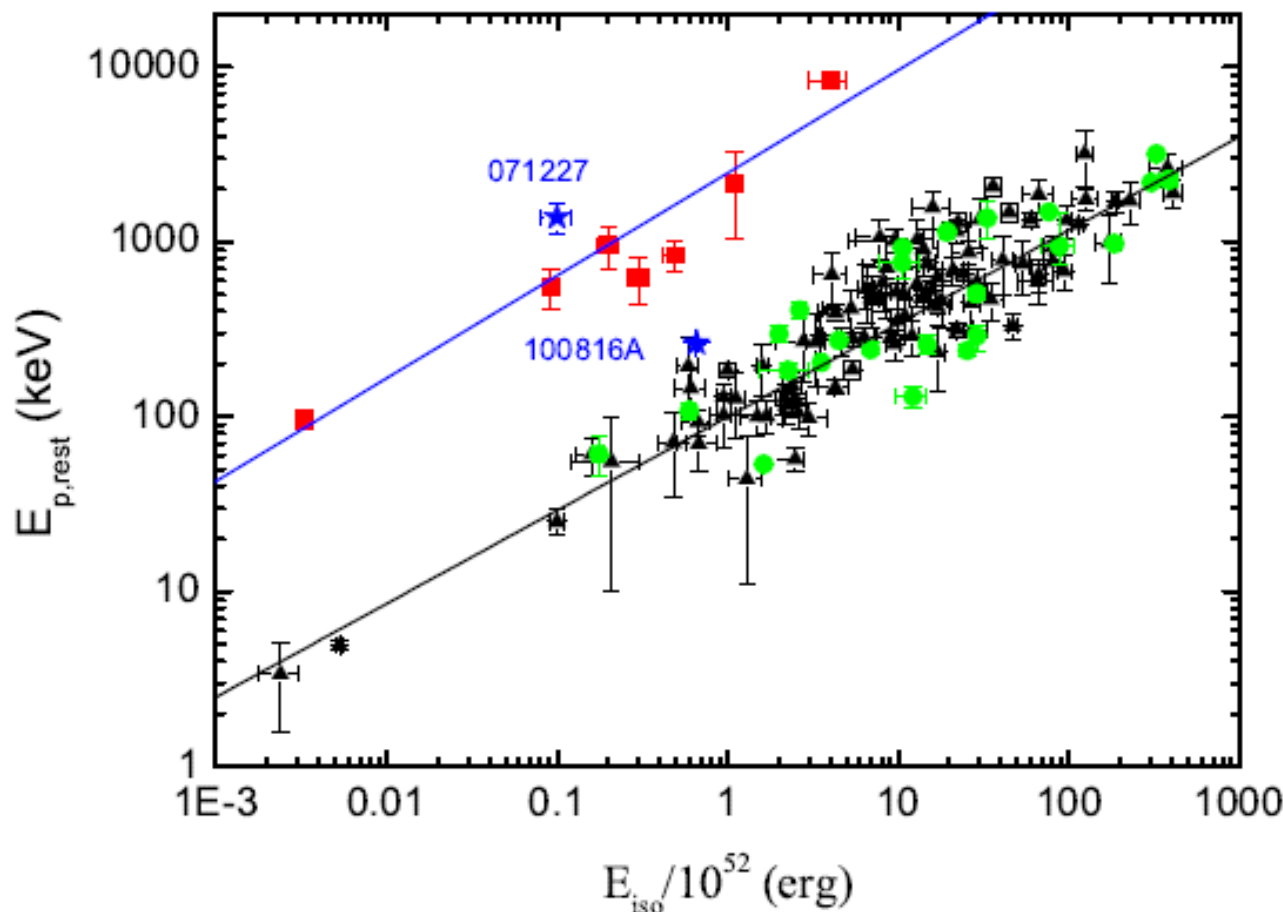


Fig. 8.— The correlations between the rest frame peak energy ($E_{p,\text{rest}}$) and the isotropic total energy (E_{iso}) for the short GRBs (squares) and long GRBs (The triangles represent Pre-Fermi GRBs taken from Amati et al. (2010) and the references therein and the circles represent Fermi GRBs listed in Table 3). The stars are the two controversial GRBs, GRB 071227 and GRB 100816A. The solid lines are the best fit correlations: $E_{p,\text{rest}} = 2455 \times (\frac{E_{\text{iso}}}{10^{52}})^{0.59}$ for short GRBs and $E_{p,\text{rest}} = 100 \times (\frac{E_{\text{iso}}}{10^{52}})^{0.51}$ for long GRBs.

time resolved spectra,
 $kT \sim 100 \text{ keV}$

But in such a model the compact source must always have some radiating surface (but not an event horizon) and, respectively, always occupy some finite volume. Such an object can have both a strong regular magnetic field and a nonuniformly-radiating surface connected with it. Thus, it may turn out that GRB sources do not belong to black holes, because properties of these massive compact sources are quite different.

But a problem immediately arises for distant GRB sources (e.g. [1, 2]): too large energy ($>10^{51}$ ergs) is released in the observed (for the most GRBs) soft γ -rays (< 511 keV and up to 1 MeV and more) in such a small volume for the sources at cosmological distances (> 1 Gpc). For a photon number density

$$n_\gamma \sim (10^{51} \text{ ergs} / (m_e c^2)) / (c \delta T)^3 \sim 10^{57} / (3000 \text{ km})^3 \sim 10^{32} \text{ cm}^{-3}$$

two γ -ray photons with a *sum energy* larger than $2m_e c^2$ could interact with each other and produce electron positron pairs. The optical depth for pair creation is given approximately by

$T_{e-e+} \sim n_\gamma r_e^2 (c \delta T) \sim 10^{16}$, where r_e is the classical electron radius $e^2/(m_e c^2)$ (the cross-section for pair production is $\sim r_e^2$ or $\sim 10^{-25} \text{ cm}^2$ at these semirelativistic energies).

It is the essence of a so-called “compactness problem”: the optical depth of the relatively low energy photons (~ 511 keV) must be so large that these photons could not be observed.

Модель асимметричного взрыва GRB/SN прадителя

...a strongly non-spherical explosion may be a generic feature of core-collapse supernovae of all types.

...Though while it is not clear that the same mechanism that generates the GRB is also responsible for exploding the star.

astro-ph/0603297
Leonard, Filippenko et al.

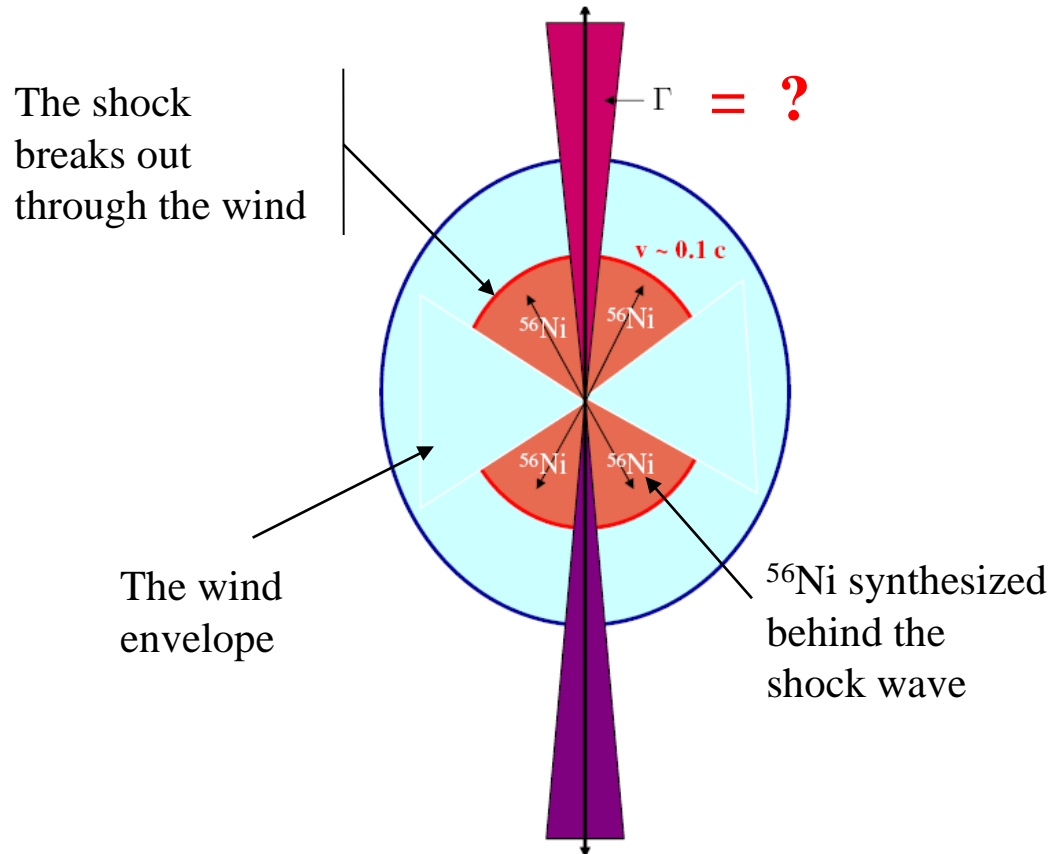


Fig. from Astro-ph/0604131, Woosley and Heger

Хотя само явление необычное, но объект-источник не так уж и уникален !/? Чем ближе GRB-вспышка, тем больше признаков СН.

Table 1. Rates in an average galaxy

	Rate (yr^{-1})
Core-collapse supernovae	7×10^{-3}
Radio pulsars (Galactic)	4×10^{-2}
SNe Ib/c	1×10^{-3}
Hypernovae	$\sim 10^{-5}$
GRBs (for different effective beaming angles θ)	
$\theta = 1^\circ$	6×10^{-4}
$\theta = 5^\circ$	3×10^{-5}
$\theta = 15^\circ$	3×10^{-6}
Massive stars	
$> 20 M_\odot$	2×10^{-3}
$> 40 M_\odot$	6×10^{-4}
$> 80 M_\odot$	2×10^{-4}

GRBs for $\theta \sim 0.1^\circ$ **7×10^{-3}**

II. Типичные спектры гамма-всплесков и соотношение между пиковой и изотропной энергией ($E_p E_i$ or the Amati law) может быть наблюдательным следствием компактной модели источника GRB

The suggested compact GRB scenario allows also predicting the behavior of **superluminal radio components** (which have been observed for GRB 030329 (Taylor et al., 2004)).

Most likely there is no considerable deceleration of the narrow jet (or bullet) with the Lorentz factor of order 10.

Hence we expect that the superluminal radio components related to the jet have the following properties:

- 1) the radio component will move with the **constant** observed superluminal velocity;
- 2) the characteristic observed velocity of the superluminal component is of the order of the Lorentz factor, i.e. of order 10 c.

The Angular Size and Proper Motion of the Afterglow of GRB 030329

G. B. Taylor¹, D. A. Frail¹, E. Berger² & S. R. Kulkarni²

ABSTRACT

The bright, nearby ($z=0.1685$) gamma-ray burst of 29 March 2003 has presented us with the first opportunity to directly image the expansion of a GRB. This burst reached flux density levels at centimeter wavelengths more than 50 times brighter than any previously studied event. Here we present the results of a VLBI campaign using the VLBA, VLA, Green Bank, Effelsberg, Arecibo, and Westerbork telescopes that resolves the radio afterglow of GRB 030329 and constrains its rate of expansion. The size of the afterglow is found to be ~ 0.07 mas (0.2 pc) 25 days after the burst, and 0.17 mas (0.5 pc) 83 days after the burst, indicating an average velocity of 3.5c. This expansion is consistent with expectations of the standard fireball model. We measure the projected proper motion of GRB 030329 in the sky to < 0.3 mas in the 80 days following the burst. In observations taken 52 days after the burst we detect an additional compact component at a distance from the main component of 0.28 ± 0.05 mas (0.80 pc). The presence of this component is not expected from the standard model.

EMMI Rapid Reaction Task Force Meeting on “Quark Matter in Compact Star”

The recent measurement of 20 pulsars has initiated an intense discussion on its impact on our understanding of the high-density matter in the cores of NSs.

A task force meeting was held from October 7-10, 2013 at the Frankfurt Institute for Advanced Studies to address the presence of quark matter in these massive stars.

During this meeting, the recent observational astrophysical data was reviewed.

The possibility of pure **quark** stars, **hybrid** stars and the nature of the **QCD phase transition** were discussed and their observational signals delineated.

Самые первые спектры ОТ GRB 060218

($z = 0.0331$)

Telescope	$T_{\text{first_Sp}}$	astro-ph/
MDM (2.4m)	1.95 days	0603686 (Mirabal et al.)
BTA (6m)	2.55 days	GCN GRB Report No 4809
ESO VLT (8m)	2.89 days	0603530 (Pian et al.)
NOT (2.56m)	3.78 days	0603495* (Sollerman et al.)
MMT (6.5m)	3.97 days	0603377 (Modjaz et al.)

...

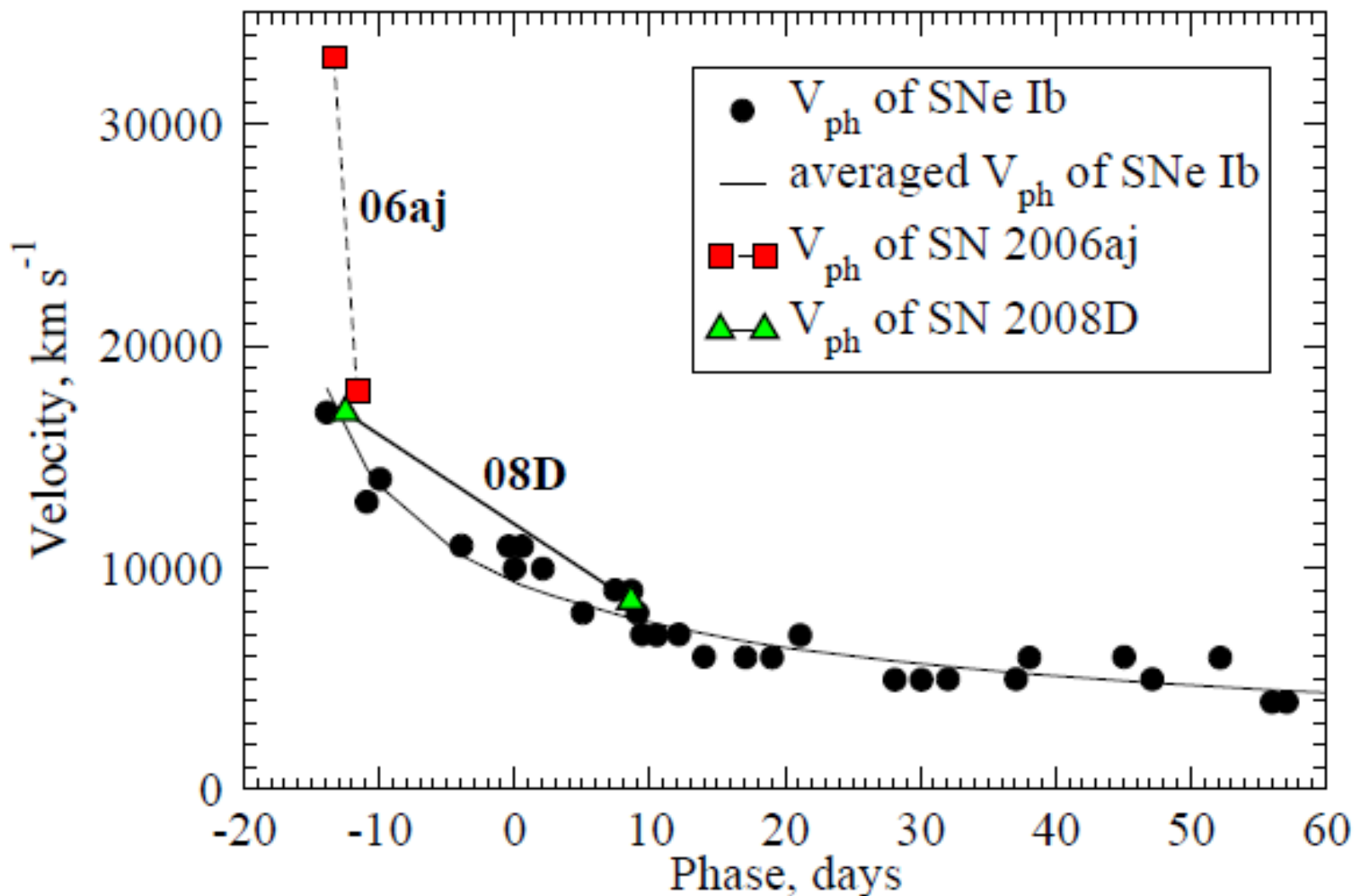
...

...

$T_{\text{first_Sp}}$ - время после GRB 060218

0603495* - Sollerman et al., directly in Abstract that:
"Our first spectra are earlier than spectra for any other GRB-SN."
Jesper Sollerman сильно ошибается потому, что

Спектры GRB 060218/SN 2006aj, полученные на БТА, как и для
GRB 030329/SN 2003dh ($z = 0.1685$), снова оказываются в числе
самых первых спектров двух самых близких GRB/SN-вспышек.
UV-избытки в ранних спектрах – это взаимодействие ударной волны
со звездным ветром массивной звезды (**the SN Ic shock break-out**)



Velocity at the photosphere, as inferred from Fe II lines, is plotted against time after maximum light. The line is a power-law fit to the data, with SN 1998dt at 32 days (open circle) excluded (Figure 22 from Branch, D. et al. 2002, ApJ, 566, 1005). Squares (SN 2008D) and Diamonds (SN 2006aj) are photosphere velocities, inferred from our spectra.

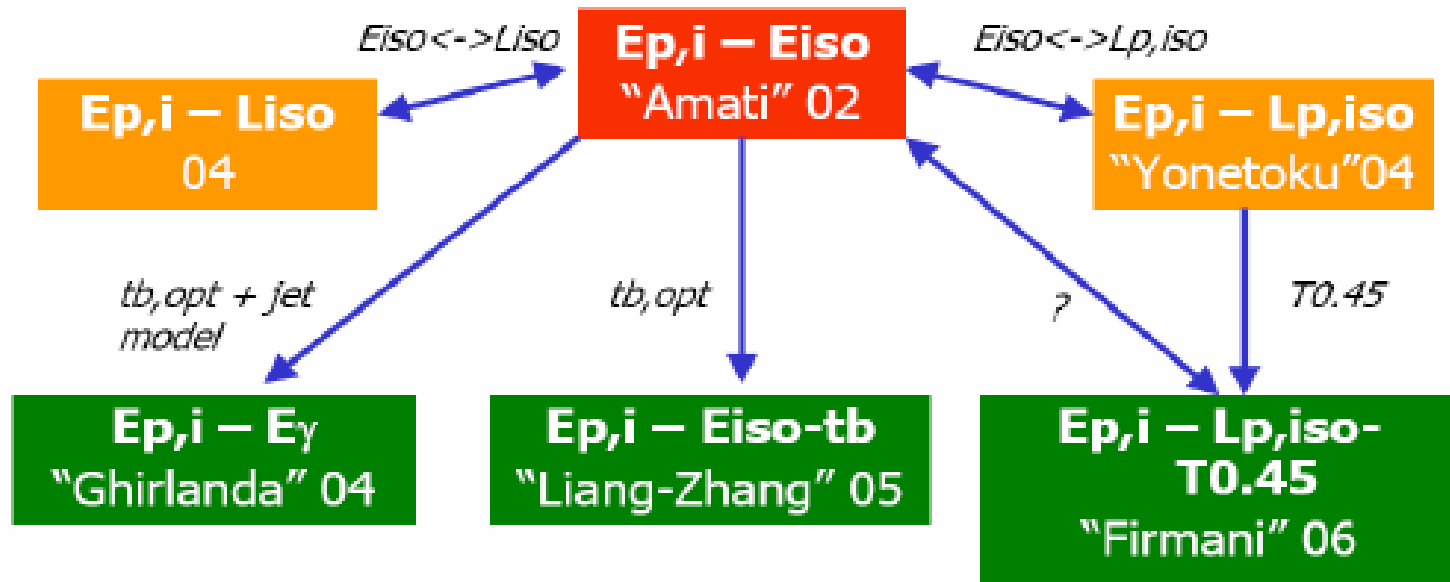
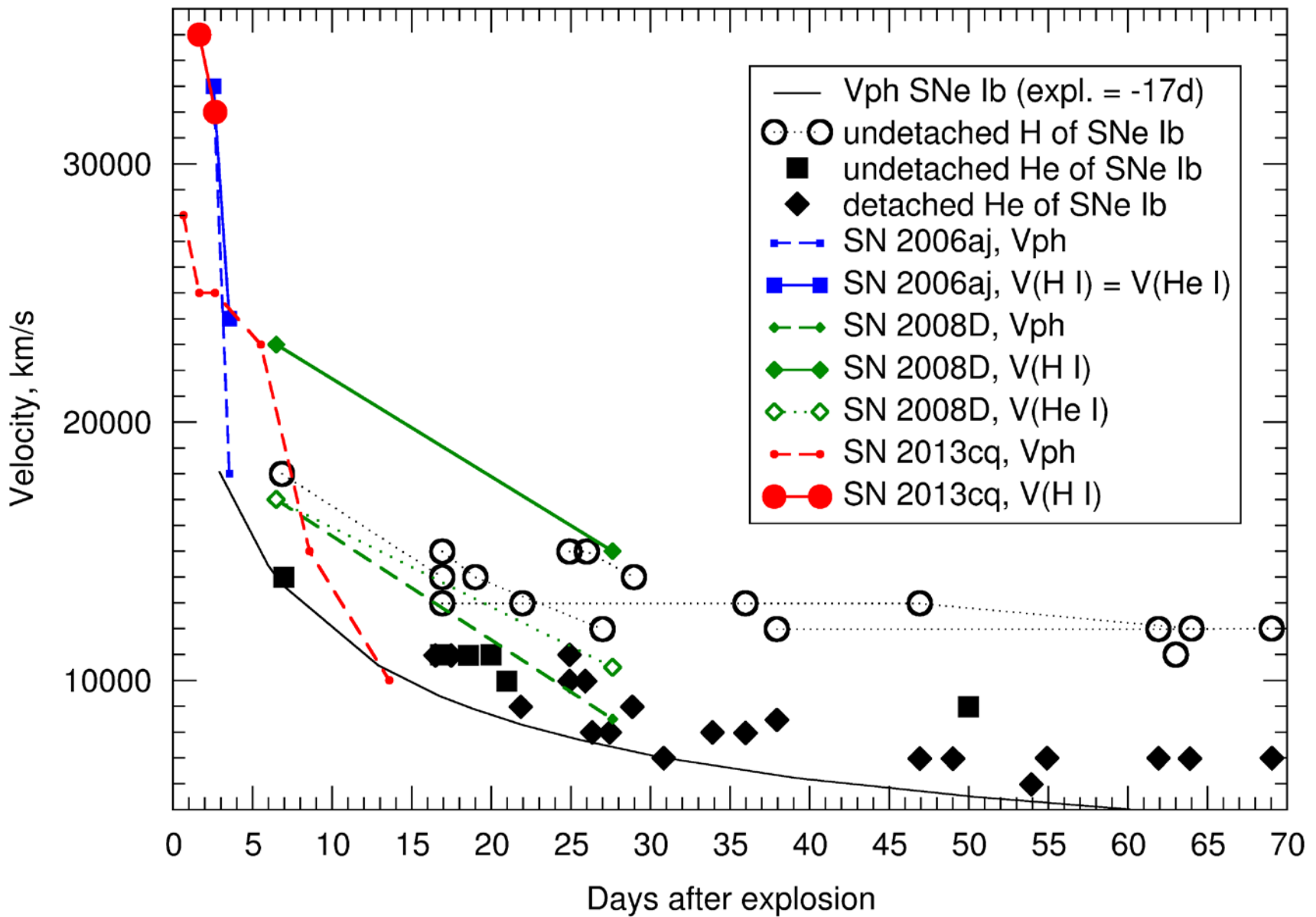


FIGURE 2. The “genealogy” of spectrum-energy correlations. The “name” often found in the literature is reported below each correlation, together with the year. Also shown are the link between the correlations (arrows) and the relevant observables.



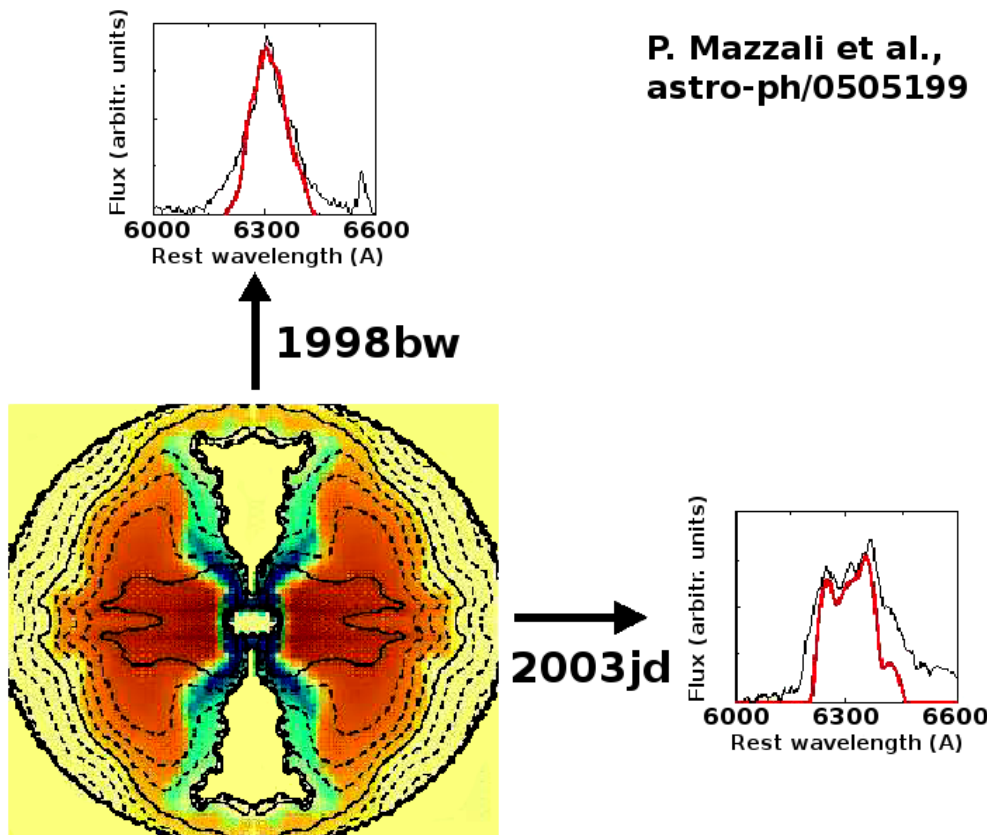
exponentially decaying mass distribution with a cutoff given by

$$P(M; M_{\text{scale}}, M_c) = \frac{\exp(M_c/M_{\text{scale}})}{M_{\text{scale}}} \\ \times \begin{cases} \exp(-M/M_{\text{scale}}), & M > M_c \\ 0, & M \leq M_c \end{cases} \quad (9)$$

This choice of the mass distribution is motivated by theoretical expectations based on the energetics of supernova explosions, as well as the density profiles and mass distributions of pre-supernova stars. The typical value of the mass scale is expected to lie in the range $M_{\text{scale}} \sim 5.5\text{--}9 M_\odot$ (as we infer from the various figures in Fryer & Kalogera 2001), whereas the cutoff mass is simply expected to be the maximum neutron-star mass. Our goal is to find the values of the mass scale M_{scale} in the exponential and the cutoff mass M_c that maximize a properly defined likelihood and to estimate their uncertainties. We will show below that the particular choice of the functional form of the mass distribution does not affect the main conclusions of the paper.

Nebular phase

The general belief is that core collapse supernovae connected with XRF/GRBs event can be naturally explained by the aspherical axially-symmetrical explosion of massive SNe. The common assumption is that in the case of an XRF type flash the observer is located outside the cone where for some reasons the bulk of gamma-ray radiation is concentrated. The asphericity is generally observed in the nebular phase observations.



We can not see any GRB event connected with SN2003jd

Thus, the doubled peaked [OI] emission must be observed for SNe which were not accompanied with GRBs, like SN2008D. And the single peak of [OI] emission is observed in the **nebular phase** of SNe which are accompanied with GRBs, as in the case of GRB060218/SN2006aj.